FEL Theory in the Ion Channel Wiggler

by

Sijia Chen

A dissertation submitted in partial fulfillment

of the requirements for the degree of

Doctor of Philosophy

Department of Physics

University of Strathclyde

September 2016

Professor Dino Jaroszynski

Declaration of Authenticity and Author's Rights

This thesis is the result of the authors original research. It has been composed by the author and has not been previously submitted for examination which has led to the award of a degree.

Signed: 陈慧丽

Date: 10/25/2016

Acknowledgements

This thesis is completed with the indispensable help of many people, first among whom must be mentioned is my supervisor Prof. Dino Jaroszynski, whose strong support of this work has been most valuable, and whose optimism has always encourged me. I am much indebted to the numerous discussions and suggestions along the way during the development of this theory, and the tireless reviewing of my thesis by Dr. Bernhard Ersfeld, with whom I have worked most closely, and always with pleasure.

My appreciation also goes to Qin Beibei for helping me with drawing plots and her encouragement.

The greatest I owe to my mother for her patience and continous support for me, without which I could not have finished this work.

Contents

Role of the Author

The author develops and extends the theory of the ion channel laser (ICL) by Whittum [1, 2], to make it applicable to free electrons oscillating with large betatron amplitudes, through a Hamiltonian-based approach. The linear ICL equations and steady state results are derived using Bonifacio's [3] universal scaling approach, a work done in collaboration with Bernhard Ersfeld and published in Ref. [4]. The author also develops for the first time a one-dimensional (1D) spatio-temporal ICL theory based on the time-dependent FEL theory, which includes a high-harmonics theory of the ICL, along with the numerical modeling and results for the spatio-temporal theory. In addition, an error in Whittum's original phase equation under eikonal formalism has been corrected.

Publication Arising from this Thesis

- B. Ersfeld, R. Bonifacio, S. Chen, R. Islam, P. Smorenburg and D. Jaroszynski, New J. Phys. **16**, 093025 (2014).
- B. Ersfeld, R. Bonifacio, S. Chen, R. Islam, and D. Jaroszynski,Proc. SPIE. **9509**, 95090L (2015).

Abstract

The ion channel laser (ICL) is an ultra-compact version of the free-electron laser (FEL), with the wiggler replaced by an ion channel. Given its small size and the large wiggler field that can be created within a small volume, it has enormous potential for generating high-frequency coherent radiation. Previous studies of the ICL [1,5], however, have assumed transverse momentum amplitudes that are unrealistically small for experiments, and thus concluded that high-gain high-frequency coherent radiation generation using the ICL is infeasible. In contrast, this thesis shows that this restriction can be removed by correctly taking into account the dependence of the resonance between oscillations and emitted field on the betatron amplitude, which must be treated as variable. The ICL model with this essential addition is described using the well-known formalism for the FEL [3]. Both steady-state and spatio-temporal analyses of the resulting scaled equations show a realistic prospect of building a compact ICL source for fundamental wavelengths down to the UV, with harmonics potentially extending to X-rays. The gain parameter ρ can attain values of the order of 0.01-0.1, which permits driving an ICL with electron bunches with realistic emittance and achieving a radiation power gain comparable to FEL over a small distance.

In addition, we present the first results of superradiant simulations for the ICL, also within the framework of the scaled formalism for the FEL, taking into account propagation effects, as well as a full SASE simulation using shot noise as the startup.

Chapter 1

Introduction

The possibility of generating coherent radiation in an ion channel wiggler was first proposed by D. Whittum in 1990 [1], and a theory using an eikonal formalism in [2]. This theory provides a satisfactory model for ion channel radiation with electrons performing small-amplitude transverse oscillations, but has significant limitations in practice: the theory does not correctly describe the interaction of electron beam and radiation field when the betatron amplitude is large, which imposes severe and artificial limits on the design parameters of an ion channel laser [5]. Moreover, when beams with large betatron amplitude are used, a number of additional high-order effects arise, which are not accounted for in Whittum's theory framework, let alone propagation effects (slippage), and high-order harmonics.

In this chapter, we briefly review the two subjects of study on which the ion channel laser theory is based: free-electron laser and laser-plasma interaction. The latter is discussed mainly in the context of the creation of an ion cavity using a high-power laser beam.

1.1 Overview of Free-Electron Laser Theory and Devices

The free-electron laser (FEL), as any conventional laser, transforms the energy of electrons into electromagnetic (e.m.) radiation. The state of electrons generating radiation in FELs, however, is different from the bound electrons of traditional lasing media, which are restricted to quantum transition energies between states, and thus can usually only produce a fixed lasing frequency. Instead, free electrons, usually moving at highly relativistic axial velocity $v_{\parallel}$, pass through a periodic magneto-static structure, which for FELs are strong magnetic fields,

produced either by arrays of permanent magnets with alternating polarities or bipolar helical coils with current circulating in opposite directions. To an electron, in its rest frame the magnetic field appears like a counter-propagating radiation field, with a Lorentz-contracted wavelength $\lambda'_w = \lambda_w/\gamma_\parallel$, where λ_w is the wiggler period and $\gamma_\parallel = \sqrt{1 - v_\parallel^2/c^2}$ the Lorentz factor corresponding to $v_\parallel$, with c the vacuum speed of light. In the Weizsäcker-Williams approximation, the electrons interact with the virtual quanta of the static magnetic field and scatter them into real photons of the stimulating field . In such a picture, the electron acts as a "relativistic mirror" that reflects the pseudo-radiation via Compton back-scattering. Thanks to the huge kinetic energy carried by the free electrons, which is easily tunable, a FEL can be tuned over an unusually broad spectrum, ranging from microwaves to hard X-rays ($\lambda \approx 0.1\,\mathrm{nm}$). In addition, the FEL has the advantage that radiation occurs in vacuum, with no thermal dispersion or breakdown effects of the medium to worry about; the latter properties are also shared by the ICL, which uses a plasma wiggler.

When electrons are randomly distributed, the FEL is simply a synchrotron device, whereas stimulated emission occurs when radiation resonantly co-propagates with the electron beam. Both of these processes are discussed in the next subsection, while spontaneous emission in the plasma wiggler is discussed in a further subsection.

1.1.1 FEL Spontaneous Emission

A really "free" charge in vacuum is unable to radiate, due to the electron-photon energy-momentum conservation relation introduced in Einstein's theory of special relativity [6]. The emission of photons by electrons, therefore, has to occur under the influence of a field, which can be a static magnetic field (an undulator), an electromagnetic field (laser wiggler), a symmetric electrostatic field (ion channel), or even a periodic electric field generated by a plasma wake [7]. In short, FEL radiation is really synchrotron radiation, *i.e.* the radiation emitted by an electric charge moving at relativistic speed with a transverse force applied to it. The focus of FEL theory is usually on the electron motion under the influence of a static magnetic field.

For a static magnetic wiggler, its simplest realization can be made in two ways: The easier one to model is the helical wiggler consisting of two intertwined helical coils, while the one made of two arrays of magnets with alternating polarities is called a "planar wiggler". In both cases, the electrons inside the wiggler are periodically deflected by the Lorentz force (or "$\mathbf{v} \times \mathbf{B}_w$", where $\mathbf{v}$ is the electron velocity) generated by the wiggler field. The magnetic field $\mathbf{B}_w$ is usually periodic due to the alternating polarities of the magnets or coils, respectively.

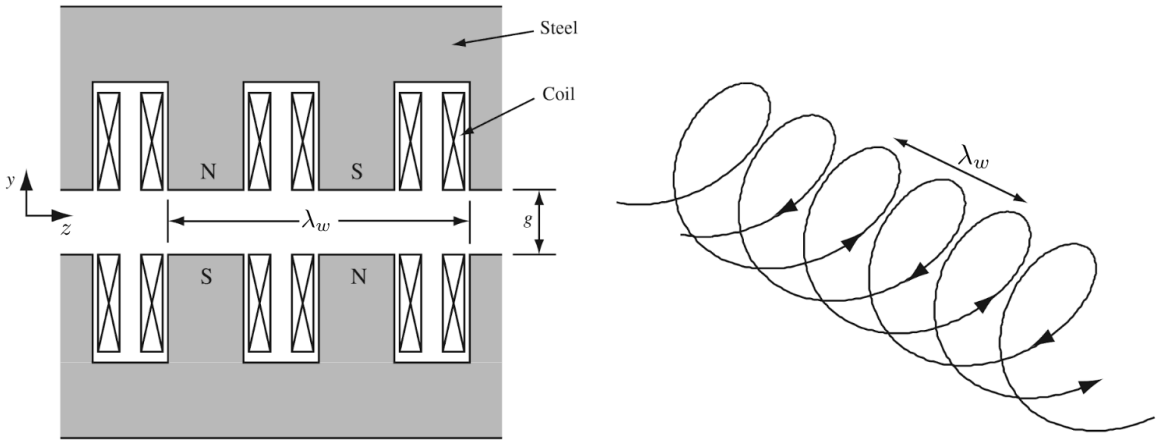

Figure 1.1: sketches of two different types of FEL wigglers adapted from the book [8], with λ_w representing the wiggler period, and g the gap length. The planar wiggler on the left is composed of two two arrays of magnets with alternating polarities, while the helical wiggler on the right is simply a bifilar helical coil

For a helical wiggler, the approximate expression for the vector potential is

$$\mathbf{A}_w = \frac{B_w}{k_w} \begin{pmatrix} [1 + k_w^2(3y^2 + x^2)/8] \sin(k_w z) - (k_w^2 xy/4) \cos(k_w z) \\ [1 + k_w^2(3x^2 + y^2)/8] \cos(k_w z) - (k_w^2 xy/4) \sin(k_w z) \\ 0 \end{pmatrix},$$

where B_w and k_w are the magnetic field amplitude and wave number of the wiggler field, respectively. Close to the axis, $\mathbf{A}_w$ can be further approximated as

$$\mathbf{A}_w = \frac{B_w}{k_w} \begin{pmatrix} \sin(k_w z) \\ \cos(k_w z) \\ 0 \end{pmatrix}.$$

Under the influence of such a field, electrons with high axial momentum (along z) will oscillate transversely with almost identical transverse velocity, thereby emitting synchrotron radiation that is circularly polarized. The main features of such radiation are the following:
i) Its intensity is proportional to the electric current and thus the number of electrons N_e in the beam, *i.e.*, the radiation is incoherent, with each electron emitting a field with random phase to that of the others.
ii) The emitted radiation is confined in a narrow cone along the direction of electron motion, the wiggler axis, within an angle of order of $1/\gamma_{\|}$ if the wiggler parameter a_w, defined in

Eq. (1.7) below as the normalized vector potential, is much smaller than unity.
iii) The bandwidth is narrow, with on-axis spectral distribution (*i.e.*, intensity I per unit intervals of solid angle Ω and frequency ω, respectively)

$$\frac{d^2I}{d\Omega d\omega} \propto \mathrm{sinc}^2\left(\pi N_w \frac{\omega-\omega_s}{\omega_s}\right), \tag{1.1}$$

where $\mathrm{sinc}(x) = \sin(x)/x$, and N_w is the number of wiggler periods. Therefore, the spectrum is peaked around a frequency $\omega_s = 2\pi c/\lambda_s$, with λ_s given by:

$$\lambda_s = \frac{1-\beta_\parallel}{\beta_\parallel}\lambda_w, \tag{1.2}$$

where $\beta_\parallel = v_\parallel/c$, with $v_\parallel$ the average longitudinal velocity of the electron beam, and $\lambda_w = 2\pi/k_w$ is the wiggler period. Its FWHM spectral linewidth is

$$\frac{\Delta\omega}{\omega} = \frac{0.886}{N_w}. \tag{1.3}$$

This equation shows that the bandwidth of the spontaneous radiation decreases with increasing number of wiggler periods. This result is most easily explained in the frame of co-moving electrons: each electron "sees" the wiggler field as a counter-propagating pseudo-radiation field, with N_w periods, and Lorentz-contracted wavelength $\lambda'_w = \lambda_w/\gamma_\parallel$. Hence it executes N_w periods of oscillation, emitting a wave packet with a length of $N_w\lambda'_w$, and a frequency centered at $2\pi c/\lambda'_w$; its bandwidth is therefore the reciprocal of the duration of the wave packet, using the Gabor limit from signal-processing theory. In fact, the one-dimensional sinc spectral distribution can be obtained by Fourier-transforming a plane wave truncated after N_w oscillations, resulting in the FWHM(full width at half maximum) relative bandwidth given by Eqn. (1.3). The bunch acts as a "relativistic mirror" where the radiation is reflected by Compton back-scattering, with the Compton shift neglected because of the classical assumption. The relationship between the wavelength of the emitted radiation and the wiggler period can also be derived in the laboratory frame. In the time an electron takes to travel one wiggler period, λ_w, the electromagnetic radiation will slip over it by one radiation wavelength, λ_r. The wiggler and the radiation wavelengths satisfy a "resonance condition"

$$\lambda_w/(\lambda_r+\lambda_w) = v_\parallel/c. \tag{1.4}$$

Using $v_\parallel = dz/dt$ and $\lambda_w/(\lambda_r + \lambda_w) = k_r/(k_w + k_r)$, with$k_w$ and k_r being the wiggler and radiation wavenumber respectively, we can rewrite this equation as $(k_w + k_r)dz/dt - \omega_r = 0$. The resonance relation is obtained by imposing that the phase difference between the electron motion and radiation field is constant,

$$k_w z + k_r z - \omega_r t = C. \tag{1.5}$$

The longitudinal velocity, $v_\parallel = c\beta_\parallel$, is obtained from the total Lorentz factor γ using the relation $1/\gamma^2 = 1 - \beta_\perp^2 - \beta_\parallel^2$; the modulus of $\beta_\perp$ will be shown in the next section to be

$$|\beta_\perp| \approx \frac{a_w}{\gamma}, \tag{1.6}$$

where

$$a_w = \frac{e\lambda_w B_w}{2\pi m_e c}, \tag{1.7}$$

with m_e the electron mass, is the wiggler parameter, which is the amplitude of the normalized transverse momentum $p_\perp/(m_e c)$. Combining this expression with the definition of the Lorentz factor, we obtain

$$\frac{1}{\gamma_\parallel^2} = \frac{1 + a_w^2}{\gamma^2}. \tag{1.8}$$

Finally, after the resonance relation is applied to the above equation, in the ultra-relativistic limit $\gamma_\parallel \gg 1$, the relation between the wiggler period and the resonant radiation wavelength is obtained

$$\lambda_s = \frac{1 - \beta_\parallel}{\beta_\parallel}\lambda_w \approx \lambda_w \frac{1 + a_w^2}{2\gamma^2}. \tag{1.9}$$

This relation shows the wide tunability and large frequency up-shift factor of an FEL. The wavelength can be tuned by changing γ, λ_w, or B_w, and the emitted wavelength can reach the hard X-ray regime if γ is large enough.

1.1.2 FEL Stimulated Emission

We know from solid-state laser theory that an electron emits "stimulated radiation" when it is stimulated by an incident photon with the same energy as its transition energy, hence

the released photon will have the same energy, and therefore frequency, as the incoming one. Unlike the conventional lasing, which can only be described fully by quantum mechanics, the free-electron lasing effect can be accurately modelled classically, although the requirements on incident photons seem somehow comparable: both require the photons to have a certain "resonant frequency", but for the "free" electrons, the frequency of the emitted radiation is freely tunable by changing their kinetic energies rather than being limited by the differences between the discrete energy levels of orbital electrons. Furthermore, "free" electrons with different phases relative to the radiation field would not end up with equal kinetic energies even if they were equal at the start of the interaction, not to say that any realistic electron bunch would have an intrinsic initial energy spread. Despite all these differences, a FEL can still be employed as a high-power, high-tunability coherent light source with relatively narrow bandwidth, which can be further improved using a resonant cavity.

The FEL stimulated emission takes place when a radiation field with wavelength $\lambda_r \approx \lambda_s$, co-propagates with the electron beam inside the wiggler. From the resonance relation one can define the resonant electron energy

$$\gamma_r = \sqrt{\frac{\lambda_w(1 + a_w^2)}{2\lambda_r}}. \tag{1.10}$$

It can be observed that if the electron energy and the radiation wavelength satisfy the above relation, then the relative phase between the transverse oscillations of the electrons and the radiation remain constant. Depending on the value of this relative phase, and the initial power of the radiation field one of the following process occurs for each electron:

- the electron gives energy to the field and decelerates, *i.e.* stimulated emission, which provides gain, or
- the electron takes energy from the field and accelerates, *i.e.* absorption.

If the first of these two processes dominates, then the injected radiation field is amplified as in the first FEL amplifier experiment [9]. Moreover, if the wiggler is long enough or if the process happens in an optical cavity, then the spontaneous emission is amplified, as in the first FEL oscillator experiment [10]. If the second of these two processes dominates, then the electrons are accelerated as in the inverse FEL [11].

A simplified picture of FEL gain can be obtained using perturbation theory, which neglects the change of the electric field in the equations of motion and leads to Madey's small

signal regime [12] theory. This theory considers a "long" electron pulse with initial electron phases randomly distributed over each radiation wavelength. In the case of a nearly mono-energetic and resonant electron beam, on average half of the electrons will decelerate and half of them will accelerate, resulting in no net gain. Madey's small signal regime occurs, therefore, when the average energy of the electrons is slightly above resonance, so that gain prevails over absorption [12].

1.1.3 Electron Bunching and the High-gain Regime

The gain which can be achieved via energy-detuning in Madey's small signal regime is quite small. Such low gain, however, is not the limit of the potential of electrons for amplifying an electromagnetic radiation field, because electron phases can evolve toward a common value. As shown in the low-gain model, acceleration and deceleration of the electrons by the radiation field will cause them to "bunch" spatially, which results in dense electron bunches with a separation of λ_r and thus in a large number of electrons radiating coherently. Such bunching allows the radiation field to be amplified far beyond the low fields of the initial seeding, in the so-called "small-signal high-gain regime". The variable representing how strongly the electrons are bunched, is the bunching parameter

$$\mathcal{B} = \frac{1}{N_e} \sum_{j=1}^{N_e} e^{-i\theta_j}, \tag{1.11}$$

where N_e is the number of electrons in the bunch previously defined, and $\theta_j = k_w z_j + k z_j - \omega t$ is the (slowly changing) difference between the respective phases of an electron at position z_j and the laser field. We see that $\mathcal{B}$ is a measure of the longitudinal modulation of the electron beam on the scale of the radiation wavelength. A uniform distribution of phases on $[0, 2\pi]$ will give a bunching factor of 0, while ideal bunching with $\|\mathcal{B}\| = 1$ implies that all electrons are perfectly in phase. We shall see that a collective instability for the system leads to electron self-bunching and to exponential growth of radiation until saturation of amplification limits the conversion of kinetic electron energy into radiation energy; this is the so-called "high-gain steady-state regime", where the saturated radiation power is proportional to $N_e^{4/3}$, due to the collective radiation effect, whereas in the incoherent radiation case the power scales as N_e.

The behaviour of the FEL is modified when beam transport and propagation effects, and the initial spread in velocities of the electrons are taken into account. This is known

as slippage, where the radiation pulse moves ahead with respect to the electron pulse by a radiation wavelength λ_r for every wiggler period λ_w, *i.e.* by $L_s = N_w\lambda_r$ at the end of a N_w period wiggler. From analytical and numerical studies it has been shown [13, 14] that when the slippage length L_s is large with respect to the "gain length", the FEL can operate in a different regime, called the superradiant regime, in which the peak intensity of the radiation no longer saturates and scales as N_e^2. The slippage effect allows us to exploit the potential of generating weakly amplified coherent radiation without an external input, yet it is not only with strong slippage that superradiance can be achieved; when a very long, almost "steady-state" like electron pulse is used, strongly amplified coherent radiation with intensity and power scaling with N_e^2 can be observed if the electron bunch is seeded with an external source. (Radiation intensities scaling as N_e^2 may also arise from coherent synchrotron radiation emitted by electron which have been pre-bunched by an external source [15].)

A FEL can also utilize incoherent synchrotron radiation as a 'startup', with electrons entering the wiggler in an unprepared state, in which case the initial emission is provided by the shot noise of the electron bunch. The random nature of this seeding field implies that the bandwidth of the spontaneous emission spectrum is broader than that of the FEL amplifier, which leads to such self-emission FEL being always tuned to the resonant frequency with the largest growth rate, and a spiky radiation pulse. The FEL self-emission phenomenon in which the propagation effects are considered is called the **S**elf -**A**mplified **S**pontaneous **E**mission (**SASE**) [16] mode of operation. The SASE mode of operation is important at wavelengths for which conventional radiation sources usually cannot be used for seeding, such as the XUV or the far-infrared regime. The single-pass SASE FEL has been realised in several projects such as the LCLS(Linac Coherent Light Source) [17] at Stanford, USA, and SACLA [18] in Japan, and the future XFEL at DESY in Hamburg. These FELs are all based on the classical theory of SASE, which models a source that radiates a pulse with a broad spectrum composed of many random superradiant spikes [19–21]. It has recently been proposed that a FEL can operate in a quantum regime (QFEL) [22], in which the spiking behaviour observed in SASE mode disappears and the spectrum reduces to a single narrow line, thanks to its much increased cooperation length.

1.1.4 Laser Wigglers

Magnetostatic wigglers can be hundreds of metres long and very expensive. This has led to a search for other types of undulators. The limitations of magnetostatic wigglers become

increasingly conspicuous in the design and construction of X-ray FEL and QFEL wigglers. A possible alternative is to utilise a counter-propagating electromagnetic wave as a wiggler. An infrared pulse from a high-power Nd or CO_2 laser, with a wavelength of 1 or 10 μm, would yield FEL radiation in the range of tens of nanometers with electrons of only a few MeV, with the interaction region that defines the wiggler length only meters long. The resonance relation becomes

$$\gamma = \sqrt{\frac{\lambda_L(1+a_0^2)}{4\lambda_r}}, \tag{1.12}$$

where λ_L is the laser wavelength and $a_0 = eA_0/(m_e c)$ is the laser wiggler parameter equal to its normalised vector potential. This dispenses with the need for large high-energy accelerators, and long magnetostatic undulators. However, the laser wiggler suffers from a small effective FEL gain parameter, and tight tolerances on the field, which severely limits the achieveable efficiency of the wiggler and requires a currently unrealistic small energy spread to operate.

1.1.5 Plasma Wiggler

Another candidate for a short-period wiggler is the purely electric plasma wave wiggler first proposed by C. Joshi *et al.* in [25], which is formed by a relativistic plasma density wave. This plasma wave can be excited in several ways, such as with two beating laser beams, a short laser pulse as proposed in the laser wakefield accelerator scheme (LWFA), or a relativistic short electron pulse propagating through a plasma channel. The geometry of a beating wave driven plasma wiggler is illustrated in Fig 1.1. In this simplified picture, the wiggler consists of a purely electric field oscillating perpendicular to the injected electron beam at the plasma frequency $\omega_p = \sqrt{n_p e^2/(m_e \epsilon_0)}$, where n_p is the plasma electron density, $-e$ is the electric charge and m_e is the mass of the electron, and ϵ_0 is the permittivity of free space, but with no spatial dependence since the wave vector of the radiation is transverse to that of the plasma wave. The electric field E_{pw} of the plasma wave deflects the electron to the side where the electron density is smaller; since both the electrons and the plasma wave are moving at close to the speed of light, by the time the electrons move by half a plasma wavelength $\lambda_p = 2\pi c/\omega_p$, the plasma wave moves orthogonal to it by $\lambda_p/2$ as well. This reverses the polarity of the electric field, which now deflects the electrons to the opposite side. Thus, the apparent wiggler wavelength is λ_p, and the time-dependent electrostatic field

can be expressed as

$$E_{pw} = \frac{e\delta n_p}{\epsilon_0 k_p} \sin(k_p z - \omega_p t), \tag{1.13}$$

where δn_p is the amplitude of the electron density perturbation. Using a plasma wave as a wiggler is attractive for two reasons. First, the effective wiggler wavelength ($2\pi c/\omega_p$, typically of order 100 μm) is shorter than that available with conventional magnetic wigglers; second, the effective wiggler strength can reach values equivalent to 100 MG for a magnetic field. The major obstacle to realize such a plasma wave wiggler is to produce a uniform and transversely wide plasma wave, which has yet to be demonstrated in experiments.

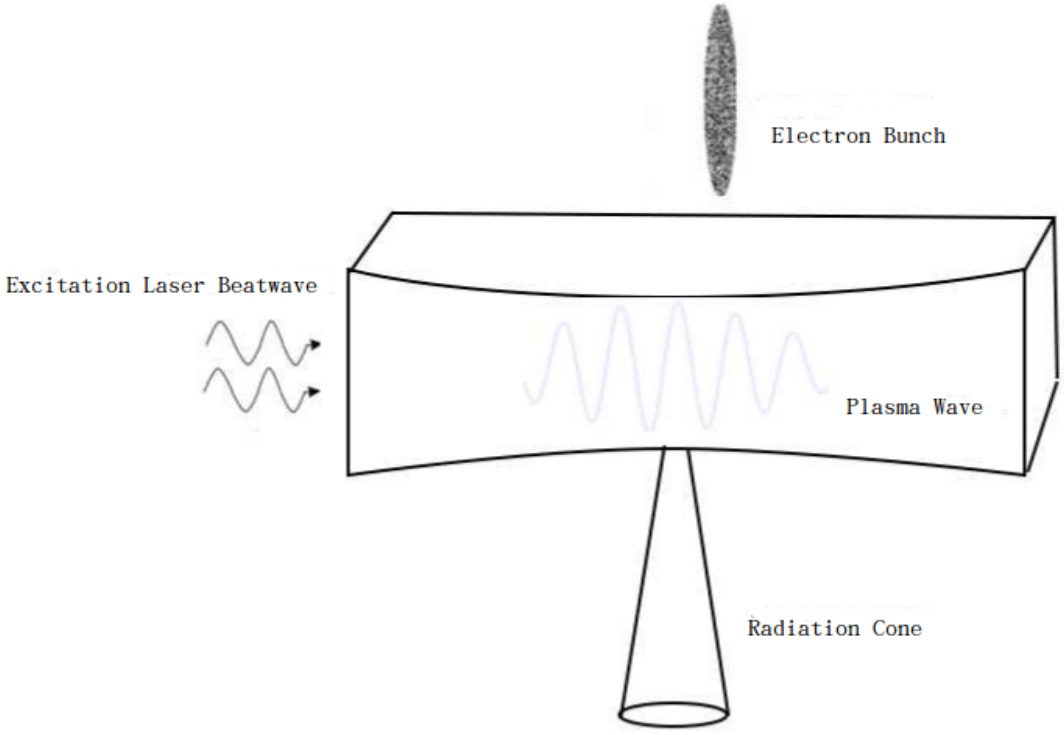

Figure 1.2: Schematic of the geometry of Joshi's plasma wiggler FEL

1.2 Ion Channel Wiggler

1.2.1 Creation of an Ion Channel Wiggler Using an Electron Beam

When the ionizing electric field from a laser pulse or an electron bunch is strong enough to remove the plasma electrons directly from a neutral gas medium, and the pulse length is shorter than the time scale for the expelled electrons to return to the plasma, then instead of an electron density modulation as in the plasma wave wiggler, a plasma channel is formed. The plasma channel produces a strong electrostatic field which wiggles the electrons and in the process, as shown in Fig. 1.2, generates intense betatron radiation. The plasma channel can be categorized as "underdense" or "overdense", depending on whether the channel plasma density is lower or higher than the beam plasma density. When the channel is ionized by an electron beam with density larger than the plasma density, the plasma electrons pushed out of the channel will stream backward to neutralize the ions in the plasma channel. The approximate time for these electrons to return to the channel is π/ω_p, half a plasma period, therefore the main body of a short electron bunch will propagate inside an ion channel free of plasma electrons as long as its duration is shorter than that. Meanwhile, if the electron bunch length is comparable to the channel length, its own electrostatic field should be able to maintain the steady state of the electron vacuum. Electrons within such a plasma channel are focused by the radial electrostatic field due to the ions. If the plasma density is higher than the beam density of a long enough ionizing bunch, the plasma electrons are not completely expelled from the channel, instead they are spatially configured so that the plasma ions cancel the beam space charge and thus allow the beam to pinch under its magnetic self-forces.

The transverse size of an ion channel formed by a relativistic electron bunch (REB) can be simply estimated by requiring all plasma electrons at the edge of the plasma channel to experience zero net transverse electrostatic force. E.g., in the case of ionized helium gas, with channel radius $b > \sigma_r$, the RMS(root-mean-sqaure) radius of the electron beam, we can express the balancing equation of an ion channel in the steady state as:

$$F_\perp = F_{REB} + F_{ion} = \sigma_r^2 n_b e^2 (1 + v_p/c)/(2b\epsilon_0) - b n_p e^2/(2\epsilon_0) = 0, \tag{1.14}$$

where v_p is the longitudinal velocity of plasma electrons pulling back towards the beam axis,

and n_b and n_p are beam and channel plasma density respectively. The above equation gives

$$\frac{b}{\sigma_r} = \sqrt{\frac{(1+v_p/c)n_b}{n_p}}, \tag{1.15}$$

which for $v_p/c \ll 1$ is approximately

$$\frac{b}{\sigma_r} = \sqrt{\frac{n_b}{n_p}}. \tag{1.16}$$

From (1.16), it is clear why a beam-driven plasma channel is not suitable for a large betatron amplitude ICL: Given that b is larger than the betatron amplitude r_β and $r_\beta/\sigma_r \gg 1$, and the ionising beam density is in the range of $10^{17} - 10^{19}$ cm^{-3} (see e.g. [26]) the plasma density produced in the channel would have to be in the range of $10^{15} - 10^{17}$ cm^{-3}, which would lead to a relatively weak electrostatic field and thus rather small gain, which scales with the field strength.

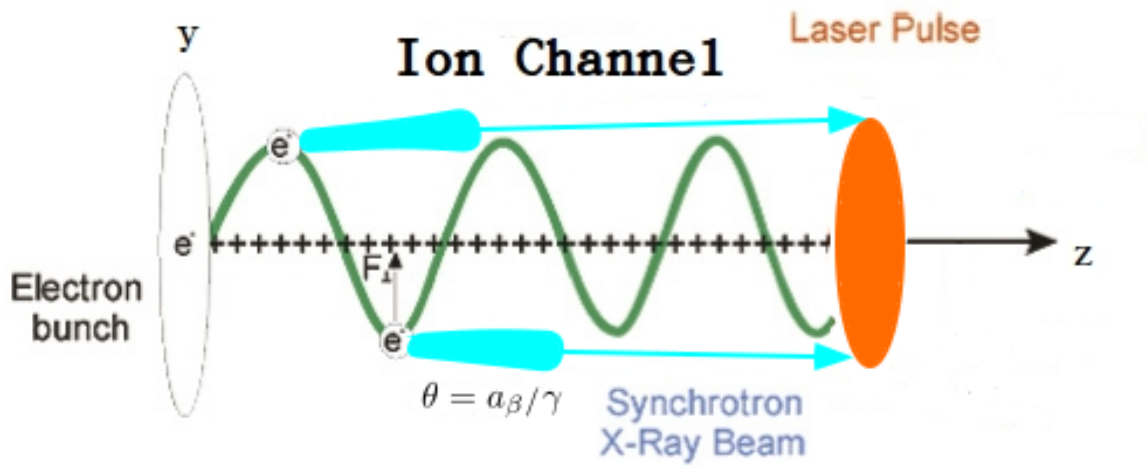

Figure 1.3: Schematic of an ion channel wiggler with an electron bunch driven by the channel field radiating at the extremities of their oscillations, with an opening angle of $\theta = a_\beta/\gamma$ for the radiation cones, where $a_\beta = \sqrt{\gamma/2}\omega_p r_\beta/c$ is the betatron parameter and γ is the Lorentz factor of the radiating electron.

1.2.2 Barrier Suppression Ionisation with a Laser Field

It is possible to produce ion channels with much higher density using an intense laser pulse. The first step is plasma formation by ionizing a neutral gas, which requires the laser intensity

to exceed the ionization intensity of $10^{13} - 10^{14}$ W/cm^2, beyond which the liberated electrons are able to escape freely from the atoms. The upper limit for the intensity needed for this to occur can be estimated using the Bohr model of a hydrogen atom in which an electron is on its orbit around a proton at a distance of a Bohr radius a_B. The electric field strength E_a, that keeps the electron on the orbit, can be calculated classically

$$E_a = \frac{e}{4\pi\epsilon_0 a_B^2} \approx 5.1 \times 10^{11} \text{ V/m}, \tag{1.17}$$

which translates to an atomic unit of intensity

$$I_a = \frac{\epsilon_0 c}{2}|E_a|^2 \approx 3.45 \times 10^{16} \text{ W/cm}^2. \tag{1.18}$$

If the atom is placed in a laser field with an intensity exceeding I_a, formally the atomic Coulomb potential binding the electrons would be completely suppressed. However, higher ionisation rates than predicted by the quantum tunneling model [27] have been observed with much lower field intensities, which leads to the conclusion that at much lower intensities the laser electric field must have a significant impact on the atomic potential field already. In a simple model developed by Bethe and Salpeter, ionization is explained by the distortion of the atomic binding potential due to the electric field of the laser [28]. The model predicts an appearance intensity, I_{app}, at which ionization occurs. The starting point is the superposition of the nuclear potential and a static external electric field. In the direction of the laser polarisation where the barrier is most deeply suppressed, this superposition reads

$$V(x) = -\frac{Ze^2}{4\pi\epsilon_0 x} - eEx, \tag{1.19}$$

with Z the charge of the ion that will be produced and E the external electric field strength. Energetically, the region of lower energy for the electron is separated by a reduced potential, The position of the barrier, x_{max}, can be derived by setting $\partial V(x)/\partial x = 0$, yielding $x_{max} = \sqrt{Ze/(4\pi\epsilon_0 E)}$. By assuming $V(x_{max}) = \epsilon_{ion}$ where ϵ_{ion} is the ionisation energy, the critical electric field strength, E_{crit}, is given by

$$E_{crit} = \frac{\pi\epsilon_0 \epsilon_{ion}^2}{Ze^3}. \tag{1.20}$$

Since in this case the electric field of the laser is so strong that the Coulomb barrier is suppressed, the electron can escape freely. This ionization process is termed barrier suppression

ionization (BSI). The minimum laser intensity required for ionisation is given by

$$I_{BSI} = \frac{\pi^2 c \epsilon_0^3 \epsilon_{ion}^4}{2Z^2 e^6}. \tag{1.21}$$

In the case of a hydrogen atom, one finds:

$$I_{BSI} = \frac{I_a}{256} = 1.37 \times 10^{14} \frac{\mathrm{W}}{\mathrm{cm}^2}, \tag{1.22}$$

using the definition of I_a in (1.18). For different elements, the relation (1.21) is confirmed over several orders of magnitude of intensity [29].

1.2.3 The Non-relativistic Ponderomotive force

With intensities significantly larger than required for BSI, modern high power lasers can easily liberate electrons from the atomic potential, following which they are completely subjected to the Lorentz equation

$$\frac{d\mathbf{p}}{dt} = -e(\mathbf{E} + \mathbf{v} \times \mathbf{B}), \tag{1.23}$$

where the time-dependent electric field of the laser at the position of the electron is denoted by $\mathbf{E}$, the magnetic field by $\mathbf{B}$, the velocity of the electron is $\mathbf{v}$, and its momentum $\mathbf{p} = \gamma m_e \mathbf{v}$. In this subsection we address the non-relativistic case of constant $\gamma \approx 1$. For an electron oscillating within a plane electromagnetic wave travelling in the z direction, its transverse velocity in the y direction is

$$v_y = -v_q \sin(\omega t - kz), \tag{1.24}$$

where

$$v_q = \frac{eE_0}{m_e \omega}, \tag{1.25}$$

which is known as the quiver velocity. For such an electron executing harmonic motion, its cycle-averaged energy is

$$U_p = \frac{e^2 E_0^2}{4 m_e \omega^2}, \tag{1.26}$$

which is also known as the ponderomotive potential of the laser.

Due to the radial intensity profile in focus, however, the electric field of the laser is far from being a homogeneous plane wave. Assuming a Gaussian intensity distribution, the peak intensity is achieved on the beam axis and a gradient across the field distribution is present. This gradient introduces radially an additional cycle-averaged acceleration of the quivering electrons in the direction of lower intensities. By averaging the dynamics over an oscillation cycle, a ponderomotive force can be identified. Its origin is usually a spatial gradient in laser intensity due to focusing. To derive the strength of the ponderomotive force, assume a plane electromagnetic wave traveling in z-direction with the electric field component in y-direction. The strength of the E-field may vary with y (*e.g.* $E_0(y) = E_{0,max}\exp(-y^2/w^2)$) with a Gaussian width w and a peak electric field strength of $E_{0,max}$.
Hence

$$\mathbf{E}(y,z,t) = E_0(y)\mathbf{e}_y\cos(\omega t - kz), \tag{1.27}$$

where $\mathbf{e}_y$ is the unit vector. The zeroth order motion of an electron under this electric field is simply the oscillation in the y direction, with the average of its velocity remaining constant, the zeroth order force however will cause the electron to explore the gradient of $\mathbf{E}(y)$, which causes the average to drift and accelerate in the y direction,under a combination of electric and Lorentz force. The electrons would also be subjected to a Lorentz force in x direction if E_0 also depends on x, such a force however, is vanishingly small in the non-relativistic regime.

The ponderomotive force can be derived by solving the right hand side of (1.23) with the expressions of $\mathbf{E}(y,z,t)$ and $\mathbf{B}(y,z,t)$ and the zeroth order approximation of v_y (1.24)

$$\mathbf{F}_p = -\frac{e^2}{4m_e\omega^2}\nabla E^2, \tag{1.28}$$

with the term $\cos(2(\omega t - kz))$ omitted, which averages to zero over a cycle.

1.2.4 Relativistic Ponderomotive Force

The aforementioned treatment of ponderomotive force loses its validity for super-intense laser fields. Relativistic nonlinearity in the electron dynamics occurs when the laser pulse used is ultra-short, with its strength satisfying a Gaussian distribution, in a similar way to the non-relativistic case. Differences in the dynamics arise from the relativistic mass increase

at high quiver velocities and a non-vanishing, much stronger B-component in the Lorentz force, which leads to a much larger $\mathbf{v} \times \mathbf{B}$ force in the x-direction when E_0 depends on x. A relativistic generalization of the ponderomotive force has been derived by Bauer *et al.* [30] as well as Quesnel and Mora [31]. It is given by

$$\mathbf{F}_p = -\frac{e^2}{4\gamma m_e \omega^2} \nabla E^2, \tag{1.29}$$

where γ is the local relativistic, cycle-averaged γ-factor in a linearly polarized wave according to

$$\gamma = \sqrt{1 + a_0^2/2}, \tag{1.30}$$

for a laser beam with a normalized amplitude of the vector potential $a_0 = eE_0/(m_e \omega c)$ and an initial transverse momentum $p_\perp = 0$. The relativistic ponderomotive force is responsible for the average electron motion observed in the laboratory frame and can be written as the negative gradient of a relativistic ponderomotive potential, $U_p = (m_e^2 c^4 + c^2 e^2 E^2/\omega^2)^{1/2}$. Quesnel and Mora [31] have shown with the help of 3D-simulations, that in the relativistic case the electrons are pushed isotropically out of focus. Besides a radial acceleration, the electrons are accelerated also in the laser propagation direction due to the magnetic field. Here the electrons, scattered out of the focus, can gain a maximum kinetic energy $E_{kin} = (\gamma - 1)mc^2$, close to the ponderomotive potential of the pulse.

1.2.5 Modelling Electron Cavitation in the Wake of an Ultra-intense Laser Pulse

The ponderomotive force, described in the previous two sections, exerts a slowly-varying force on the electrons, which allows us to model the evolution of the number density n_0 of the plasma electrons.

We start with the electron momentum equation, reformulatedin terms of the field potentials

$$\frac{d\mathbf{p}}{dt} = -e\left(-\frac{\partial \mathbf{A}}{\partial t} - \nabla_\perp \psi + \mathbf{v} \times (\nabla_\perp \times \mathbf{A})\right), \tag{1.31}$$

written using the scalar field potential ψ and vector potential $\mathbf{A}$ instead of field strengths. Given that the pulse duration of the field is much smaller than the plasma period, (1.31)

can be transformed by substituting the following Quasistatic Approximation (QSA) of field potentials:

$$\mathbf{A} = \mathbf{A}_0(z_1, \epsilon x, \epsilon y, \epsilon z) + \epsilon \mathbf{A}_1(z_1, \epsilon x, \epsilon y, \epsilon z), \tag{1.32}$$

$$\psi = \psi_0(z_1, \epsilon x, \epsilon y, \epsilon z) + \epsilon \psi_1(z_1, \epsilon x, \epsilon y, \epsilon z), \tag{1.33}$$

with $z_1 = z - ct$ and $\epsilon \ll 1$, into the Lorenz gauge condition

$$\nabla \cdot \mathbf{A} + \frac{1}{c^2}\frac{\partial \psi}{\partial t} = 0. \tag{1.34}$$

In zeroth order we have

$$\frac{\partial}{\partial z_1}(A_{0z} - \psi_{0z}) = 0 \tag{1.35}$$

which when substituted into (1.31) will produce

$$\frac{\partial p_{0z}}{\partial z_1} = 0, \tag{1.36}$$

and

$$\mathbf{p}_0 = e\mathbf{A}_0, \tag{1.37}$$

where $\mathbf{p}_0$ is the electron momentum in the zeroth order. We now introduce the dimensionless units we will use later in this chapter:

$$\begin{aligned}
&\mathbf{p} \to \mathbf{p}/(m_e c),\\
&\mathbf{A} \to e\mathbf{A}/(m_e c),\\
&\mathbf{E} \to e\mathbf{E}/(m_e c\omega_p),\\
&\mathbf{B} \to e\mathbf{B}/(m_e \omega_p),\\
&\psi \to e\psi/(m_e c^2),\\
&t \to \omega_p t,\\
&\mathbf{r} \to (\omega_p/c)\mathbf{r}\\
&n_0 \to n_0/n_p.
\end{aligned} \tag{1.38}$$

Using (1.34), (1.36), (1.37), the momentum equation (1.31) can be reduced to

$$\begin{aligned} \nabla_\perp \psi &= \mathbf{v} \times (\nabla_\perp \times \mathbf{A}) \\ &= \nabla_\perp \gamma, \end{aligned} \tag{1.39}$$

Substituting this relation into the wave equation of the scalar electromagnetic field potential yields

$$\left(\nabla_\perp^2 - \frac{\partial^2}{\partial t^2}\right) \psi = n_0 - 1, \tag{1.40}$$

where n_0 is the electron number density, n_p is its ambient value, and ϵ_0 being the vacuum permittivity. We obtain the following evolution equation for the number density n_0 [32] under the QSA:

$$n_0 = 1 + \nabla_\perp^2 \gamma. \tag{1.41}$$

With $\gamma = \sqrt{1 + a_0^2/2}$, the distribution of n is entirely determined by the transverse distribution of the laser field strength. For an ultra-short Gaussian laser pulse, electrons are mostly expelled out of the centre of the beam, as shown by simulations in [32–34].

1.2.6 Laser Pulse Propagation in the Homogenous Plasma

Group Velocity Dispersion (GVD)

At frequencies far above its highest resonant frequency, the dielectric function of a dielectric medium takes the simple form of

$$\epsilon(\omega) \approx 1 - \frac{\omega_p^2}{\omega^2}, \tag{1.42}$$

according to [6]. Therefore, the refractive index of the medium is frequency-dependent, $\eta(\omega) = [\epsilon(\omega)]^{1/2} = (1 - \omega_p^2/\omega^2)^{1/2}$. It can be expanded in a Taylor series around the central frequency of the laser:

$$\eta(\omega) = \eta_0 + \left(\frac{d\eta}{d\omega}\right)_{\omega=\omega_0} (\omega - \omega_0) + \frac{1}{2}\left(\frac{d^2\eta}{d\omega^2}\right)_{\omega=\omega_0} (\omega - \omega_0)^2 + ... \tag{1.43}$$

The mode-propagation constant $\beta(\omega) = \eta(\omega)\omega/c$, which determines the variation of the amplitude and phase of a wave mode in the medium can be expanded similarly:

$$\beta(\omega) = \beta_0 + \beta_1(\omega - \omega_0) + \beta_2(\omega - \omega_0)^2/2 + ..., \tag{1.44}$$

with $\beta_1 = \left(\frac{d\beta}{d\omega}\right)_{\omega=\omega_0}$ and $\beta_2 = \left(\frac{d^2\beta}{d\omega^2}\right)_{\omega=\omega_0}$. Substituting the expression for $\eta(\omega)$ we obtain

$$\beta(\omega) = \frac{\omega}{c}\eta(\omega) = \frac{\omega}{c}\left(1 - \frac{\omega_p^2}{\omega^2}\right)^{1/2}. \tag{1.45}$$

Thus,

$$\beta_1 = \frac{1}{c\sqrt{1 - \omega_p^2/\omega_0^2}}, \tag{1.46}$$

$$\beta_2 = \frac{\omega_p^2}{c\omega_0^3(1 - \omega_p^2/\omega_0^2)^{3/2}}. \tag{1.47}$$

Following Agrawal [35], β_1 is the first order dispersion or the reciprocal of the group velocity, while β_2 is related to the group velocity dispersion, which directly contributes to the temporal broadening of the laser pulse; for $\omega_p \ll \omega$ however, such broadening effect is not significant.

Self-focusing of a Laser Beam in Plasma

At high laser intensities, the refractive index of a medium starts to show an intensity-dependence of the form

$$\eta = \eta_0 + \eta_2 I, \tag{1.48}$$

where η_0 and η_2 are linear and nonlinear refractive indexes depending on the medium. For solid-state media, this is the optical Kerr effect. For positive η_2, a laser pulse with highest intensity near the propagation axis will cause a refractive index profile which is also higher near the axis. This implies that the medium will act like a continuous focusing lens, which suppresses diffraction and creates higher and higher peak intensity as the laser pulse propagates. In the case of the optical-Kerr effect, the critical power above which the self-focusing

effect overcomes diffraction is [35]

$$P_{cr} = \alpha \frac{\lambda^2}{4\pi\eta_0\eta_2},$$

with $\alpha \approx 1.8962$ for a Gaussian beam. The critical power for plasma self-focusing is instead [32]

$$P_{cr} = \frac{4\pi\epsilon_0 m_e^2 c^5 \omega^2}{e^2\omega_p^2} \approx 17 \left(\frac{\omega}{\omega_p}\right)^2 \text{GW},$$

where ω and ω_p are the wave and plasma frequencies respectively.

Similarly, self-phase modulation of a laser pulse propagating in plasma can be treated in analogy to self-phase modulation of a laser pulse in a fiber: The refractive index will also vary in time due to the temporal variation of the intensity, which means that different parts of the pulse experience different responses from the medium. The variation in refractive index causes a self-induced phase shift in the pulse, that increases with propagated distance according to

$$\begin{aligned} \phi &= \beta z - \omega_0 t = \frac{\omega_0 \eta(z,t) z}{c} - \omega_0 t \\ &= \frac{\omega_0 \eta_0 z}{c} + \frac{\omega_0 \eta_2 I(z,t) z}{c} - \omega_0 t. \end{aligned} \tag{1.49}$$

The phase ϕ can be divided into a linear part $\phi_L = \omega_0\eta_0 z/c - \omega_0 t$, and an intensity-dependent nonlinear phase shift $\phi = \omega_0\eta_2 I(z,t)z/c$ due to nonlinear refraction. Since the instantaneous frequency of the pulse is given by the time derivative of the phase, it will also show an intensity dependence according to

$$\omega = -\frac{\partial\phi}{\partial t} = \omega_0 - \frac{\omega_0\eta_2}{c}\frac{\partial I}{\partial t} z. \tag{1.50}$$

It is thus clear that new frequency components will be generated as the pulse propagates in the medium. Depending on the sign of $\partial I/\partial t$, the spectrum will be either blue- or red-shifted. For the leading edge of the pulse, $\partial I/\partial t > 0$ and the spectrum correspondingly shifts towards the red. For the trailing edge, $\partial I/\partial t < 0$, the spectrum instead shifts towards the blue. This phenomenon is referred to as self-phase modulation (SPM); it is the temporal counterpart to self-focusing due to the optical Kerr-effect. The spectral broadening due to SPM is associated with an oscillatory structure over the entire frequency range, where the

outermost peaks are the strongest. Due to the generation of new frequencies as the pulse propagates, SPM induces a chirp in the pulse. Unlike GVD the induced chirp is nonlinear, which makes the pulse impossible to compress [35]. If however SPM and GVD act together on equal footing, a spectral broadening will occur simultaneously with a linear chirp, which can be used to compress pulses. If normal dispersion prevails, the pulse stretches more rapidly compared to the situation when only GVD is present. This can be explained by the fact that SPM generates red-shifted frequency components at the leading edge of the pulse and blue-shifted at the trailing edge. Since low frequencies travel faster than high for normal dispersion, the pulse shows an enhanced temporal stretching. Due to the decrease in intensity, the SPM-induced phase shift decreases, according to equation (1.50). If the dispersion is anomalous instead, the pulse initially stretches at a much lower rate than if only GVD were present and eventually reaches a steady state. Since the SPM-induced chirp is positive for the central part of the pulse, while the dispersion-induced chirp is negative, the two contributions will counteract each other, thus limiting the temporal stretching of the pulse, and the broadening of the spectrum.

1.3 Plasma Bubble Wiggler

The ion channel, despite all its advantages as a wiggler, is very difficult to create and maintain; especially when the required length is long. The maintenance of channel symmetry and plasma density uniformity both become great experimental challenges. However, an ion channel is not the only form of plasma cavity that can be used to contain a laser-electron beam resonant interaction. A strongly nonlinear "bubble" regime has been observed in simulations and confirmed by experiments [36]. In this regime, the background electrons are completely evacuated from the first period of the plasma wave excited behind the laser pulse, as shown in Fig 1.3, and an "electron bubble" is formed. The ion density in this bubble is many orders of magnitude higher than those observed in beam-plasma interaction experiments using ionising beams with low density. For example, the ion density in the bubble can be as high as 10^{19} cm^{-3}, which is 10^5 times higher than the highest achievable plasma density using beam-plasma interaction. Therefore the radiated power in the laser-produced channel can be 10^{10} times higher than available with a beam-driven plasma channel using the formula derived in [37]. The bubble moves with the group velocity of the laser pulse, which is close to the speed of light. A relativistic electron bunch injected into the bubble can propagate inside the bubble over a very long distance. Hence, in spite of the small length of

the bubble, the electrons can oscillate in the bubble for a long time, if the acceleration force from the plasma wave excited by the laser pulse can be sufficiently suppressed.

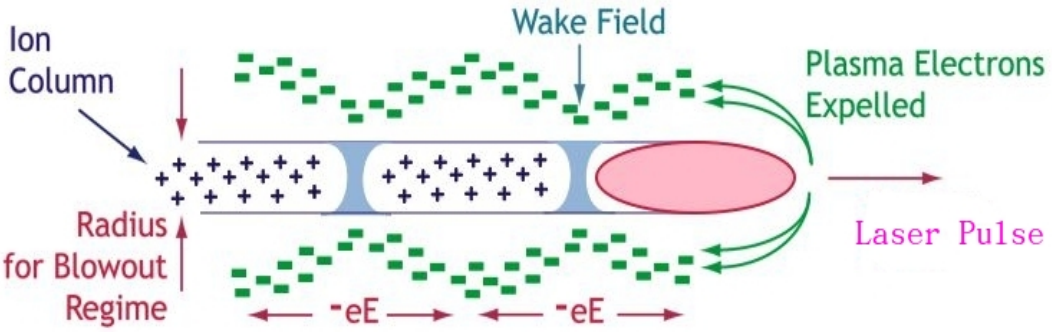

Figure 1.4: Schematic of wakefield bubbles trailing a laser pulse in the blowout regime, from [38]

1.3.1 The Plasma Bubble Structure

We start with Kostyukov's [39] results for fields within an ionic sphere at rest, before moving on to the relativistic cavity moving in plasma. The electromagnetic field of the uniformly charged sphere at rest is purely electrostatic. The electric field and the scalar potential inside the sphere with radius R and with the charge density en_0 are

$$\mathbf{E} = \frac{\mathbf{r}}{3}, \tag{1.51}$$

$$\mathbf{B} = 0, \tag{1.52}$$

$$\phi = 1 + \frac{R^2}{6} - \frac{r^2}{6}, \tag{1.53}$$

where we choose the boundary condition of the potential $\phi(R)$ to be equal to unity at the sphere boundary, and normalize the fields to the units defined in (1.38). r is the distance from the centre of the bubble. If the ionic sphere travels at the relativistic velocity $\beta_g \approx 1$ along the z-axis then the fields inside the sphere are:

$$E_z = 0, \quad E_y = B_x = \frac{y}{2}, \tag{1.54}$$

$$B_z = 0, \quad E_x = -B_y = \frac{x}{2}, \tag{1.55}$$

after neglecting terms proportional to $\gamma_0^{-1} \ll 1$. We now investigate the fields inside a spherical electron cavity moving in plasma. Contrary to the case discussed above, the ions are now immobile in the cavity while the cavity moves at the relativistic velocity $v_0 \approx 1$ along the z-axis. The ion dynamics is neglected because the cavity radius is assumed to be smaller than the ion response length $\approx c/\omega_{pi}$, where $\omega_{pi} = (Ze)^2 n_i/(\epsilon_0 m_i)$ is the ion plasma frequency, with Ze the ion charge and m_i their mass. To calculate the fields we notice that under the similar ultra-relativistic and quasi-static approximation used in 1.2.5 the Lorenz gauge (1.34) admits another solution

$$A_z = \frac{\Phi}{2} = -\phi, \tag{1.56}$$

which can be used to obtain the Maxwell equations for potentials

$$\Delta\Phi = 1 - n_e\left(1 - \frac{p_z}{\gamma}\right) + \left(\frac{\partial}{\partial t} + \frac{\partial}{\partial z}\right)\left[\nabla\cdot\mathbf{A} + \frac{1}{2}\frac{\partial}{\partial t}\left(\frac{\partial}{\partial t} - \frac{\partial}{\partial z}\right)\Phi\right], \tag{1.57}$$

$$\nabla\times(\nabla\times\mathbf{A}) + n_e\frac{\mathbf{p}}{\gamma} + \frac{\partial}{\partial t}\left(\frac{\partial\mathbf{A}}{\partial t} - \frac{\nabla\Phi}{2}\right) = 0. \tag{1.58}$$

Here we use the wake field potential $\Phi = A_z - \phi$ instead of the scalar one, n_e is the electron density, and $\mathbf{p}$ is the electron momentum. Solving the two equations of potentials with spherical symmetry we get

$$\Phi = 1 - \frac{R^2}{4} + \frac{r^2}{4}. \tag{1.59}$$

The Lorentz force acting on a relativistic electron with $\beta_z = 1$ inside the cavity is thus

$$F_z = -\frac{\partial\Phi}{\partial\xi} = -E_z = \frac{\xi}{2}, \tag{1.60}$$

$$F_y = -\frac{\partial\Phi}{\partial y} = -E_y - B_x = -\frac{y}{2}, \tag{1.61}$$

$$F_x = -\frac{\partial\Phi}{\partial x} = -E_x + B_y = -\frac{x}{2}. \tag{1.62}$$

Note that the x-component is not needed assuming that the electron remains in the y-z-plane. The wake potential Φ can be considered as the potential of the Lorentz force on electrons with $v_z = 1$. The Lorentz force approaches its peak as the velocity of an electron approaches $v_z = v_0 \approx 1$ while it approaches zero the electron with speed close to $v_z = -1$ because of the relativistic compensation of the electrostatic force by the self-magnetic force. Notice that this effect is opposite to that of the relativistically moving ionic sphere. This is because the displacement current in the cavity is opposite to the ion current in the relativistically moving ion sphere.

Let us now consider now an electron moving in the bubble field, with trajectory $\mathbf{r}(t)$. If at some point $d\xi/dt = 0$, with $\xi(t) = z(t) - v_0 t$, i.e., $v_z = v_0$, the electron can be "trapped" within the bubble as it moves at the same velocity as the cavity base. If ξ remains slowly varying, the electron Hamiltonian can be separated into a sum of parts corresponding to transverse and longitudinal motion,

$$H = \gamma_{\parallel} + h_{\perp} + \frac{\xi^2}{4}. \tag{1.63}$$

Where $\gamma_{\parallel} \approx p_z$ represents the kinetic energy corresponding to longtudinal motion, and $h_{\perp} \approx R_{\beta}^2/4$ corresponds to the haromic motion in the transverse direction, with R_{β} being the amplitude of the oscillation. The conservation of $h_{\perp}$ under the zeroth-order approximation to $\mathbf{A}$ allows us to apply the analysis of the resonant electron-radiation interaction in the ion channel, which will be developed in Chapter 2, to electrons in the plasma bubble as well.

1.3.2 Resonance-Enhanced Betatron Oscillation in the Ion Channel

If the electron beam co-propagates in the plasma channel or the moving bubble cavity with a high-power laser beam, for which $eA_y \gg cp_y$, where p_y is the (average) transverse electron momentum, and $\partial A_y/\partial t$ is non-negligible (the large-signal condition), and if furthermore the betatron phases of the transverse electron oscillations match the phase of the laser field, the betatron amplitude experiences a large growth [40–42]. This phenomenon gives rise to a large-betatron amplitude oscillation of the electron beam, whose theoretical potential as a source of coherent radiation will be explored in the following chapter. This can be described by a similar theoretical model to the more rigorous one developed in Chapter 2. We use the so-called 'transverse energy' term $h_{\perp}$ defined in (1.63) for the ion channel Hamiltonian, which expresses the maximum kinetic energy of the electron undergoing betatron oscillation.

It is easy to see that, in non-normalized units,

$$h_\perp \approx \frac{m\omega_p^2 R_\beta^2}{4}, \tag{1.64}$$

where R_β is the unnormalised amplitude of the betatron oscillation. Since the extremities of oscillation, where the transverse kinetic energy is fully converted to the harmonic potential, are the points where $y = R_\beta$, the maximum of the harmonic potential energy can not exceed $m\omega_p^2 R_\beta^2/4$. We can then further express the Hamiltonian of an electron interacting with a linearly polarized laser field in an ion channel, while oscillating in the y-z plane (a choice made for simplicity's sake, as a 3D model would be similar), which is

$$H = \sqrt{m^2c^4 + (cp_z - eA_z)^2 + (cp_y - eA_y)^2} + \frac{m\omega_p^2 y^2}{4}, \tag{1.65}$$

in the form of longitudinal and transverse energy, namely $H = cp_z + mc^2/(\gamma_\parallel + p_z/mc) + h_\perp$. The variation equation for the transverse energy can then be written as

$$\frac{dh_\perp}{dt} = v_y \left(\frac{\partial}{\partial t} + c\frac{\partial}{\partial z} \right) A_y. \tag{1.66}$$

When the electron is in resonance with a laser field with large field amplitude, the electrons start to absorb energy from the laser field and their R_β values no longer remain constant. If the vector potential is so large that the loss of laser energy is negligible with respect to A_y but not $h_\perp$, it satisfies the wave equation in its free-space form

$$\frac{\partial^2 A_y}{\partial z^2} - \frac{\partial^2 A_y}{c^2 \partial t^2} = 0, \tag{1.67}$$

which has a solution in the form

$$A_y = A_+(z - ct) + A_-(z + ct), \tag{1.68}$$

where A_+ and A_- are arbitrary functions. As the electron beam moves in the $+z$ direction, the resonant interaction only takes place between the beam and a radiation field moving in the same direction, i.e., fields of the form $A_+(z - ct)$. Assuming the laser pulse has a Gaussian shape and central wave number k, the expression for $A_y(z,t)$ will be $A_y(z,t) = a_0 \cos(k(z - ct))$, with $a_0 = A_0 \exp[-(z - z_c)^2/\Delta z_L^2]$ where A_0 is the maximum vector potential amplitude, Δz_L is the pulse length, and $z_c = R + v_g t$, where in turn v_g is the group velocity

of the pulse and R is the position of the centre of the bubble at $t = 0$. Substituting this expression into Eq. (1.66) we obtain:

$$\frac{dh_\perp}{dt} = 2mcv_y(c - v_g)\frac{(z - v_g t - R)A_0 \exp[-(z - z_c)^2/\Delta z_L^2]\cos(k(z - ct))}{\Delta z_L^2}. \tag{1.69}$$

Recalling that in the wave equation, v_y is just the transverse current velocity term driving the generation/absorption of the wave field, Eq. (1.66) can be transformed into the following equation:

$$\left\langle \frac{dh_\perp}{dt} \right\rangle = \frac{2mc^2}{\omega_b^2}\left[\left(\frac{\partial^2}{\partial z^2} - \frac{\partial^2}{c^2\partial t^2}\right)a_1\cos(k(z - ct))\right]\left(\frac{\partial}{\partial z} + \frac{\partial}{c\partial t}\right)a_0\cos(k(z - ct)), \tag{1.70}$$

where the angle brackets denoting the averaging over the whole ensemble of electrons, ω_b is the plasma frequency of the electron beam, and a_1 is the normalized amplitude of the wave field generated by the collective movement of the electrons. Assuming $a_0 \gg a_1$, applying the slowly varying envelope and amplitude assumptions [43]:

$$\left|\frac{\partial a_1(z,t)}{\partial z}\right| \ll k|a_1(z,t)|, \tag{1.71}$$

$$\left|\frac{\partial a_1(z,t)}{\partial t}\right| \ll \omega|a_1(z,t)|, \tag{1.72}$$

which we will return to in Chapter 2, equation (1.70) can be further simplified to contain only total time derivatives $d/dt \approx \partial/\partial t + c\partial/\partial z$:

$$\left\langle \frac{dh_\perp}{dt} \right\rangle = \frac{2\omega mc^2}{\omega_b^2}\left(\frac{da_1}{dt}e^{-i(k(z-ct))} + c.c.\right)\frac{da_0}{dt}\cos(k(z - ct)). \tag{1.73}$$

After integrating both sides, and eliminating the oscillating $\cos(2(k(z-ct))$ term, the slowly varying envelope approximation is applied once again to eliminate terms proportional to d^2a_1/dt^2

$$\begin{aligned}\langle h_\perp\rangle &\approx h_0 + \frac{2\omega mc^2}{\omega_b^2}a_1' a_0 + c.c. \\ &\approx h_0 + \langle v_\beta a_0 \exp(-i\psi)\rangle,\end{aligned} \tag{1.74}$$

where $v_y = v_\beta \cos(\omega_\beta t)$ has been assumed. Eq. (1.74) demonstrates that within a co-propagating Gaussian pulse, the electrons with betatron oscillation frequencies equal to (i.e. in resonance with) the frequency of the laser field will be driven to oscillate at an amplitude that depends on the magnitude of the laser vector potential. High-frequency radiation from such highly resonant betatron oscillations has been observed by, e.g., Cipiccia *et al.*, [40], both in experiment and simulation. The following OSIRIS [44] simulation results showing the resonant growth of the betatron amplitudes of a monoenergetic ultrashort electron pulse in the strongly damped, weakly and strongly resonant regimes are reproduced from Ref. [40]:

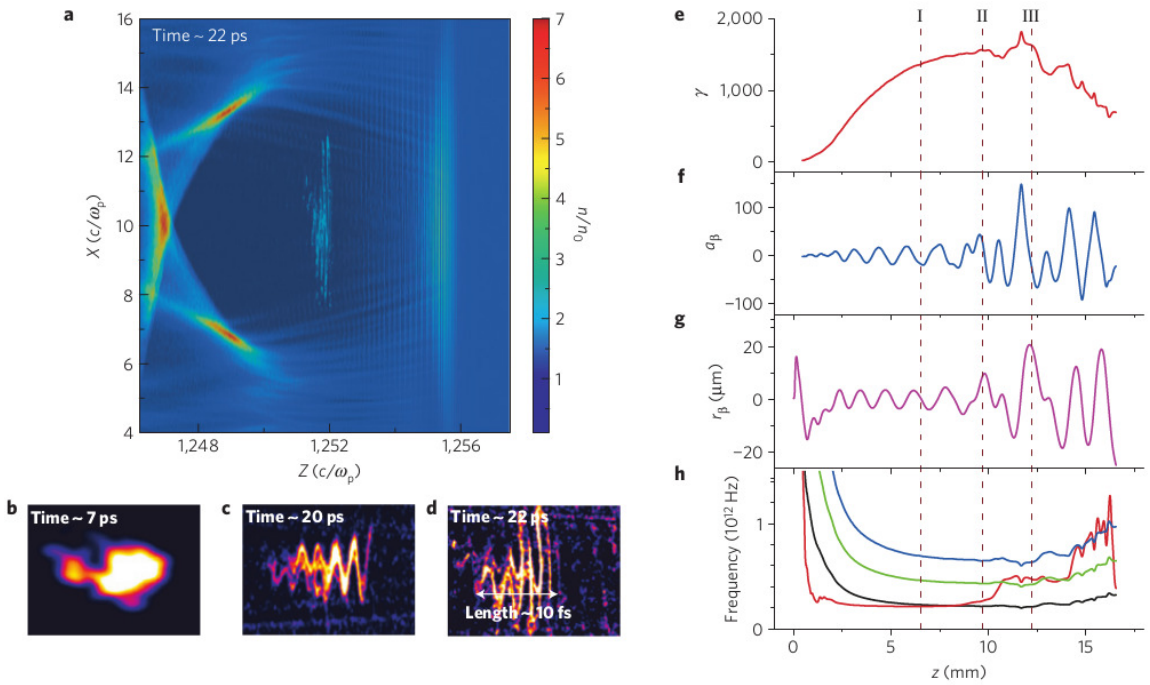

Figure 1.5: (a). Snapshot of the electron distribution from Cipiccia *et al.*, [40]. (b)-(d), Electron beam trajectories for the strongly damped (b), weakly resonant (c) and strongly resonant (d) case.(e)-(h), The evolutions, for a selected trajectory, are shown of γ (e), $a_\beta = \gamma.r_\beta$, (f), r_β (g), and the first (black line), second (green line) and third harmonics (blue line) of ω_β, and ω, the Doppler-shifted laser frequency as seen by the electrons (red line) (h). The three vertical dashed lines indicate the three different regimes that can occur with almost the same γ. Parameters used in simulation: $n_e = 1.8 \cdot 10^{18}\text{cm}^{-3}$ λ= 800 nm, laser spot size 35 μm, laser pulse duration 70 fs and initially $a_0 = 3$. The normalized transverse momentum varies from $a_\beta = 5.6$ for $r_\beta = 1\,\mu$m to $a_\beta = 150$ for $r_\beta = 20\,\mu$m, at $\gamma = 1,600$.

Chapter 2

Electron Motion in an Ion Channel

2.1 Electron Dynamics and Particle Equations

In this section, the single-electron dynamics for small initial radiation field in an ion channel will be investigated using the Hamiltonian-separating method. In this method, the relativistic Hamiltonian is separated into parts corresponding to electron motion in the longitudinal and the transverse direction, respectively, and equations of motion are obtained for each. We first consider the small-signal model of a single electron interacting with a co-propagating monochromatic wave along the z-axis in an ion channel. We restrict ourselves to slab geometry with electrons oscillating only in the $y-z$ plane, which, we will show later, is a good approximation to electrons in a 3D model, where the harmonic potential depends on both the x and y coordinates. The ion channel is assumed to be perfectly ionized and void of free electrons, with a radius much larger than the laser beam radius, so that there is no waveguiding and the phase velocity of light is equal to that in the vacuum. The initial transverse momentum of the electron at its injection point, p_{y0}, is considered to be negligibly small in comparison to the transverse momentum generated by the channel electric field, so that the electron is pulled towards the channel axis immediately at the injection point. We write down the Hamiltonian for such a model as given by [1]:

$$H = \sqrt{m^2c^4 + c^2p_z^2 + (cp_y - eA)^2} + \frac{m\omega_p^2 y^2}{4}, \tag{2.1}$$

where A is the transverse vector potential of the laser field, p_y and p_z are the canonical momenta along the y and z axis, respectively. Furthermore, $\omega_p = \sqrt{n_p e^2/(m_e\epsilon_0)}$ is the

plasma frequency, with $n_p = Zn_i$ the electron density that would neutralize the ions, where Ze is the ion charge and n_i is their number density in the ion channel. Unlike in [45], the time variable t, rather than z, is chosen to be independent, largely because the ion channel beam electrons do not oscillate in a spatially periodic field as in a FEL wiggler. Instead, the field strength the electron experiences is entirely dependent on its distance from the axis, i.e., its y coordinate, which is in turn dependent on its initial position and the time variable, but independent of z.

We derive the equations of motion using the following units normalized to ω_p, wave number $k_p = \omega_p/c$, and wavelength $\lambda_p = 2\pi/k_p$, in SI units

$$\begin{aligned}
&y, z \to k_p y, k_p z,\\
&v_y, v_z \to v_y/c, v_z/c,\\
&p_y, p_z \to p_y/mc, p_z/mc\\
&A \to eA/mc,\\
&\Phi \to e\Phi/mc^2,\\
&t \to \omega_p t,\\
&k, \omega \to k/k_p, \omega/\omega_p.
\end{aligned} \tag{2.2}$$

Following this normalization, the Hamiltonian can be expressed as

$$H = \sqrt{1 + p_z^2 + (p_y - A)^2} + \frac{y^2}{4}. \tag{2.3}$$

Separating the Hamiltonian into two parts representing the kinetic energy and the electrostatic potential energy, respectively, we obtain

$$H = \gamma + \frac{y^2}{4}, \quad \gamma = \sqrt{1 + p_z^2 + (p_y - A)^2}. \tag{2.4}$$

If the maximum excursion of the electron from the channel axis (known as the betatron amplitude of the electron) is much smaller than the ion channel radius and the width of the radiation pulse, the transverse variation of the laser field can be neglected. The vector potential can be expressed as $A = A_0 \sin(kz - \omega t + \phi)$, where A_0 and ϕ are considered to vary on a length scale much longer than the radiation wavelength, and can thus be treated as

constant on this scale. The equations of motion can thus be obtained from the Hamiltonian,

$$y' = \frac{p_y - A}{\gamma}, \tag{2.5}$$

$$z' = \frac{p_z}{\gamma}, \tag{2.6}$$

$$p_y' = -\frac{y}{2}, \tag{2.7}$$

$$p_z' = \frac{p_y - A}{\gamma} k A_0 \cos(kz - \omega t + \phi), \tag{2.8}$$

where the prime denotes the time derivative. All the wave and particle equations can be transformed into a "harmonic oscillator" form, where the variables corresponding to slow bunching motion and rapid betatron oscillation can be separated. Using the relation $\frac{dH}{dt} = \frac{\partial H}{\partial t} = \frac{\omega}{k}\frac{dp_z}{dt} = \frac{dp_z}{dt}$, assuming that $\omega = k$ in the last step, we obtain the following constant of motion:

$$a^2 \equiv H - p_z = const. \tag{2.9}$$

Explicitly,

$$a^2 = \gamma - p_z + \frac{y^2}{4} = \frac{\gamma^2 - p_z^2}{\gamma + p_z} + \frac{y^2}{4}. \tag{2.10}$$

Substituting $\gamma^2 - p_z^2 = 1 + (p_y - A)^2$ into the last equation, we obtain the transformed Hamiltonian:

$$H = p_z + \frac{1 + (p_y - A)^2}{\gamma + p_z} + \frac{y^2}{4}. \tag{2.11}$$

For $p_z \gg 1$, the term $\frac{1}{\gamma + p_z}$ will remain nearly constant throughout the interaction time; therefore, we can define the betatron amplitude r_β in terms of a new constant of motion, the "transverse energy" term $\frac{r_\beta^2}{4} = a^2 - \frac{1}{\gamma + p_z} \approx a^2 - \frac{1}{\gamma_0 + p_{z_0}}$, and further express y and the transverse velocity v_y in terms of r_β and the betatron oscillation phase θ

$$y = r_\beta \sin(\theta), \tag{2.12}$$

$$v_y = r_\beta \theta' \cos(\theta). \tag{2.13}$$

Combining (2.5) with (2.13), we can derive the betatron frequency ω_β, which is the first order derivative of the betatron phase,

$$\omega_\beta \equiv \theta' = \frac{\sqrt{\gamma + p_z}}{2\gamma}. \tag{2.14}$$

The laser frequency as experienced by the electron (due to its axial velocity) is

$$\omega - kv_z = \omega \frac{\gamma - p_z}{\gamma} = \omega \left(\frac{1}{2\gamma^2} + \frac{r_\beta^2 \cos^2(\theta)}{8\gamma} \right). \tag{2.15}$$

In the unscaled form, the frequency expressions are:

$$\omega_\beta = \omega_p \frac{\sqrt{\gamma + p_z}}{2\gamma}, \tag{2.16}$$

$$\tag{2.17}$$

$$\omega - kv_z = \omega \left(\frac{1}{2\gamma^2} + \frac{\omega_p^2 r_\beta^2 \cos^2(\theta)}{8\gamma} \right). \tag{2.18}$$

The $\cos^2(\theta)$ term gives rise to higher-order harmonics and a reduced coupling between the electron beam and the fundamental harmonic. This coupling factor approaches its lowest value, 0.7, when $\gamma r_\beta \gg 1$ [46]. As the effective change in the amplitude of the field is less than 30%, we will assume $r_\beta^2 \approx r_\beta^2 \cos^2(\theta)/2$. in this chapter, and return to the discussion of high harmonics and formally define the coupling factor in Chapter 4. The betatron amplitude r_β, on the other hand, remains constant during the entire interaction with the laser field as long as the variation in the envelope of field vector potential is much smaller than the oscillation in amplitude within one betatron period, as will be elaborated later in this chapter.

2.1.1 The Resonance Condition

Efficient energy exchange between radiation field and the bunched electrons in the ICL, as in the FEL, can only occur if the electrons are "in resonance" with the radiation field. That is, the phase difference between the electron oscillation and the radiation field oscillation, defined as

$$\psi = \theta + kz - \omega t, \tag{2.19}$$

must vary on a time scale much longer than the betatron oscillation period.

There are two ways of defining the electron oscillation phase. Both involve separation of the rapidly varying from the slowly varying components of the electron motion. In Whittum's original work, the phase is defined by expressing the transverse momentum in an eikonal form $p_y = q_y \sin(\theta_y)$, where θ_y is the rapidly varying phase. In this thesis, however, we define the rapidly varying term as the betatron oscillation phase of the position variable y, and the slowly varying term as the betatron amplitude r_β. We favour this approach for a number of reasons:

1. The definitions are simple and easily understandable, and capable of describing the rapid evolution of both y and v_y.

2. The formal expression of the betatron phase is similar to the FEL synchrotron oscillation phase $k_w z$.

3. The eikonal formulation will introduce a slowly varying term proportional to the ponderomotive phase into the phase variation equation, significantly complicating the analysis.

The differential equation for the slowly varying phase is obtained simply by differentiating the RHS of (2.19), using the definitions (2.17), (2.18)

$$\psi' \approx \omega_\beta - \omega \left(\frac{1}{2\gamma^2} + \frac{\omega_p^2 r_\beta^2}{8\gamma c^2} \right). \tag{2.20}$$

The electrons are then said to be in resonance with the radiation field, when their betatron frequencies are equal to the wave frequency, i.e., $\psi' = 0$, which leads to the following equation:

$$\frac{1}{\gamma^{3/2}} + \frac{\omega_p^2 r_\beta^2}{4\gamma^{1/2} c^2} = \sqrt{2}\, \frac{\omega_p}{\omega}. \tag{2.21}$$

We can thus define the γ value satisfying this resonance condition as γ_r, which is important for establishing the energy of the electron bunch to be used for generating radiation of a particular wavelength.

2.1.2 Generalization to 3D theory

Although the relation (2.21), and the ICL theory that follows from it, have been derived using slab geometry, they can be extended to model electrons in 3D, when the laser wave

electric field is linearly polarised in the y direction, by simply redefining r_β^2 as

$$r_\beta^2 = 4\left(\frac{p_x^2 + (p_y - A)^2}{\gamma + p_z} + \frac{x^2}{4} + \frac{y^2}{4}\right). \tag{2.22}$$

It can then be checked that the constancy of r_β^2 is preserved as the relation $r_\beta^2/4 \approx H - p_z - 1/(\gamma_0 + p_{z_0})$ still holds regardless of which definition of r_β^2 is used, whereas the ponderomotive phase of each electron will see a constant phase factor dependent on the direction of electron oscillation added to it. The formulation of ICL theory can therefore be directly applied to a 3D model.

2.2 High-Gain Steady-State Theory of the ICL

2.2.1 Introduction

In the previous section, we showed that for slowly-varying field envelope, the betatron amplitude of an oscillating electron in an ion channel is not influenced by the energy exchange between electron and the radiation field. Therefore, the initial betatron amplitude $r_{\beta,0}$ can be solely defined by the electron's initial transverse position y_0 at injection into the channel, and its initial phase θ_0, through the relation

$$y_0 = r_{\beta,0}\cos(\theta_0). \tag{2.23}$$

If the electron is injected parallel to the channel axis, we have $\theta_0 = 0$ and $y_0 = r_\beta$, i.e., the maximum excursion of the electron from the axis is just its initial y value.

So far, we have considered a single electron. When referring to one of the electrons (the jth) in a bunch or beam, we shall denote the corresponding electron variables by an additional subscript j.

The method of injection used has a significant influence on the amplification. In the ICL theory proposed by Whittum [1], a round beam with a finite betatron amplitude spread centered on axis is proposed, as shown in Fig. 2.1. This assumption restricts the mean betatron amplitude to be $r_b/\sqrt{2}$, where r_b is the beam radius. Additionally, in this case the value of r_b must be much smaller than $2/\sqrt{\gamma}$, otherwise the spread, which depends on r_β, will grow so large that it prevents amplification from taking place. In this section, we investigate a new form of injection: off-axis injection of an electron beam displaced from the channel axis by a distance larger than the beam radius. For an ion channel with a channel

radius defined as r_a, and $r_a \gg r_b$, it is possible to adjust the mean betatron amplitude of an electron bunch, R_β, to give a large initial mean transverse displacement from the axis that is independent of the beam radius and also the betatron amplitude spread, with $R_\beta \gg r_b$. The mean initial betatron phases of the electrons θ_{β_0} will thus be non-zero, which suggests that injecting electrons on-axis at an angle may lead to similar results. An electron bunch with a large initial r_β and a narrow betatron phase distribution could possibly be produced experimentally by harmonically driving them with a high-power laser during their acceleration phase in the wakefield accelerator, as described in Chapter 1 and shown in Figure 1.5.

Compared with on-axis injection described in Whittum's paper [2], off-axis injection has a number of advantages, including allowing adjustment of the betatron amplitude independently from the beam radius, which enables the use of a much larger wiggler parameter value a_β than feasible for a traditional FEL. ($a_\beta = r_\beta \omega_p \sqrt{\gamma/2}$, as described in Whittum's work, is analogous to the FEL wiggler parameter a_w.) A high a_β value will also improve amplifier efficiency, in addition to reducing the requirement for a small intrinsic energy and betatron amplitude spread. The disadvantage of off-axis injection is that it makes coherent amplification of high-frequency electromagnetic radiation, especially in the X-ray regime, theoretically very difficult to achieve without using a very high energy beam, which can be partly compensated for by amplification using high-harmonic production, a topic of discussion in Chapter 3. In reality, however, the production of an electron beam with sufficiently small mean betatron amplitude is so difficult that using off-axis injection maybe the only realistic option for building an ICL to generate high-frequency radiation.

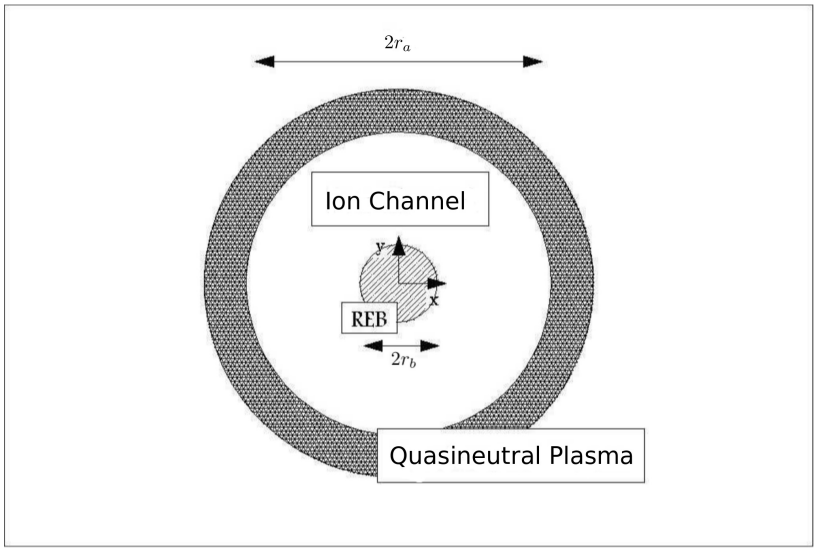

Figure 2.1: On-axis injection using a round beam with a step radial profile with beam radius r_b in an ion channel with radius r_a, surrounded by quasi-neutral plasma.

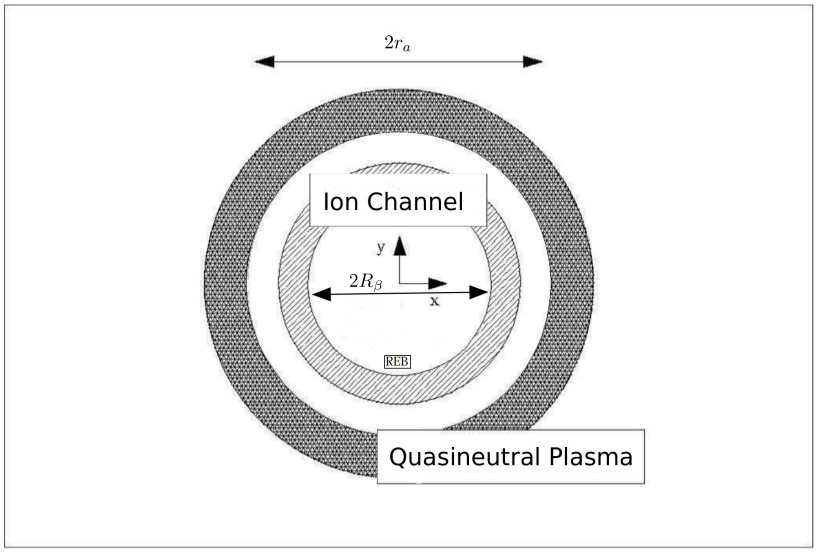

Figure 2.2: Scehmatic plot of the cross section of an ion channel when a ring-shaped beam with $\sigma(r_\beta) \ll R_\beta$ and uniform θ_x and θ_y, is injected off-axis.

A ring-shaped injection beam as shown in the Figure 2.2 would be very difficult to realize experimentally. However, injection of a small segment of the ring, as shown in Fig. 2.3 is sufficient. The motion of electrons injected in such a manner can also be adequately modeled using slab geometry if, for a co-propagating wave with linear polarization along y, say, the

initial excursion and momentum in x direction are negligible. The equations of motion can then be formulated without the x coordinate.

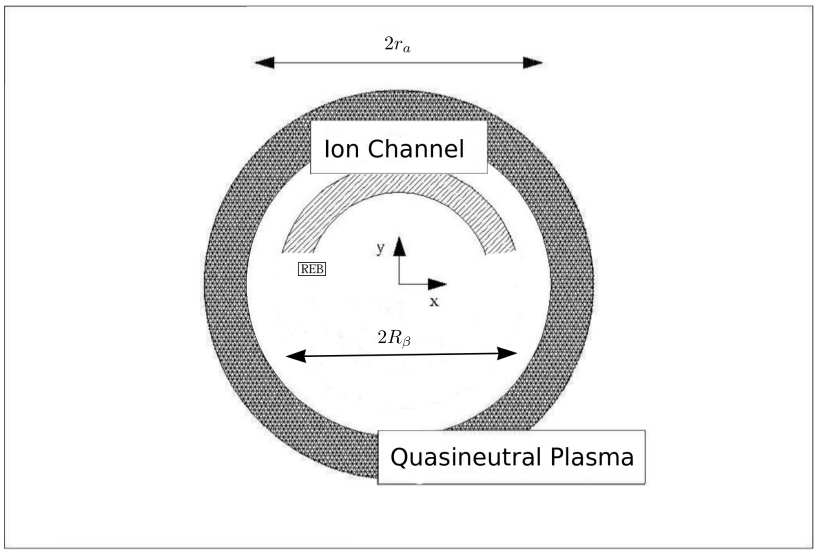

Figure 2.3: Off-axis injection at the channel entrance using a segment-shaped rather than a ring-shaped beam with $\sigma(r_\beta) \ll R_\beta$.

2.2.2 The Wave Equation

The following unscaled inhomogeneous wave equation for the vector potential A_y of the laser field can be deduced from from the Maxwell equations

$$\left(\nabla_\perp^2 + \frac{\partial^2}{\partial z^2} - \frac{1}{c^2}\frac{\partial^2}{\partial t^2}\right) A_y = -\mu_0 J_y, \tag{2.24}$$

where μ_0 is the vacuum permeability and J_y the transverse current density. The latter can be expressed in terms of delta functions representing individual electrons (Klimontovich distribution) as

$$J_y(\vec{r},t) = \sum_j J_{y,j}(\vec{r},t), \text{ with } J_{y,j}(\vec{r},t) = -ev_{y,j}(t)\delta(\vec{r} - \vec{r}_j(t)), \tag{2.25}$$

where $\vec{r}_j(t)$ is the trajectory of the j-th electron and $v_{y,j}$ is the y-component of its velocity. The Coulomb gauge, which removes the dependence of the vector potential on the longitudinal current, is chosen so that the Hamiltonian in (2.3), which does not depend on A_z, can be used in this analysis.

The y-dependence of the single-electron current density $J_{y,j}(\vec{r},t) = -e\, g_j(y,t)\, \delta(x - x_j(t))\, \delta(z - z_j(t))$ is given by

$$g_j(y,t) = v_{y,j}(t)\delta(y - y_j(t)), \text{ where } y_j(t) = r_{\beta,j} \sin\theta_j \text{ and thus } v_{y,j}(t) = \omega_{\beta,j}\, r_{\beta,j}\, \cos\theta_j, \tag{2.26}$$

with θ_j being the betatron phase of the electron and $\omega_{\beta,j} = \omega_p\sqrt{\gamma_j + p_{z,j}}/(2\gamma_j)$. This can be expanded in a Fourier series

$$\begin{aligned} g_j(y,t) &= \sum_{m=0}^{\infty} g_{m,j} \cos(m\theta_j) + \sum_{m=1}^{\infty} h_{m,j} \sin(m\theta_j) \\ &= \sum_{m=0}^{\infty} g_{m,j} \mathrm{T}_m(\cos(\theta_j)) + \sum_{m=1}^{\infty} h_{m,j} \mathrm{U}_{m-1}(\cos(\theta_j))\hat{y}_j, \end{aligned} \tag{2.27}$$

where $\hat{y}_j = y_j/r_{\beta,j}$, $\mathrm{T}_m(\cos(\theta_j)) = \cos(m\theta_j)$ and $\mathrm{U}_m(\cos(\theta_j)) = \sin((m+1)\theta_j)/\sin(\theta_j)$ are Chebyshev polynomials of the first and second kind, respectively. The coefficients $g_{m,j}$ and $h_{m,j}$ can therefore be evaluated by projecting the current density onto the Fourier series:

$$\begin{aligned} g_{m,j} &= \int_{-\pi/2}^{3\pi/2} d\theta_j \cos(m\theta_j)\omega_{\beta,j} r_{\beta,j} \cos(\theta_j)\delta(y - y_j) \\ &= \frac{\omega_{\beta,j} r_{\beta,j}}{\pi}\Big(\int_{-1}^{1} d\hat{y}_j\, \mathrm{T}_m(\sqrt{1-\hat{y}_j^2})\delta(\hat{y} - \hat{y}_j) + \int_{1}^{-1} d\hat{y}_j\, \mathrm{T}_m(-\sqrt{1-\hat{y}_j^2})\delta(\hat{y} - \hat{y}_j)\Big), \\ h_{m,j} &= \int_{-\pi/2}^{3\pi/2} d\theta_j \sin(m\theta_j)\omega_{\beta,j} r_{\beta,j} \cos(\theta_j)\delta(y - y_j) \\ &= \frac{\omega_{\beta,j} r_{\beta,j}}{\pi}\Big(\int_{-1}^{1} d\hat{y}_j\, \mathrm{U}_{m-1}(\sqrt{1-\hat{y}_j^2})\hat{y}\delta(\hat{y} - \hat{y}_j) + \int_{-1}^{1} d\hat{y}_j\, \mathrm{U}_{m-1}(-\sqrt{1-\hat{y}_j^2})\hat{y}\delta(\hat{y} - \hat{y}_j)\ \Big). \end{aligned} \tag{2.28}$$

Using the relation $\delta(\hat{y} - \hat{y}_j) = \delta(\hat{y}_j - \hat{y})$, and $\sqrt{1-\hat{y}^2} = \cos(\theta)$the entire series expansion of $g_j(y,t)$ is obtained:

$$g_j(y,t) = \frac{\omega_{\beta,j} r_{\beta,j}}{\pi}\big((T_1(\cos(\theta)) - T_1(-\cos(\theta)))\cos(\theta_j) + (U_0(\cos(\theta)) - U_0(-\cos(\theta)))\hat{y}\sin(\theta_j) + ...\big) \tag{2.29}$$

Applying the symmetry properties of the Chebyshev polynomials to the expansion we have

$$g_j(y,t) = \frac{2\omega_{\beta,j} r_{\beta,j}}{\pi}(\cos(\theta)\cos(\theta_j) + \sin(2\theta)\sin(2\theta_j) + ...). \tag{2.30}$$

The expression (2.30) shows that the fundamental Fourier term of the current density of each electron is a smooth function of $\hat{y} = \cos(\theta)$ with effective size comparable to the betatron amplitude, and the strongest feedback occuring at the axis of the ion channel, which decreases linearly towards the extremities of the betatron oscillation. For 2-D geometry to be applicable, the bunch width in the perpendicular (x) direction should be small compared to the betatron amplitude.

The source size determines how strongly the emitted radiation diffracts. We postpone the discussion of diffraction and assume for the moment that it can be neglected. This leads to the wave equation in one dimension (1-D)

$$\left(\frac{\partial^2}{\partial z^2} - \frac{1}{c^2}\frac{\partial^2}{\partial t^2}\right) A_y = -\mu_0 J_y. \tag{2.31}$$

As in FEL theory, coherent radiation emission is a collective process involving electrons that initially oscillate at different phases, with the radiation field acting as a medium for transmitting information between the electrons, creating a feedback loop that amplifies the initial radiation field. Therefore, a model using collective variables is more suitable for describing this process. The main difference from the FEL, however, is that the transverse velocity of each electron is determined by its own betatron amplitude and phase through the relation (2.26) Therefore the wave equation can be written as

$$\left(\frac{\partial^2}{\partial z^2} - \frac{1}{c^2}\frac{\partial^2}{\partial t^2}\right) A_y = \mu_0 e n_x \sum_j g_j(y,t)\delta(z - z_j(t)), \tag{2.32}$$

where $n_x = N_e \Pi(2x/\Delta_x)/\Delta_x$ represents the electron number density in the $y-z$ plane after the average over a top hat distribution $\Pi(2x/\Delta_x)$ in the x direction, with Δx being the effective width of the distribution.

2.2.3 The Slowly-Varying Envelope Approximation

The wave equation Eq.(2.31) can be expressed in complex exponential form by introducing the complex vector potential amplitude A_r defined by

$$A_y = -iA_r \exp[ik(z-ct)+i\phi]/2 + c.c., \tag{2.33}$$

where *c.c.* denotes the complex conjugate of the preceding term. We substitute this expression into the wave equation (2.32) (using $\omega = ck$)

$$\frac{1}{2}\left[-i\left(\frac{\partial^2 a_r}{\partial z^2}-\frac{\partial^2 a_r}{c^2\partial t^2}\right)+2k\left(\frac{\partial a_r}{\partial z}+\frac{\partial a_r}{c\partial t}\right)\right]e^{i(kz-\omega t)}+c.c. = \mu_0 e n_x \sum_j g_j(y,t)\delta(z-z_j(t)), \tag{2.34}$$

The collective complex amplitude $a_r = A_r e^{i\phi}$ of the radiation wave varies on the scale of the interaction length, which is usually much larger than the radiation wavelength. For the steady-state propagation model, this condition is always satisfied. The wave equation can thus be simplified using the following relations, called the Slowly Varying Envelope Approximation(SVEA):

$$\left|\frac{\partial a_r(z,t)}{\partial z}\right| \ll k|a_r(z,t)|, \tag{2.35}$$

$$\left|\frac{\partial a_r(z,t)}{\partial t}\right| \ll \omega|a_r(z,t)|. \tag{2.36}$$

Now the wave equation can be reduced to the following form, with second order derivatives of A_r neglected

$$\frac{1}{2}\left[\left(\frac{\partial}{\partial z}+\frac{1}{c}\frac{\partial}{\partial t}\right)a_r\right]e^{i(kz-\omega t)}+c.c. = \frac{\mu_0 e n_x}{2k}\sum_j g_j(y,t)\delta(z-z_j(t)). \tag{2.37}$$

If we multiply both sides of the equation by $e^{-i(kz-\omega t)}$, terms varying on the scale of the radiation wavelength can be further removed from both sides of the equation, as can be found from (2.30), only the term oscillating at the fundamental betatron frequency will remain after integrating both sides of the resulting equation over the domain occupied by

the electron bunch in the phase space $\chi_{[a,b;-R_\beta,R_\beta]}$ with $a < z < b$ and $-R_\beta < y < R_\beta$,

$$\begin{aligned}\left(\frac{\partial}{\partial z}+\frac{1}{c}\frac{\partial}{\partial t}\right)a_r &= \frac{\mu_0 e n_x}{kN_e}\sum_j \int_{-R_\beta}^{R_\beta} dy \int_b^a dz\; v_{y,j}(t)\exp[-i(kz-\omega t)]\delta(y-y_j(t))\delta(z-z_j(t)) \\ &= \frac{\mu_0 e n_x}{kN_e}\sum_j \int_{-1}^{1} d\hat{y}\omega_{\beta,j} r_{\beta,j}\sqrt{1-\hat{y}^2}\delta(\hat{y}-\hat{y}_j)\exp[-i(kz_j-\omega t)] \\ &= \frac{\mu_0 e n_x}{2kN_e}\sum_j \omega_{\beta,j} r_{\beta,j}\exp[-i(\theta_j+kz_J-\omega t)] + \omega_{\beta,j} r_{\beta,j}\exp[i(\theta_j-kz_j+\omega t)]\end{aligned} \tag{2.38}$$

The second exponential expression in Eq. (2.38) can be neglected, as a resonance relation that will make it slowly-varying can never be satisfied due to the speed of the light limit. Representing the slowly-varying phase difference between the rapidly-varying betatron and radiation phases with the variable $\psi_j = \theta_j + kz_j - \omega t$, introduced in Eq. (2.19). The angle bracket symbols can be used to denote the averaging in the source term, as in Chap.1, which leads to the unscaled wave equation of ICL

$$\left(\frac{\partial}{\partial z}+\frac{1}{c}\frac{\partial}{\partial t}\right)a_r = \frac{\mu_0 e n_x}{2k}\langle \omega_{\beta,j} r_{\beta,j} e^{-i\psi_j}\rangle. \tag{2.39}$$

Normalise the field potential with (2.2), we will have

$$\left(\frac{\partial}{\partial z}+\frac{1}{c}\frac{\partial}{\partial t}\right)A = \frac{\omega_b^2}{2\omega c^2}\langle \omega_{\beta,j} r_{\beta,j} e^{-i\psi_j}\rangle \tag{2.40}$$

where $\omega_b^2 = \omega_p^2 n_b/n_p$, with n_b being the electorn bunch density and n_p the plasma density, $A = (mc/e)a_r$ is the normalised field potential.

2.2.4 The Steady-State ICL Equations

The Particle Equations of Motion

The coordinate ψ represents the difference between the betatron and radiation phase, which is just the slowly varying variable we were looking at in the first section. Using relations obtained in the first section, it is straightforward to write down the first order equation of

motion for this coordinate as a function of γ_j and $r_{\beta,j}$, for each electron:

$$\frac{d\psi_j}{dt} = \frac{\omega_p}{\sqrt{2\gamma_j}} - \omega\left(\frac{1}{2\gamma_j^2} + \frac{\omega_p^2 r_{\beta,j}^2}{8\gamma_j c^2}\right). \tag{2.41}$$

The energy variation equation expressed in slowly-evolving variables can also be obtained:

$$\frac{d\gamma_j}{dt} = \frac{\omega_p r_{\beta,j}}{4\sqrt{2\gamma_j}}\exp(i\psi_j)\left(ka_r - i\frac{\partial a_r}{\partial z}\right) - i\frac{\omega_b^2}{\omega}\langle\exp(-i\psi_j)\rangle\exp(i\psi_j) + c.c.. \tag{2.42}$$

The wave equation obtained using the slowly varying envelope approximation is a first order PDE with the mean beam electron velocity very close to the speed of light (e.g., for a electron with $\gamma = 400$, the longitudinal velocity $\beta_z \approx 0.999997$). The highly relativistic nature of the electron is not only vital for the electron to maintain a small ponderomotive phase drift with its co-propagating radiation field (i.e., to satisfy the resonance condition), but also to approximately maintain its relative position to the radiation profile. In this case the radiation field 'sees' an almost infinitely long bunch and is considered to be in a "steady state".

In this chapter, we investigate the situation where the slippage between electrons and radiation can be neglected (*i.e.* $v_z \approx c$). In this case, the wave equation can be transformed into an ODE using the following relation:

$$\left(\frac{\partial}{\partial z} + \frac{1}{c}\frac{\partial}{\partial t}\right)a_r = \frac{1}{c}\left(c\frac{\partial}{\partial z} + \frac{\partial}{\partial t}\right)a_r \approx \frac{1}{c}\left(v_z\frac{\partial}{\partial z} + \frac{\partial}{\partial t}\right)a_r = \frac{1}{c}\frac{da_r}{dt},$$

which gives us the steady-state wave equation for the normalised field potential

$$\frac{dA}{dt} = \frac{\omega_b^2}{2\omega c}\langle\omega_{\beta,j} r_{\beta,j} e^{-i\psi_j}\rangle \tag{2.43}$$

Space Charge Effects

The repulsive force between electrons can inhibit the formation of a bunched electron beam. To investigate the influence of the space charge effect on bunching, the longitudinal electrostatic field $E_{sc,z}$ can be approximated by neglecting the transverse derivatives in

$$\nabla\cdot\vec{E}_{sc} \approx \frac{\partial}{\partial z}E_{sc,z} = \frac{e}{\epsilon_0}\left(n_p - \frac{1}{\Delta x}\sum_{j=1}^{N}\delta(y-y_j)\delta(z-z_j)\right). \tag{2.44}$$

Assuming that the field is periodic on the scale of the radiation wavelength we can expand the RHS into a Fourier series with respect to $\hat{\psi}$, to obtain

$$\frac{\partial}{\partial z}E_{sc,z} = \frac{e}{\epsilon_0}\left(n_p - \frac{k}{\Delta x \Delta y}\sum_{j=1}^{N}\delta(\psi-\psi_j)\right) = \frac{e}{\epsilon_0}\left(n_p - n_b\sum_{n=-\infty}^{\infty}\exp(in\psi)\langle\exp(-in\psi)\rangle\right). \tag{2.45}$$

By integrating this equation we find

$$e_{sc} = \frac{eE_{sc,z}}{m_e\omega c} = \frac{\omega_p^2}{\omega^2}z + i\frac{\omega_b^2}{\omega^2}\sum_{n=-\infty}^{\infty}\frac{\exp(in\psi)\langle\exp(-in\psi)\rangle}{n}. \tag{2.46}$$

We keep only the first harmonic term, as is appropriate for the linear analysis of the ICL equations carried out in the next section.

$$e_{sc} \approx i(\omega_b/\omega)^2\exp(i\psi)\langle\exp(-i\psi)\rangle + c.c.\,. \tag{2.47}$$

The right hand side is proportional to the bunching factor $\langle e^{-i\tilde{\psi}}\rangle$, which means that the electrons will tend to repel each other more as the bunching progresses.

Collective Radiation Feedback on the Betatron Amplitude and Frequency

The space charge force is not the only bunching-induced effect that needs to be considered. The radiation envelope A_0's exponential growth causes the electrons to oscillate asymmetrically in the transverse direction, those with $\sin(\psi) > 0$ will gain transverse energy, while those with $\sin(\psi) < 0$ will lose it, which leads to an increase or decrease in their betatron amplitudes and betatron frequencies, respectively. The influence of bunching on the evolution of betatron amplitude and frequency can be directly obtained with the Hamiltonian approach, by using the single-electron Hamiltonian in the split form (2.11)

$$\begin{aligned} r'_\beta \approx (a^2)'/(2r_\beta) &= (H-p_z)'/(2r_\beta) \\ &= [iA'\exp(i\psi) + c.c.]/[(8\gamma)^{1/2}]. \end{aligned} \tag{2.48}$$

The expression of betatron frequency can then be written by substituting (2.48) into the equation

$$r_\beta \frac{\omega_p \sqrt{\gamma + p_z}}{2\gamma} \sin(\theta) = r_\beta \theta' \sin(\theta) - r'_\beta \cos(\theta), \tag{2.49}$$

which gives:

$$\theta' = \frac{\omega_p \sqrt{\gamma + p_z}}{2\gamma} + \frac{icA' \exp(i\psi) + c.c.}{2\omega_p (2\gamma)^{1/2} r_\beta}. \tag{2.50}$$

Linearisation of the ICL Equations in the Compton Regime

With the ponderomotive phase and energy evolution equations at hand, the electron beam dynamics can be described by utilizing the concept of the bunching factor, which is defined as

$$b = \langle e^{-i\psi} \rangle. \tag{2.51}$$

Its evolution equation can be obtained as

$$b^{'} = -i\langle \psi' e^{-i\psi} \rangle. \tag{2.52}$$

As pointed out in the first chapter, the ICL betatron phases θ_j evolve rather independently from the wave phase $kz - \omega t$. We now have a set of self-consistent equations ((2.41)-(2.43) and (2.48)) expressed in slowly-evolving variables which can fully describe the fundamental physics of collective electron-radiation interaction within the ICL. This set of equations, however, cannot be solved using analytical methods, though approximate solutions do exist, see [47]. However, the essential dynamics of the ICL can be captured using a linearized model, as in the FEL [3], if the average of the kinetic energies and betatron amplitudes of the electrons in the bunch remain close to their resonance values throughout the whole interaction, i.e.

$$\frac{\Delta\gamma}{\gamma_r} = \frac{\langle (\gamma - \gamma_r)^2 \rangle^{1/2}}{\gamma_r} \ll 1. \tag{2.53}$$

If the betatron amplitude variation is sufficiently small, the right hand side of the phase evolution equation can be expanded in the so-called Compton limit, for a particular $r_{\beta,r}$to

be:

$$\frac{d\psi_j}{dt} = \left(-\frac{\omega_p}{2\sqrt{2\gamma_r}} + \frac{\omega}{\gamma_r^2} + \frac{\omega\omega_p^2 r_{\beta,r}^2}{8\gamma_r}\right)\frac{\Delta\gamma_j}{\gamma_r} + O\left(\left(\frac{\Delta\gamma_j}{\gamma_r}\right)^2\right) \tag{2.54}$$
$$\approx \frac{\omega_p}{\sqrt{2\gamma_r}}\left(\frac{1}{2} + \frac{1}{1+\omega_p^2 r_{\beta,r}^2\gamma_r/(4c^2)}\right)\frac{\gamma_j-\gamma_r}{\gamma_r}.$$

The difference from the FEL ponderomotive phase equation is evident: the amplitude of the FEL total dimensionless vector potential $|a_w e^{k_w z} + a_r e^{i(kz-\omega t)}|$ contains no slowly varying term in the lowest order under the condition $a_w \gg a_r$, while its counterpart in the ICL resonance relation, the betatron parameter a_β is a variable depending on both γ_r and $r_{\beta,r}$. Equally important is the slowly varying betatron frequency term: although the combined ponderomotive phase evolves in much the same way as in the FEL theory, the betatron phase evolves in direct proportion to the wave phase. Thanks to the γ dependence of the betatron frequency, which introduces a slowly varying term into the betatron phases, the transverse oscillation velocities of the electrons converge under the ponderomotive force, which leads to the electrons forming a microbunch transversely on a scale much smaller than r_β, with their phases centered around a value corresponding to $\sin(\theta_0) = 0$. This slowly varying term, as will be discussed in the Chapter 3, will contribute to the enhancement of the amplification of the fundamental harmonics through the longitudinal jittering term $\cos^2(\theta)$. As a result of both effects, the first-order coefficient in the linear term will be dependent on both γ_r and $r_{\beta,r}$ instead of being a constant. If $\omega_p^2 r_{\beta,r}^2\gamma_r/(4c^2) \gg 1$ then the coefficient tends towards $\omega_p/(2\sqrt{2\gamma_r})$. For the small-betatron amplitude scenario ($r_{\beta,r} \sim 0.5 - 1\ \mu$m), which is useful in the X-ray regime, due to the large value of γ_r the full expression must be used, and the coefficient can vary between $\omega_p/(2\sqrt{2\gamma_r})$ and $3\omega_p/(2\sqrt{2\gamma_r})$.

Utilizing this expansion in γ, the linearized first order ODE for the bunching factor can be written as

$$\frac{db}{dt} \approx -i\frac{\omega_p}{\sqrt{2\gamma_r}}\left(\frac{1}{2} + \frac{1}{1+\omega_p^2 r_{\beta,r}^2\gamma_r/(4c^2)}\right)\left\langle p\frac{r_\beta}{\sqrt{2\gamma_r}}\, e^{-i\psi}\right\rangle, \tag{2.55}$$

where $p_j = (\gamma_j - \gamma_r)/\gamma_r$. We can therefore write down the linearized equation for $\langle p(r_\beta/\sqrt{2\gamma_r})e^{-i\tilde{\psi}}\rangle$ to complete the linearization, with R_β being defined as the average of the r_β of the electrons,

$$d\left\langle p\frac{r_\beta}{\sqrt{2\gamma_r}}\, e^{-i\tilde{\psi}}\right\rangle \Big/ dt \approx \frac{\omega_p R_\beta^2 k a_r}{8\gamma} - i\frac{\omega_b^2}{\omega}\langle e^{-i\tilde{\psi}}\rangle. \tag{2.56}$$

2.2.5 Universal Scaling and Dimensionless Compton ICL Equations

A dimensionless scaling [3] of the variables can be introduced so that no experimental parameter appears explicitly in the equations of motion, which greatly simplifies our analysis of the ICL interaction in a way that only fundamental physical process are included. We first define the parameter ρ which is central to the universal scaling, for an electron distribution that is uniform in r_β

$$\rho = \left[\frac{\omega_b^2 R_\beta^2}{\gamma_r c^2} \left(\frac{1}{2} + \frac{1}{1 + \omega_p^2 R_\beta^2 \gamma_r / (4c^2)} \right) \right]^{1/3}. \tag{2.57}$$

If we apply the following universal scaling to the coordinates

$$\begin{aligned} \hat{p}_j = \frac{1}{\rho} p_j, \quad \hat{a}_r = 4c^3 \rho a_r / \omega_b^2 \omega_\beta R_\beta^3, \\ \overline{z} = (\rho \omega_\beta / 2c) z, \quad \overline{t} = (\rho \omega_\beta / 2) t, \end{aligned} \tag{2.58}$$

we obtain the following dimensionless ICL equations

$$\frac{d\psi_j}{d\overline{t}} = \hat{p}_j, \tag{2.59}$$

$$\frac{d\hat{p}_j}{d\overline{t}} = -(\hat{a}_r e^{i\psi_j} + c.c), \tag{2.60}$$

$$\frac{d\hat{a}_r}{d\overline{t}} = \langle e^{-i\tilde{\psi}} \rangle, \tag{2.61}$$

with the space charge effect, which is of the order of ρ, neglected in this section. (It will be re-introduced later along with the betatron variation effect in a more uniform way.) As we focus the discussion on ICL dynamics in the Compton limit, it can be immediately noticed that the scaled and linearized ICL equations in the Compton limit are identical to those of the scaled and linearized FEL equations [3]. The collective scaled equations for an ideal cold

beam will also be of an identical form

$$\overline{p}(0) = \frac{\gamma_0 - \gamma_r}{\rho\gamma_r} = \delta, \tag{2.62}$$

$$\overline{p}_j = \hat{p}_j - \delta, \tag{2.63}$$

$$\overline{\psi}_j = \psi_j - \delta t, \tag{2.64}$$

$$\overline{a}_r = \hat{a}_r \, e^{i\delta t}. \tag{2.65}$$

In this way the detuning parameter appears explicitly in the equations, which read (dropping the primes)

$$\frac{d\overline{\psi}_j}{d\bar{t}} = \overline{p}_j, \tag{2.66}$$

$$\frac{d\overline{p}_j}{d\bar{t}} = -(\overline{a}_r \, e^{i\psi} + c.c.), \tag{2.67}$$

$$\frac{d\overline{a}_r}{d\bar{t}} = \langle e^{-i\psi} \rangle + i\delta\overline{a}_r. \tag{2.68}$$

The scaled ICL equations can thus be written in a collective form after defining the following collective variables

$$\mathcal{A} = \overline{a}_r, \tag{2.69}$$

$$\mathcal{B} = \langle e^{-i\psi} \rangle, \tag{2.70}$$

$$\mathcal{P} = \langle \overline{p} \, e^{-i\psi} \rangle. \tag{2.71}$$

Neglecting the second order terms as in Sec 3.3, we obtain a closed set of equations

$$\frac{d\mathcal{B}}{d\bar{t}} = -i\mathcal{P}, \tag{2.72}$$

$$\frac{d\mathcal{P}}{d\bar{t}} = -\mathcal{A}, \tag{2.73}$$

$$\frac{d\mathcal{A}}{d\bar{t}} = \mathcal{B} + i\delta\mathcal{A}. \tag{2.74}$$

The similarity between the Compton regime ICL equations, after the scaling (2.58) is applied, and the classical scaled FEL equations used in [3] allows us to apply the same linear analysis

to the ICL equations. A single linear differential equation for only $\mathcal{A}$ can thus be constructed:

$$\frac{d^3\mathcal{A}}{d\bar{t}^3} - i\delta\frac{d^2\mathcal{A}}{d\bar{t}^2} - i\mathcal{A} = 0. \tag{2.75}$$

Assuming a solution of the form $\mathcal{A} \propto e^{i\lambda\bar{t}}$, we obtain the following characteristic equation, which determines the instability (existence of a root of the dispersion relation with positive real part) of the system

$$\lambda^3 - \delta\lambda^2 + 1 = 0. \tag{2.76}$$

Depending on the value of δ, equation (2.76) can have three real roots or two complex conjugate roots in addition to one real root. In the former case, there will be no growth of the radiation amplitude and the system will remain stable. In the latter case, one of the complex roots will lead to exponential growth of the field until non-linear effects become non-negligible.

It is straightforward to find that the imaginary part of λ is maximum when $\delta = 0$, exactly at resonance; in this case, (2.76) has three solutions

$$\lambda_1 = 1, \qquad \lambda_2 = \frac{-1 - \sqrt{3}i}{2}, \qquad \lambda_3 = \frac{-1 + \sqrt{3}i}{2}, \tag{2.77}$$

where λ_3 is responsible for the growth of the radiation field.

If instead of choosing an ideal cold beam we assume an initial energy distribution $f(p_0)$ with a finite energy spread, then (2.76) is modified to

$$\lambda - \delta_p + \int_{-\infty}^{+\infty} \frac{f(p_0)}{(\lambda + p_0)^2} dp_0 = 0, \tag{2.78}$$

according to [46]. The above integral can be analytically solved in certain cases. For the case of a rectangular distribution in kinetic energy with a half-width δ_p, the characteristic equation will become

$$(\lambda - \delta_p)(\lambda^2 - \mu^2) + 1 = 0, \tag{2.79}$$

where $\mu^2 = \langle p^2 \rangle - \langle p \rangle^2$ is the kinetic energy spread. When the betatron amplitude spread is also considered, the characteristic equation will taken on a more complex form, which will be the topic of section 2.2.8.

2.2.6 Constants of Motion and Efficiency

In addition to the conserved transverse energy, Equations (2.66)-(2.68) also admit two constants of motion that can help gaining more physical insight into the interaction process. The first is

$$\langle \overline{p} \rangle + |\overline{a}_r|^2 = \mathrm{C}, \tag{2.80}$$

where C is a constant.This conservation law shows that the energy of the radiation beam is extracted from the energy of the electron beam and can be used to estimate the saturation power of the radiation beam in the linear regime

$$|a_r|^2_{sat} \approx \Delta |a_r|^2 = \frac{2\omega_b^2}{\omega^2} \Delta \langle \gamma \rangle \approx \frac{2\omega_b^2 \rho}{\omega^2} \gamma_r. \tag{2.81}$$

where $\Delta|a_r|^2$ and $\Delta\langle\gamma\rangle$ represent the changes in $|a_r|^2$ and $\langle\gamma\rangle$, respectively. From the above relation, we find that the saturation power $|a_r|^2_{sat} \propto \omega_b^2 \rho \propto n_e^{4/3}$, which implies the existence of collective behaviour within the electron beam. The efficiency of the ICL can also be found:

$$\upsilon = \frac{\epsilon_0 |E_0|^2}{mc^2 \gamma_r n_e} = \frac{\rho}{4}. \tag{2.82}$$

The second constant of motion is the total Hamiltonian of the electrons and the radiation field, similar to the one introduced in [45]:

$$H_{tot} = \sum_{j=1}^{N_e} \frac{\overline{p}_j^2}{2} + i[A_r \mathcal{B} - c.c.]. \tag{2.83}$$

2.2.7 Gain Parameter and Raman Regime of the ICL

The Definition of Gain Parameter and the Range of its Value

Given the definition of $\bar{t}$ in (2.59) and the exponential form of $\mathcal{A}$, it is helpful to define a gain length

$$L_g = \frac{\lambda_\beta}{\sqrt{3}\pi\rho}, \tag{2.84}$$

which corresponds to the distance the wave needs to travel for its power to grow by a factor of e in the linear regime. With L_g we can also define a saturation length

$$L_{sat} \approx L_g \ln(9P_{sat}/P_0), \tag{2.85}$$

where P_{sat} is the saturation power, and P_0 is the initial power of the beam. From Eq. (2.84) it is immediately clear that the gain of the radiation amplitude in the wiggler is directly determined by ρ and λ_β, which is the reason why the ρ parameter is also called the gain parameter.

The formulation of ICL equations under Compton limit is sufficient when the value of ρ is small ($\rho \ll 0.1$). This, however, is not always the case for an ICL, even when an electron beam with $\gamma \gg 1$ is used for amplification of short-wavelength radiation. This can be seen by estimating the value of ρ for realistic ICL parameters. We first express the ρ value in terms of parameters with equal dimensions:

$$\rho = \left[\frac{\omega_b^2 R_\beta^2}{\gamma c^2}\left(\frac{1}{2} + \frac{1}{1+\omega_p^2 R_\beta^2 \gamma_r/(4c^2)}\right)\right]^{1/3} \approx \left[\frac{4I\pi R_\beta^2}{I_A S_b}\left(\frac{1}{2} + \frac{1}{1+\omega_p^2 R_\beta^2 \gamma_r/(4c^2)}\right)\right]^{1/3}, \tag{2.86}$$

where S_b is the cross section of the electron beam and I is the current of the electron beam, and $I_A = I_0 \gamma_r \beta_z$ where $I_0 = 4\pi\epsilon_0 mc^3/e$ is the Alfven limiting current. With $I = 4$ kA and $\gamma = 400$, parameters routinely attainable in wakefield acceleration experiments, $\rho \approx 0.105$ (which corresponds to a ρ value of 0.027 defined using FEL scaling in [3], hereafter referred to as a 'FEL equivalent' ρ value) when the betatron amplitude is equal to the beam radius, assuming $R_\beta = r_b$ and no guiding effect. Therefore, for plausible experimental conditions, the value of ρ can be large enough to require high density effects to be taken into account. In addition, the value of ρ for a fixed wavelength can also be large for reasons other than high electron beam density or low wiggler wavelength, e.g., a correlation in the transverse betatron phases introduced through pre-bunching. Compared with an electron beam with uncorrelated initial betatron phases, a beam with correlated betatron phases could have a smaller beam radius.

It is worth pointing out that the definition of (2.86) ρ for the ICL reveals an important difference between the ICL and FEL. For both paraxial oscillation and very large R_β scenarios, the value of ρ of the ICL is independent of the strength of the external electrostatic field. (The gain, however, does depend on ω_p, which determines the strength of the electrostatic

field.) This property is useful in the following analysis of the influence of space charge effects on the amplification process.

For large ρ values (Raman regime), a number of effects must be accounted for in the linearized ICL formulation, namely the space charge effect, betatron amplitude and frequency variations. We will repeat the process of linearizing the ICL equations, but now include all terms up to the first order of ρ. We start by extending the scaling (2.59) to include:

$$s_j = r_{\beta,j}/R_\beta - 1, \tag{2.87}$$

$$s = \langle s_j \rangle, \tag{2.88}$$

$$a_\beta = \frac{\omega_p R_\beta \sqrt{\gamma_0/2}}{c}. \tag{2.89}$$

and use q instead of p to denote the momentum change variable. (2.41)-(2.43), (2.48) can thus be expressed in the following form by using the resonance relation:

$$\overline{a}'_r = (1+\delta_{r_\beta})\langle (1+s)\exp(-i\psi)/(1+q)^{1/2}\rangle, \tag{2.90}$$

$$\begin{aligned}\psi'_j = (2/\rho)\{&(1+q_j)^{-1/2} - \frac{\rho^3 \overline{a}'_r}{1+1/a_\beta^2} - (1+a_\beta^2)^{-1}(1+q)^{-2} \\ &- (1+s_j)^2(1+\delta_{r_\beta})^2/[(1+\delta_\gamma)^{1/2}(1+1/a_\beta^2)(1+q_j)]\},\end{aligned} \tag{2.91}$$

$$\begin{aligned}q'_j = &-\rho\overline{a}_r(1+s_j)(1+\delta_{r_\beta})\exp(i\psi_j)/(1+q_j)^{1/2} \\ &- 2i\rho^2\frac{(1+a_\beta^2)^2}{(3+a_\beta^2)a_\beta^2}(1+\delta_t)\langle\exp(-i\psi)\rangle\exp(i\psi_j) + c.c.,\end{aligned} \tag{2.92}$$

$$s'_j = -i(\rho^2/8)\langle(1+\delta_t)\exp(-i\psi)\rangle\exp(i\psi_j)/(1+q_j)^{1/2} + c.c., \tag{2.93}$$

where the primes denote derivatives with respect to τ, and $a_\beta = \omega_p r_{\beta,r}\sqrt{\gamma_r/2}$, where in turn $r_{\beta,r}$ and γ_r are combinations of r_β and γ values that satisfy the resonance relation (2.21) for ω and ω_p, with their detunings being defined by δ_{r_β} and δ_γ respectively, which sum to the total detuning δ_t.

Comparing Equations (2.90) -(2.93) with the linearized ICL equations in the Compton regime and the FEL equations, we notice several important differences, which will be discussed below.

When feedback of the beam bunching on the betatron amplitude is taken into account, we find that the derivative of the betatron amplitude s_j becomes proportional to the bunching factor and is similar to the longitudinal space charge force contributing to q'_j. The term describes a transverse bunching force that is a counter force to the repulsive space charge

force. The coefficient of the q_j term in the linearized phase variation equation depends on a_β: The RHS of the phase variation equation will approach $(q_j + \delta_\gamma)/\rho$ for $a_\beta \gg 1$, and $3(q_j + \delta_\gamma)/\rho$ for a_β approaching zero.

The space charge contribution also depends on a_β; the value of its coefficient can be approximated with ρ in the large a_β case, and tends toward infinity as a_β approaches zero, which can be understood through the definition of ρ, which tends to zero as R_β approaches zero. As a result the bunching effect of the beam will diminish with ρ, whereas the space charge coefficient will remain above $2\omega_b^2/(\omega_p^2\gamma_r)$. This shows that a small r_β ion channel laser, as proposed in [1] and [48], is not only technically difficult to build, but would also be theoretically undesirable since the space charge effects of the electron beam could be more than two orders of magnitude larger than achievable for large r_β. When $a_\beta^2 < \rho/7.6$ (as under parameters provided on p. 295 of Whittum's thesis [2]) the characteristic equation of the system will have three real roots and amplification will not occur.

Assuming $a_\beta \gg 1$ and applying the scaling

$$\overline{q}_j = q_j/\rho,\ \overline{s}_j = 4s_j/\rho^2, \text{ and } \overline{\delta} = 2\delta_t/\rho \tag{2.94}$$

to eqns. (2.90)-(2.93), where $\delta_t = -2\delta_{r_\beta} + \delta_\gamma/2$, these eqns. can be linearized by expanding their right-hand sides into Taylor series in ρ and keeping only the zeroth and first order terms:

$$\overline{a}\,'_r = -i\langle \Delta\psi \exp(-i\psi_0)\rangle + i\rho\langle \overline{q}\exp(-i\psi_0)\rangle/2, \tag{2.95}$$
$$\psi'_j = (1+2\delta_t)\overline{q}_j - (1+\delta_t)\rho\overline{s}_j + \overline{\delta}, \tag{2.96}$$
$$\overline{q}\,'_j = -[\overline{a}_r + 2i\rho\langle\exp(-i\psi - i\overline{\delta}\,\overline{t})\rangle]\exp(i\psi_j) + c.c., \tag{2.97}$$
$$\overline{s}\,'_j = -i\overline{a}'_r \exp(i\psi_j)/2 + c.c.. \tag{2.98}$$

with $\Delta\psi$ representing the first-order phase variation. We redefine the collective variables as:

$$\mathcal{B} = \langle \Delta\psi \exp(-i\psi_0)\rangle, \tag{2.99}$$
$$\mathcal{P} = \langle \overline{q}\exp(-i\psi_0)\rangle, \tag{2.100}$$
$$\mathcal{A} = \overline{a}_r \exp(i\overline{\delta}\overline{t}), \tag{2.101}$$
$$\mathcal{S} = \langle \overline{s}\exp(-i\psi_0)\rangle. \tag{2.102}$$

Their evolution follows from Eqns. (2.95)-(2.98):

$$\mathcal{A}' = -i\mathcal{B} - \frac{\rho}{2}\mathcal{P} + i\overline{\delta}\mathcal{A}, \tag{2.103}$$

$$\mathcal{B}' = \mathcal{P} - \rho\mathcal{S}, \tag{2.104}$$

$$\mathcal{P}' = -\mathcal{A} - 2i\rho(\mathcal{A}' - i\overline{\delta}\mathcal{A}), \tag{2.105}$$

$$\mathcal{S}' = -\frac{i}{2}(\mathcal{A}' - i\overline{\delta}\mathcal{A}), \tag{2.106}$$

which reduces to a linear differential equation for $\mathcal{A}$, by expressing all collective variables in terms of $\mathcal{A}$ and its derivatives:

$$\mathcal{A}''' - i\overline{\delta}\mathcal{A}'' + \rho\mathcal{A}' - i(1 + 3\rho\overline{\delta}/2)\mathcal{A} = 0. \tag{2.107}$$

The characteristic equation can be obtained in the same way as in the Compton regime FEL:

$$\lambda^3 - \overline{\delta}\lambda^2 - \rho\lambda + (1 + 3\rho\overline{\delta}/2) = 0. \tag{2.108}$$

When $\overline{\delta} = 0$, the characteristic equation simplifies to:

$$\lambda^3 - \rho\lambda + 1 = 0. \tag{2.109}$$

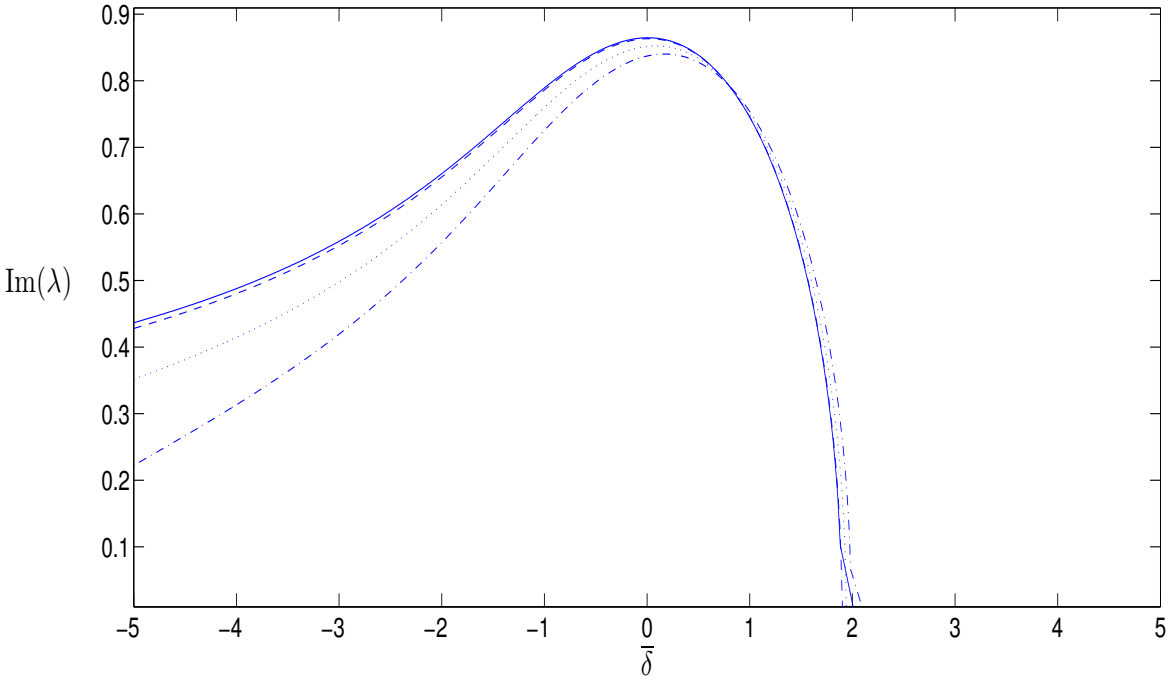

Figure 2.4: Instability domain: imaginary part of the unstable root of the dispersion relation (2.108), as a function of $\overline{\delta}$ for different values of ρ:(1) $\rho = 0.005$ (solid line). (2)$\rho = 0.01$ (dashed line). (3) ρ=0.05 (the dotted line) $\rho = 0.1$ (the dot-dashed line). The maximum value of λ is obtained when $\overline{\delta} = 0$ and $\rho = 0$, while the maximum λ for sufficiently large ρ occurs at $\overline{\delta} \approx \sqrt{\rho}$. The larger the value of ρ, the smaller $\overline{\delta}$ will be required for λ to approach zero.

The plot shows that the value of the imaginary part of λ varies with the value of scaled detuning $\overline{\delta}$. As in FEL theory, the growth rates with detuning are asymmetric between positive and negative detuning. For positive values of detuning, Im(λ) attains a maximum value at $\overline{\delta} \approx \sqrt{\rho}$ before rapidly declining to zero, at which point the instability vanishes. For negative values of detuning, the value of Im(λ) will slowly decline, but will remain positive instead of rapidly falling to zero. The saturation power is also affected differently by positive and negative detuning values, a positive detuning, as long as it is below the threshold value, can enhance the power gain, while a negative detuning will weaken it. The detuning factor also adds the term $i\overline{\delta}\mathcal{A}$ to the RHS of the differential equation (2.106) for $\mathcal{S}$. Correspondingly, $\langle s \rangle$ no longer is a conserved quantity, but follows the differential equation

$$\langle \overline{s}_j' \rangle = -\frac{\overline{\delta}}{2} \overline{a}_r \langle \exp(-i\psi) \rangle. \tag{2.110}$$

A new conserved quantity can thus be defined, in the same way as (2.80):

$$\langle \overline{s}_j \rangle + \frac{\overline{\delta}}{2} |\overline{a}_r|^2 = \mathrm{C}. \tag{2.111}$$

For a positive $\overline{\delta}$, $\langle \overline{s} \rangle$ will be reduced by a growing $|\overline{a}_r|^2$, while a negative $\overline{\delta}$ will increase it.

2.2.8 Energy and Betatron Amplitude Spread

A fundamental difference between the ICL and the FEL, is that the value of the betatron amplitude r_β, and therefore, the wiggler parameter a_β is individually defined for each electron in the beam. To model a realistic electron beam, the influence of spreads in both energy and betatron amplitude on the amplification must simultaneously be considered. We therefore consider the evolution of the electron beam in $z - p_z - r_\beta - \theta$ phase space, where electron distributions with both spreads can be best modelled using a Vlasov-Maxwell approach. We start with the general form of the Vlasov equation:

$$\left(\frac{\partial}{\partial t} + \mathbf{x}' . \frac{\partial}{\partial \mathbf{x}} + \mathbf{p}' . \frac{\partial}{\partial \mathbf{p}} \right) f = 0. \tag{2.112}$$

We will start with the equilibrium distribution f_0, which satisfies the following Vlasov equation:

$$\frac{\partial f_0}{\partial t} + z' \frac{\partial f_0}{\partial z} + p_z' \frac{\partial f_0}{\partial p_z} + y' \frac{\partial f_0}{\partial y} + p_y' \frac{\partial f_0}{\partial p_y} = 0. \tag{2.113}$$

The equilibrium phase space distribution function of the beam electrons, f_0, can be defined as a function of two variables, p_z and r_β^2:

$$f_0 = f(p_z, r_\beta^2). \tag{2.114}$$

In the linear regime, we seek a solution in the form of

$$f = f_0 + f_1 = f_0 + \overline{f}_1 e^{i\psi + i\lambda \bar{t}}. \tag{2.115}$$

Substituting the above equation into (2.112) and eliminating the rapidly oscillating terms,

we obtain the linearised Vlasov equation, written using the slowly varying coordinates:

$$\frac{\partial f_1}{\partial t} + \psi' \frac{\partial f_1}{\partial \psi} + p_z' \frac{\partial f_0}{\partial p_z} + \frac{dr_\beta^2}{dp_z} p_z' \frac{\partial f_0}{\partial r_\beta^2} = 0. \tag{2.116}$$

Assuming the condition $\frac{dr_\beta^2}{dp_z} p_z' \propto (kv_z - \omega) p_z' \ll p_z'$, which is valid for $a_\beta \gg 1$, the $\frac{\partial f_0}{\partial r_\beta^2}$ term can be removed from Eq.(2.116). Replacing the variables p_z and r_β^2 with q and s we obtain

$$\frac{\partial f_1}{\partial \overline{t}} + \psi' \frac{\partial f_1}{\partial \psi} + \overline{q}' \frac{\partial f_0}{\partial \overline{q}} = 0, \tag{2.117}$$

substituting the scaled equations of motion for ψ and $\overline{q}$ into the linearised Vlasov equation, the first-order distribution function can be written in a form that contains the derivative of f_0,

$$f_1 = -\frac{\partial f_0(\overline{q}, \overline{s})}{\partial \overline{q}} \frac{i\overline{a}_r e^{i\psi}}{(\lambda + \overline{q} - \rho\overline{s})}, \tag{2.118}$$

after some rearrangements. We then rewrite the source term of the steady-state wave equation using the distribution function

$$\frac{d\overline{a}_r}{d\overline{t}} = \int_{-r_\beta}^{r_\beta} \int_{-\infty}^{\infty} \int_{-\infty}^{\infty} f_1 e^{-i\psi} dp_y dp_z dy, \tag{2.119}$$

This equation can then be transformed using the coordinate transformation $(p_y, p_z, y \rightarrow \theta, \overline{q}, \overline{s})$, with the substitution of (2.115), to produce the following dispersion relation which rules the stability of the system

$$\int_{-\infty}^{\infty} \int_{-\pi}^{\pi} \delta(\theta - \theta_0) \frac{\partial f_0(\overline{q}, \overline{s})}{\partial \overline{q}} \frac{1}{\lambda(\lambda + \overline{q} - \rho\overline{s})} d\theta d\overline{q} d\overline{s} + 1 = 0. \tag{2.120}$$

In the case of a monoenergetic beam (i.e., $f(\overline{q}, \overline{s}) = \delta(\overline{q})\delta(\overline{s})$), this can be reduced to the familiar cubic equation $\lambda^3 - \overline{\delta}\lambda^2 + 1 = 0$. The dispersion relation starts to diverge significantly from the one for the FEL when the electron bunch is modelled with a rectangular distribution

$f(\overline{q},\overline{s}) = \Pi(\overline{q}_0)\Pi(\overline{s}_0)$with half width $\mu_{\overline{q}}$, $\mu_{\overline{s}}$

$$\Pi(\overline{q}_0) = \begin{cases} \dfrac{1}{2\mu_{\overline{q}}} & \text{if } -\mu_{\overline{q}} < \overline{q}_0 < \mu_{\overline{q}}\,, \\ 0 & \text{elsewhere,} \end{cases} \qquad \Pi(\overline{s}_0) = \begin{cases} \dfrac{1}{2\mu_{\overline{s}}} & \text{if } -\dfrac{\mu_{\overline{s}}}{\rho} < \overline{s}_0 < \dfrac{\mu_{\overline{s}}}{\rho}, \\ 0 & \text{elsewhere,} \end{cases} \tag{2.121}$$

for which the following dispersion relation can be obtained through a straightforward calculation:

$$\frac{1}{4\mu_{\overline{q}}\mu_{\overline{s}}\lambda} \ln\Big(1 - \frac{4\mu_{\overline{q}}\mu_{\overline{s}}}{(\mu_{\overline{q}}+\mu_{\overline{s}})^2 - \lambda^2}\Big) = -1, \tag{2.122}$$

Expanding the logarithmic term inside the transcendental dispersion relation yields:

$$\frac{1}{4\mu_{\overline{q}}\mu_{\overline{s}}\lambda}\Big[\frac{4\mu_{\overline{q}}\mu_{\overline{s}}}{\lambda^2 - (\mu_{\overline{q}}+\mu_{\overline{s}})^2} - \Big(\frac{4\mu_{\overline{q}}\mu_{\overline{s}}}{\lambda^2 - (\mu_{\overline{q}}+\mu_{\overline{s}})^2}\Big)^2/2 + ...\Big] + 1 = 0. \tag{2.123}$$

When $\mu_{\overline{s}} = 0$, the dispersion relation can be reduced to the form seen in the FEL literature (e.g., [46])

$$\lambda(\lambda^2 - \mu_{\overline{q}}^2) + 1 = 0. \tag{2.124}$$

A formally similar dispersion equation taking into account both $\mu_{\overline{q}}$ and $\mu_{\overline{s}}$ can be obtained from (2.123) if only the first-order term in the expansion is kept:

$$\lambda[\lambda^2 - (\mu_{\overline{q}}+\mu_{\overline{s}})^2] + 1 = 0. \tag{2.125}$$

This approximate relation shows that at the lowest order, the spreads in γ and r_β will affect the growth factor equally. In fact, this is the full dispersion relation for a beam with the following distribution function:

$$f_0(\overline{q}) = \begin{cases} \dfrac{1}{2\mu_{\overline{q}}} & \text{if } -\mu_{\overline{q}} < \overline{p}_0 < \mu_{\overline{q}}\,, \\ 0 & \text{elsewhere,} \end{cases} \qquad f_0(\overline{s}) = \delta\Big(\overline{s} + \frac{\mu_{\overline{s}}}{\rho}\Big) - \delta\Big(\overline{s} - \frac{\mu_{\overline{s}}}{\rho}\Big). \tag{2.126}$$

It is therefore imperative to include higher terms in the calculation of the growth factor, when the value of $\mu_{\overline{s}}$ is comparable to ρ. As no analytical solution exists for the equation (2.122), the gain curve has to be obtained numerically.

We numerically solve the equation (2.123) to obtain the values of λ under a number of

different conditions for the spreads:

	$\mu_{\overline{q}} = 0.2$	$\mu_{\overline{q}} = 0.5$	$\mu_{\overline{q}} = 1.0$	$\mu_{\overline{q}} = 1.5$
Im(λ) with $\mu_{\overline{s}}$=0	-0.8545	-0.7937	-0.5623	0
Im(λ) with $\mu_{\overline{s}}$=$\mu_{\overline{q}}$, solved using the full dispersion relation	-0.8429	-0.7244	-0.4221	-0.2322
Im(λ) with $\mu_{\overline{s}}$=$\mu_{\overline{q}}$, solved using the lowest order term in the dispersion relation	-0.8198	-0.5623	0	0

It can be seen from the above table that for small $\mu_{\overline{q}}$ ($\mu_{\overline{q}} < \rho$) the imaginary root value is smaller with $\mu_{\overline{s}} = \mu_{\overline{q}}$ than with $\mu_{\overline{s}} = 0$. However, when $\mu_{\overline{q}} > \rho$, the imaginary root for $\mu_{\overline{s}} = 0$ will rapidly decline to zero, while remaining positive for $\mu_{\overline{q}} = \mu_{\overline{s}}$. In fact, a complex root corresponding to the exponentially growing solution of A can theoretically always be found, however large $\mu_{\overline{s}}$ or $\mu_{\overline{q}}$ are, as long as the condition $\mu_{\overline{q}} = \mu_{\overline{s}}$ is satisfied. Although counter-intuitive, such an outcome can be explained considering that the electron distributions in $\overline{q}$ and $\overline{s}$ coordinates are uniform and symmetric. If $\mu_{\overline{q}} = \mu_{\overline{s}}$, for any electron with a $\overline{q}$ value outside the instability range corresponding to $\overline{s} = 0$, there is a finite probability for an $\overline{s}$ value in the interval that allows instability to occur with this value of $\overline{q}$. The result demonstrates that, unlike in FEL theory, larger spreads do not necessarily lead to stronger suppression of the gain in the ICL. This result, however, cannot be generalised to other more realistic forms of energy/betatron amplitude distributions, e.g., Gaussian distribution or Lorentzian distribution commonly observed in the electron beam produced by wakefield accelerators, both with less abrupt cut-offs of the tails.

2.3 Non-paraxial Extension of Whittum's ICL Formulation

In this section we will establish the connection between Whittum's [1] formulation and ours by deriving the set of equations of motion in his approach from the set of variables used in the present thesis. The derivation will show that Whittum's expression for ρ can be considered an approximation to ours in the limit of small r_β, and his equation of motion for θ is incorrect due to an inappropriate use of averaging.

2.3.1 Resonance with the Betatron Phase and the Momentum Phase

The first important differences between the two approaches are the different treatment of the notion of "resonance" and the definitions of the ponderomotive phase. In Whittum's thesis, the ponderomotive phase is defined as the difference between the oscillation phase of the momentum and the radiation wave phase, rather than the difference between the betatron oscillation phase (i.e, phase of variation in y) and the radiation wave phase, as used in our model. It is therefore useful to formally define the relation between the two phases.

We first express the momentum components of an electron under consideration in Whittum's eikonal formulation:

$$p_y = q_y \sin(\theta_y), \tag{2.127}$$

$$p_z = q_z. \tag{2.128}$$

In the above equations, θ_y is considered to vary on a much faster time scale than q_y, so that after averaging over the betatron period, terms including $\sin(n\theta_y)$, where n is an integer, will become zero, while terms without $\sin(n\theta_y)$, but including q_y, remain constant. The transverse momentum, expressed in coordinates of both systems, must be equivalent. Thus we can obtain from the Hamiltonian, in the large r_β case, with the same scaling used in Whittum's thesis,

$$q_y \sin(\theta_y) = r_\beta \frac{\sqrt{\gamma + p_z}}{2} \sin(\theta) - A_0 \sin(kz - \omega t). \tag{2.129}$$

The rapidly varying phases θ_y and θ can be expressed as:

$$\theta_y = -(kz - \omega t - \psi_1), \tag{2.130}$$

$$\theta = -(kz - \omega t - \psi_2), \tag{2.131}$$

where ψ_1 and ψ_2 are the ponderomotive phases defined for the momentum and betatron phases, respectively.

These relations can be used to rewrite Equation (2.129) as:

$$q_y[\sin(kz-\omega t)\cos(\psi_1)-\cos(kz-\omega t)\sin(\psi_1)] \\ = r_\beta\frac{\sqrt{\gamma+p_z}}{2}[\sin(kz-\omega t)\cos(\psi_2)-\cos(kz-\omega t)\sin(\psi_2)]+A_0\sin(kz-\omega t). \quad (2.132)$$

As q_y, $r_\beta\sqrt{\gamma+p_z}/2$, and A_0 are all assumed to be slowly-varying terms, we observe that to make the two sides of Eq. (2.132) always equal the following relations must be satisfied:

$$q_y\cos(\psi_1) = r_\beta\frac{\sqrt{\gamma+p_z}}{2}\cos(\psi_2)+A_0, \quad (2.133)$$

$$q_y\sin(\psi_1) = r_\beta\frac{\sqrt{\gamma+p_z}}{2}\sin(\psi_2). \quad (2.134)$$

The expression of q_y in non-canonical variables can thus be obtained:

$$q_y = \sqrt{\frac{r_\beta^2(\gamma+p_z)}{4}+A_0r_\beta\sqrt{\gamma+p_z}\cos(\psi_2)+A_0^2}. \quad (2.135)$$

We then expand both sides of Eq.(2.129) around the point $t=0$ into:

$$q_y(\sin(\psi_1)+\theta_y'\cos(\psi_1)\Delta t)+O(\Delta t^2) \\ = r_\beta\frac{\sqrt{\gamma+p_z}}{2}\sin(\psi_2)+(r_\beta\frac{\sqrt{\gamma+p_z}}{2}\theta'\cos(\psi_2)+A(kv_z-\omega))\Delta t+O(\Delta t^2). \quad (2.136)$$

Because the terms of the same order in t on the two sides of the above equation must be equal, we have:

$$q_y\theta_y'\cos(\psi_1) = r_\beta\frac{\sqrt{\gamma+p_z}}{2}\theta'\cos(\psi_2)+A(kv_z-\omega). \quad (2.137)$$

We thus find from the above equation and Eq. (2.129) that:

$$\theta_y' = \frac{r_\beta\frac{\sqrt{\gamma+p_z}}{2}\theta'\cos(\psi_2)+A(kv_z-\omega)}{r_\beta\frac{\sqrt{\gamma+p_z}}{2}\cos(\psi_2)-A}, \quad (2.138)$$

which can be rewritten using the resonance relations Equation (2.130) and (2.131) as:

$$\begin{aligned}\theta'_y &= \frac{r_\beta \frac{\sqrt{\gamma+p_z}}{2}\theta' \cos(\psi_2) + A(\psi'_2 - \theta')}{r_\beta \frac{\sqrt{\gamma+p_z}}{2}\cos(\psi_2) - A} \\ &= \theta' - A\frac{\psi'_2}{q_y \cos(\psi_1)} \\ &= \theta' - A\frac{\psi'_1 - \theta'_y + \theta'}{q_y \cos(\psi_1)}.\end{aligned} \tag{2.139}$$

I.e., $\theta'_y - \theta' = \dfrac{A\psi'_1}{A - q_y \cos(\psi_1)}$. For $\psi'_1 = 0$, we have:

$$\begin{aligned}\theta'_y &= \theta' - A\frac{(-\theta'_y + \theta')}{q_y \cos(\psi_1)} \\ &= \theta' = \omega_\beta.\end{aligned} \tag{2.140}$$

Thus we conclude that the frequency of the momentum phase is equal to that of the betatron phase, provided that the momentum phase is in exact resonance with the radiation wave phase, and q_y is slowly-varying. This result contradicts the one obtained for θ_y in Whittum's thesis, whose first-order derivative contains a term dependent on $\cos(\psi_1)$. An analysis is carried out in the following to understand the caveat in the derivation of equations of motion in Whittum's original thesis.

2.3.2 Comparison of the Equations of Motion

We start by following Whittum's procedure in deriving the eikonal equations of motion. Substituting the eikonal expression of transverse momentum into the following second-order differential equation for p_y,

$$p''_y = -\frac{p_y + A_0 \sin(kz - \omega t)}{2\gamma}, \tag{2.141}$$

which can be obtained from the Hamiltonian, will lead to the following equation

$$q''_y \sin(\theta_y) + 2q'_y\theta'_y \cos(\theta_y) + q_y\theta''_y \cos(\theta_y) - q_y \sin(\theta_y)(\theta'_y)^2 + \omega_\beta^2 q_y \sin(\theta_y) = -\omega_\beta^2 A_0 \sin(kz - \omega t). \tag{2.142}$$

Multiplying both sides by $\sin(\theta_y)$ and $\cos(\theta_y)$ respectively, and averaging over the betatron period gives:

$$q_y'' - q_y(\theta_y')^2 + \omega_\beta^2 q_y = \omega_\beta^2 A_0 \cos(\psi_1), \tag{2.143}$$

$$2q_y'\theta_y' + q_y\theta_y'' = -\omega_\beta^2 A_0 \sin(\psi_1). \tag{2.144}$$

To first order in A_0 , the above set of equations reduces to:

$$\frac{d\theta_y}{dt} = \omega_\beta\Big[1 - \frac{A_0}{2q_y}\cos(\psi_1)\Big], \tag{2.145}$$

$$\begin{aligned}\frac{dq_y}{dt} &= -\frac{q_y}{2\omega_\beta}\frac{d\omega_\beta}{dt} - \frac{1}{2}\omega_\beta A_0 \sin(\psi_1) \\ &= -\frac{1}{2}\Big(\omega_\beta + \frac{1}{4}\frac{kcq_y^2}{q_z^2}\Big)A_0 \sin(\psi_1).\end{aligned} \tag{2.146}$$

The same procedure can be applied to obtain the equations of motion in the z direction:

$$\frac{d\psi_y}{dt} = kv_z - \omega + \omega_\beta - \frac{\omega_\beta}{2q_y}A_0\cos(\psi_1), \tag{2.147}$$

$$\frac{dq_z}{dt} = -\frac{1}{2}\omega\frac{q_y}{q_z}A_0\sin(\psi_1). \tag{2.148}$$

The right hand side of the ponderomotive phase equation, which describes the resonance relation, therefore contains a slowly varying term dependent on $\cos(\psi_1)$. Such averaging over the betatron period, however, is only valid as long as no term on the left hand sides of (2.143) and (2.144) contain harmonics oscillating at frequencies higher than ω_β. While this is true for q_y and q_z, it is not for q_y' and q_z'. In fact, Eq.(2.148) comes from the Hamiltonian equation of motion for p_z:

$$\begin{aligned}\frac{dp_z}{dt} &= -kmc^2\frac{p_y}{p_z}A_0\cos(kz-\omega t), \\ &= -kmc^2\frac{q_y}{q_z}A_0\sin(\theta_y)\cos(kz-\omega t), \\ &= -kmc^2\frac{q_y}{2q_z}A_0[\sin(kz-\omega t+\theta_y)+\sin(kz-\omega t-\theta_y)],\end{aligned} \tag{2.149}$$

which gives:

$$\frac{dq_z}{dt} = -kmc^2\frac{q_y}{2q_z}A_0[\sin(kz-\omega t+\theta_y)+\sin(kz-\omega t-\theta_y)]. \tag{2.150}$$

Eq.(2.150) contains a term proportional to $\sin(kz - \omega t - \theta_y)$, oscillating at $2\omega_\beta$, which is explicitly neglected in Whittum's thesis. The existence of this term invalidates the premise of the betatron period averaging, applied to Eq.(2.142), as can be seen by evaluating the right-hand side of Eq.(2.146) using the complete expression of q_z':

$$\frac{dq_y}{dt} = -\frac{1}{2}\omega_\beta[A_0\sin(\psi_1) + A_0\sin(kz - \omega t - \theta_y)] - \frac{1}{8}kc\frac{q_y^2}{q_z^2}[A_0\sin(\psi_1) + A_0\sin(kz - \omega t - \theta_y)], \tag{2.151}$$

which can be used to obtain:

$$\begin{aligned}\langle -2q_y'\theta_y'\cos(\theta_y)\sin(\theta_y)\rangle &= \frac{1}{4}kc\omega_\beta\frac{q_y^2}{q_z^2}A_0\sin(kz - \omega t - \theta_y)\sin(2\theta_y) \\ &= \frac{1}{8}kc\omega_\beta\frac{q_y^2}{q_z^2}A_0[\cos(kz - \omega t - 3\theta_y) - \cos(\psi_1)].\end{aligned} \tag{2.152}$$

A large r_β and the resonance condition ensure that $kcq_y^2/(4q_z^2) = [\omega_\beta - kc/(2\gamma^2)]/2 \approx \omega_\beta/2$, up to first order in A_0. Therefore, the resonant term on the RHS of Eq. (2.151) can be found to be roughly $-\omega_\beta^2 A_0\cos(\psi_1)$, which is the same resonant term that appears on the RHS of Eq. (2.143). The removal of this term from Eq. (2.143) leads to the result $\theta_y' = \omega_\beta$.

For $r_\beta \ll 1$, we have $kcq_y^2/(4q_z^2) \ll \omega_\beta$, the corresponding terms on the RHS of Eq. (2.151) can therefore be negelected, with the RHS of the equation of motion for the betatron frequency in turn depends on the ponderomotive phase through the term $\omega A\cos(\psi_1)/(4q_y)$, which is still reduced by half from the value obtained in the $q_y' \approx 0$ approximation.

However, the approach we take above can only serve as a heuristic statement, as the time derivative of q_y (Eq. (2.146) is obtained from Eq. (2.144), which already contains the assumption that $\theta_y' \approx \omega_\beta$. A strict derivation that further demonstrates the power of our approach, involves expressing q_y in non-canonical variables as in Eq. (2.135), which gives:

$$\begin{aligned}\frac{dq_y}{dt} &\approx \left[r_\beta\frac{\sqrt{\gamma + p_z}}{2} + A_0\cos(\psi_2)\right]' \\ &\approx \frac{r_\beta\omega_\beta}{2}p_z' \\ &= q_y\omega_\beta^2 p_z'.\end{aligned} \tag{2.153}$$

Substituting from Eq. (2.150) for p'_z, we have:

$$\begin{aligned}\frac{dq_y}{dt} &= -kmc^2\frac{q_y^2}{4q_z^2}A_0[\sin(kz-\omega t+\theta_y)+\sin(kz-\omega t-\theta_y)],\\ &\approx -\omega_\beta A_0\sin(\psi_1),\end{aligned} \tag{2.154}$$

this result confirms the deficiency of Whittum's formulation in the derivation of Eq.(2.147) that was found using the eikonal assumption.

2.3.3 Gain Parameter Without the Small Betatron Amplitude Approximation

A more structural and important difference between the two formulations is that in Whittum's original treatment, the small betatron amplitude approximation, i.e. $q_x,\ q_y \ll 1$, is used to calculate the second-order derivative of the ponderomotive phase $\psi_y = \theta_y + kz - \omega t$ (and the bunching parameter),

$$\frac{d^2\psi_y}{dt^2} = \frac{(k_z c)^2}{4q_z^4}q_y\Big(2+\frac{3}{4}q_y^2-2\frac{\omega_\beta}{k_z c}q_z^2\Big)A\sin(\psi_y), \tag{2.155}$$

which is equal to the second-order derivative of ψ without the derivative of the betatron oscillation term $(-r_\beta^2/8\gamma)' = [r_\beta^3 k_z c/(16\sqrt{2}\gamma^{5/2})]A_0\sin(\psi)$. The value of ρ in this small betatron amplitude approximation can be obtained from our equations of motion to be:

$$\rho = \left[\frac{\omega_b^2 R_\beta^2}{\gamma_r c^2}\Big(\frac{1}{2}+\frac{1}{2}\Big)\right]^{1/3} \approx \Big(\frac{2I}{I_0\gamma_r}\Big)^{1/3}, \tag{2.156}$$

which is just the general expression of (2.86) evaluated at $r_b \approx R_\beta$ and $a_\beta \ll 1$. With the assumption of $R_\beta = r_b$, it appears that the ρ parameter for large R_β is less than ideal as formally it is always reduced by a factor of one half from the expression with equal γ_r and negligible betatron amplitude. Such an assumption, as used in Whittum's original formulation, however, is unnecessary and unrealistic. Furthermore, the ρ value obtained under large R_β condition is usually much larger than under the small-betatron amplitude limit.

2.3.4 Dielectric Guiding

For finite electron bunch width, small compared to the betatron amplitude, the size of the radiation source is determined by the latter. Under the idealized assumption that electrons radiate in vacuum, i.e., disregarding the dielectric properties of the plasma channel, the radiation will diffract within a Rayleigh length $L_R \approx \pi R_\beta^2/\lambda$, where λ is the radiation wavelength. Using the resonance condition, it can be shown that L_R is shorter than the gain length $L_g = \lambda_\beta/(\sqrt{3}\pi\rho)$, so that diffraction would suppress the gain. Therefore, diffraction cannot be neglected and waveguiding in the plasma channel must be considered. Neglecting any influence from the electron beam, the waveguide can be considered as having a step discontinuity in the dielectric constant,

$$\epsilon(r,\omega) = 1 - \frac{\omega_p^2}{\omega^2}\Theta(r - r_c),$$

where $r = \sqrt{x^2 + y^2}$ is the radial coordinate, r_c the channel radius, and Θ the Heaviside step function. Such a waveguide will always have at least one guided mode, the HE11 mode. In the limit $\omega \gg \omega_p$, the overlap between this laser mode and the beam can be calculated using the results of Marcuse [49] and Snitzer [50]. The transverse distribution of the vector potential of the HE11 mode with frequency ω and axial wave number k is

$$A_y(\mathbf{r},t) = a_r(z,t)\exp(i[kz - \omega t])F(r), \tag{2.157}$$

where

$$F(r) = \begin{cases} \mathrm{J}_0(\kappa r) & \text{for} \quad r < r_c, \\ \dfrac{\kappa \mathrm{J}_0(\hat{\kappa})}{\mu \mathrm{K}_0(\hat{\mu})}\mathrm{K}_0(\mu r) & \text{for} \quad r \geq r_c, \end{cases} \tag{2.158}$$

satisfies $[\nabla_\perp^2 + \epsilon(r,\omega)\omega^2/c^2 - k^2]F(r) = [d(r\,dF/dr)/dr]/r + \omega^2/c^2 - (\omega_p^2/c^2)\Theta(r - r_c) - k^2 = 0$ for $(\omega^2 - \omega_p^2)/c^2 < k^2 < \omega^2/c^2$, i.e., J_0 and K_0 are the zeroth order Bessel and second-kind modified Bessel functions, respectively, $\kappa = \sqrt{\omega^2/c^2 - k^2}$, $\mu = \sqrt{k^2 + (\omega_p^2 - \omega^2)/c^2}$, $\hat{\kappa} = \kappa r_c$, and $\hat{\mu} = \mu r_c$.

Substituting the vector potential (2.157) into the Helmholtz wave equation

$$\left(\nabla^2 - \frac{1}{c^2}\frac{\partial^2}{\partial t^2}\right) a_r(z,t)\exp(i[kz - \omega t])F(r) = -\mu_0 J_y(\mathbf{r},t), \tag{2.159}$$

using $[\nabla^2 - \partial^2/\partial(ct)^2]\exp(i[kz-\omega t])F(r) = 0$, and neglecting second derivatives of a_r, we obtain

$$2i\left(k\frac{\partial a_r}{\partial z} - \frac{\omega}{c^2}\frac{\partial a_r}{\partial t}\right)\exp(i[kz-\omega t])F(r) = -\mu_0 J_y(\mathbf{r},t). \tag{2.160}$$

We then move $\exp[i(kz-\omega t)$ to the RHS and project the current density profile on F(r)

$$2i\left(k\frac{\partial a_r}{\partial z} - \frac{\omega}{c^2}\frac{\partial a_r}{\partial t}\right) = -\frac{\mu_0}{\Sigma}\iint_{-\infty}^{\infty} dxdy\, F^*(r)\exp(-i[kz-\omega t])J_y(\mathbf{r},t), \tag{2.161}$$

where

$$\Sigma = 2\pi\int_0^\infty dr\, r|F(r)|^2 = \pi r_c^2\{\mathrm{J}_0^2(\hat{\kappa}) + \mathrm{J}_1^2(\hat{\kappa}) + (\hat{\kappa}/\hat{\mu})^2\mathrm{J}_0^2(\hat{\kappa})[\mathrm{K}_1^2(\hat{\mu})/\mathrm{K}_0^2(\hat{\mu}) - 1]\} \tag{2.162}$$

is the effective cross section of the radiation mode (2.158). The r.h.s. becomes slowly varying close to resonance, $\omega - kv_z = \omega_\beta$, when it can be averaged in a manner similar to (2.38) to become

$$2i\left(k\frac{\partial a_r}{\partial z} - \frac{\omega}{c^2}\frac{\partial a_r}{\partial t}\right) = -\frac{\mu_0}{\Sigma}\sum_j\iint_{-R_\beta}^{R_\beta} dxdy\, F^*(r)\sqrt{1-y^2/R_\beta^2}\exp(-i[kz_j-\omega t])\delta(y-y_j), \tag{2.163}$$

As in (2.38) , we retain only the lowest order term $\cos(\theta)\cos(\theta_j)$ in the Fourier series expansion of the current density, to calculate the intgeral for the mode (2.158), which is

$$\int_{-\pi}^{\pi} d\theta\, F^*(R_\beta\sin\theta)R_\beta\cos(\theta)^2 = \frac{\pi R_\beta}{2}\left[\mathrm{J}_0^2(\kappa R_\beta/2) + \mathrm{J}_1^2(\kappa R_\beta/2)\right]. \tag{2.164}$$

The spatial overlap factor of current density and radiation mode, obtained by comparing the wave equation with its one-dimensional equivalent, is

$$\eta = \frac{\pi R_\beta^2}{2\Sigma}\left[\mathrm{J}_0^2(\kappa R_\beta/2) + \mathrm{J}_1^2(\kappa R_\beta/2)\right] = \frac{R_\beta^2}{2r_c^2}\frac{\mathrm{J}_0^2(\kappa R_\beta/2) + \mathrm{J}_1^2(\kappa R_\beta/2)}{\mathrm{J}_0^2(\hat{\kappa}) + \mathrm{J}_1^2(\hat{\kappa}) + (\hat{\kappa}/\hat{\mu})^2\mathrm{J}_0^2(\hat{\kappa})[\mathrm{K}_1^2(\hat{\mu})/\mathrm{K}_0^2(\hat{\mu}) - 1]}. \tag{2.165}$$

For small betatron amplitude, $\kappa R_\beta \ll 1$, this simplifies to

$$\eta \approx \frac{R_\beta^2/(2r_c^2)}{\mathrm{J}_0^2(\hat{\kappa}) + \mathrm{J}_1^2(\hat{\kappa}) + (\hat{\kappa}/\hat{\mu})^2\mathrm{J}_0^2(\hat{\kappa})[\mathrm{K}_1^2(\hat{\mu})/\mathrm{K}_0^2(\hat{\mu}) - 1]}. \tag{2.166}$$

With η thus defined, the ρ parameter in the large R_β limit can be reformulated to include the effect of finite bunch width:

$$\rho = \left(\frac{\eta \omega_b^2 R_\beta^2}{2\gamma c^2} \right)^{1/3}. \tag{2.167}$$

2.4 Numerical Simulations

2.4.1 Numerical Algorithms

Phase Space Distribution Generation and Steady State Simulation

To carry out a successful ICL simulation, the first step is to generate an initial phase space distribution for the electron bunch that represents the distribution of real electrons with sufficient accuracy. To simulate a FEL electron bunch under typical conditions, the large number of electrons per bunch, typically on the order of 10^9-10^{11} and $10^4 - 10^6$ per wavelength in the X-Ray spectral regime, makes it computationally prohibitive to simulate using all the electrons. As an alternative, macro particles, each of which represents an aggregation of particles with similar dynamic variables, have to be used. The use of macro particles, however, introduces artificial numerical noise. The electron bunch generated by the wakefield acceleration experiments, however, are ultrashort (bunch length $1 - 10\ \mu m$) and usually have a lower electron number in the range of $10^6 - 10^8$. This makes it possible, in principle, to simulate all electrons independently, avoiding the numerical noise introduced by using macro particles. To make sure the unbunched electron beam generates no radiation field, the initial distributions of the electron phase and γ and r_β should be random and uniform so that the initial bunching factor is zero. We make use of the Hammersley sequence generator in the open sourced code **GENESIS** [52], and pair particles in phase. (Unfortunately, pairing does not always work for warm beams because the phase-space distribution gets mixed up very quickly erasing the effect of pairing.) Pairing is done by loading half of the macroparticles with their phases evenly distributed in the range of $0 < \psi < \pi$, and copying them into the remaining phase, while keeping other coordinates unchanged. Having a particle with exactly the same set of dynamic variables except a phase difference of π, the code proceeds to numerically solve a set of $2N_e + 1$ ordinary differential equations, Equations (2.66) - (2.68), using a fourth-order Runge Kutta integrator. In a steady-state simulation with slippage neglected, due to the absence of spatial fluctuation in the electron beam, only electrons in one wavelength need to be simulated.

2.4.2 The Coupled-Equation Solver

The Maxwell-Newtonian equations for the ICL contain two differential equations for the coordinates of each (macro) particle, and one wave equation using the sum of the particle phase factors as its source term. These equations can be solved following a simple explicit leapfrog integration procedure: For a simulation after n steps, with length Δt, we use the electron coordinates and radiation field vector potential as the initial values and source term of the particle equations (2.41), (2.42), respectively, to advance the particles by one step using the Runge-Kutta fourth-order formula:

$$y_{n+1} = y_n + \Big(\frac{k_1}{6} + \frac{k_2}{3} + \frac{k_3}{3} + \frac{k_4}{6}\Big)\Delta t, \tag{2.168}$$

with

$$k_1 = f(t_n, y_n), \tag{2.169}$$

$$k_2 = f\Big(t_n + \frac{\Delta t}{2}, y_n + \frac{k_1}{2}\Big), \tag{2.170}$$

$$k_3 = f\Big(t_n + \frac{\Delta t}{2}, y_n + \frac{k_2}{2}\Big), \tag{2.171}$$

$$k_4 = f(t_n + \Delta t, y_n + k_3). \tag{2.172}$$

After the particle coordinates are obtained, they are summed up as the source term of the wave equation, and used to advance the wave equation using the same Runge-Kutta integrator, and vice versa.

The space charge and betatron amplitude variation effects are included by simply substituting terms proportional to the "old" wave equation source term into the particle equations.

2.4.3 Parameter Selection

Two important parameters to be decided before a steady-state simulation are the number of integration steps and the number of particles used. Saturation will usually occur after 50-100 plasma wavelengths, given the range of ICL's ρ value. In order to average out the fluctuation in γ within one betatron period, enough sampling points should be used for one half of a betatron period, the number of sampling points used per plasma period should theoretically scale with $1/\sqrt{2\gamma}$, in the steady state simulation it is observed that 10-20 points per plasma period are adequate for approximating both the exponential growth in the linear regime and the synchrotron oscillation in the nonlinear regime. There is more flexibility in the choice

of the number of macro particles, depending on the radiation wavelength and the current density. To start the simulation with an uncorrelated electron bunch, however, the number of electrons must be even, so that each electron can be paired with another with exactly π difference in phase. It should also be noted that the assumption of a negligible space charge field is only valid as long as the electron density of the bunch is much smaller than the channel plasma density, so that the electrostatic field of the ions dominates. In the wakefield acceleration experiments, it is observed that the total charge of the bunch produced is in the range of 5-10 pC, which amounts to $3-6\times10^7$ electrons, and translates to an electron density of $10^{20}-10^{22}$ cm^{-3}, at least ten times bigger than the theoretically attainable plasma density for an ion channel, which is oF the order of $10^{18}-10^{19}$ cm^{-3}. Divided by the number of wavelengths that can be accommodated in an electron bunch, the number of macroparticles to be used for an X-Ray regime steady state simulation should be in the range of 10^4-10^6, with each macroparticle accounting for about 30-3000 real electrons.

2.4.4 Compton Simulation Results and Analysis

In this chapter we numerically study several examples of ion channel lasers designed for different wavelength ranges. In the first section, variants of a microwave ICL will be investigated. Because microwave propagation in the channel is strongly influenced by the dielectric guiding effect, waveguiding will be included in our analytical predictions and numerical simulations. In the second section, the simulations will be carried out for two different radiation wavelengths in the X-Ray spectral range, which is the region of interest for practical applications. With the exception of X-ray regime simulation and the large betatron amplitude simulation in the UV regime, all simulations are conducted using the parameters used in the simulation of the corresponding wavelength in Whittum's ion channel laser thesis [2], for the purpose of better comparison.

The influence of detuning spread and spread in the transverse energy will also be studied, in addition to the influence of guiding on the efficiency on the laser-electron interaction. The guiding effect is calculated using Eq.(2.157).

2.4.5 Simulations in the Microwave Regime

In this section, high gain ICL designs in the microwave region are considered using parameters in the following table, relying solely on dielectric guiding, but subject to different initial detuning and spread conditions. The channel radius is thus considered to be relatively large,

i.e., $r_c/r_b \gg 1$. The simulation is conducted using the parameters in the following table:

Table 2.1: **Microwave Parameters**

λ(cm)	1.75
E(MeV)	2
I(kA)	4
$\mathrm{n_p}(\mathrm{cm}^{-3})$	6.2×10^{10}
λ_β(cm)	36
r_b(cm)	1

At I=4 kA, the overlap between the laser beam and the electron bunch for the HE11 mode can be computed to be 0.066 using Eq.(2.166) with $V = \sqrt{\hat{\kappa}^2 + \hat{\mu}^2} = 0.9$, which gives a ρ value of 0.28 (FEL equivalent ρ of 0.07). The gain length L_g is thus 33 cm according to (2.84), the saturated beam power is expected to be $\rho E_w = Imc^2\rho\gamma/4e = 560$MW, where E_w is the electron beam power, which is about 8 GW in this case. For an initial field power P_0 of 66 kW, the power should theoretically grow 2.4×10^4 times before it reaches saturation. The minimum length of ion channel required to reach radiation power saturation can be calculated, using equation (2.85) to be $L_{sat} \approx L_g \ln(9P_{sat}/P_0) = 266$ cm, which is confirmed by the numerical result shown below.

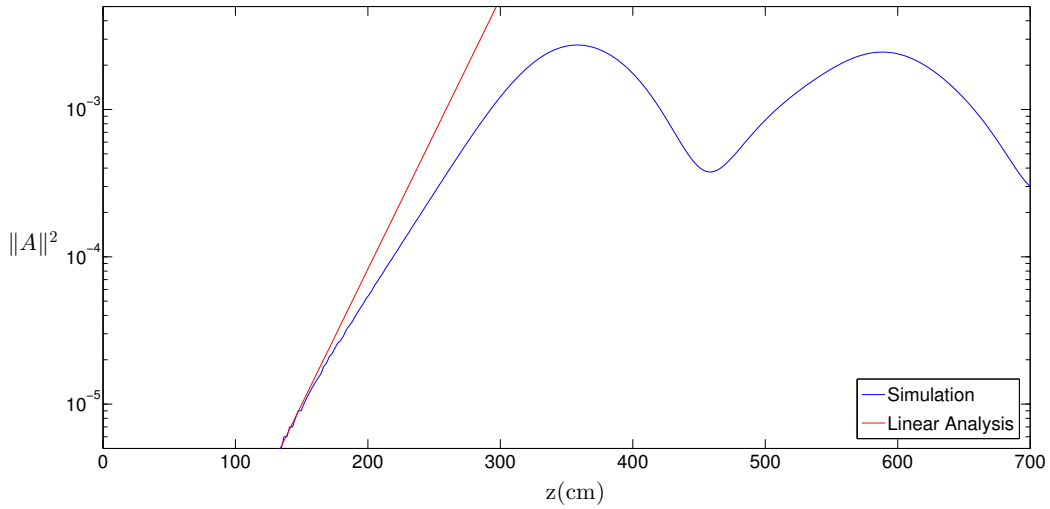

Figure 2.5: The radiation power growth versus z for $\gamma = 3.9$, $r_b = 1$ cm, $\lambda = 1.75$ cm, the red curve shows the exponential growth prediction of linear analysis, in contrast to the blue curve which is the simulation result obtained by solving (2.41)-(2.43) with the parameters in Table 2.1, plotted on a semi-log scale.

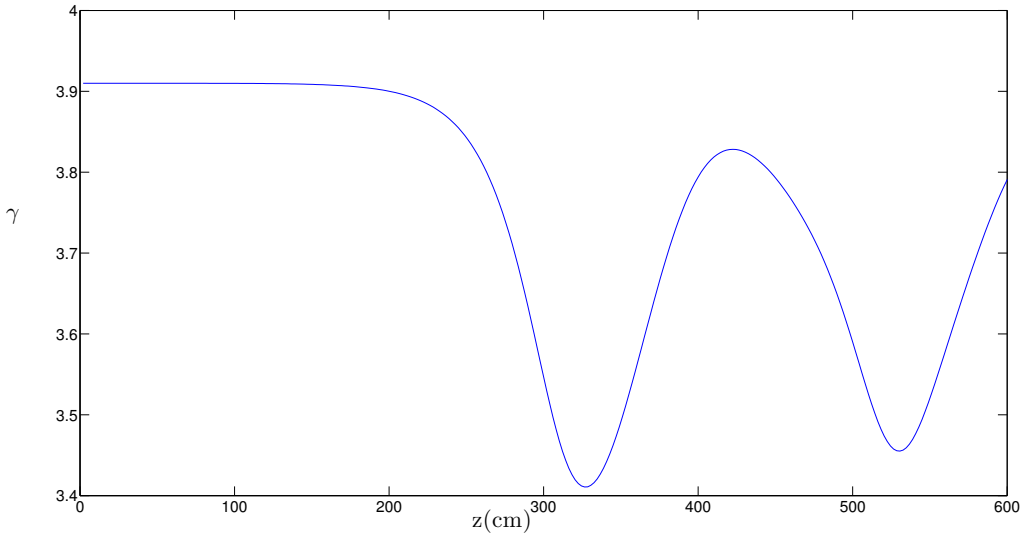

Figure 2.6: Simulated beam energy versus z for the same microwave parameters in Table 2.1.

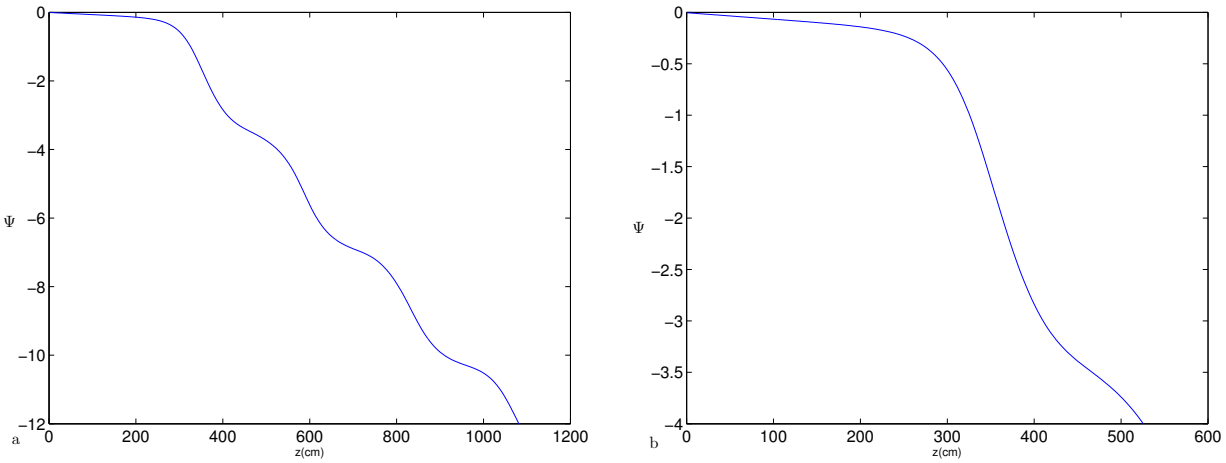

Figure 2.7: a. Averaged ponderomotive phase versus z throughout the interaction. b. close-up of the phase variation at the onset of nonlinearity. Simulated with the same parameters as in Fig. 2.5

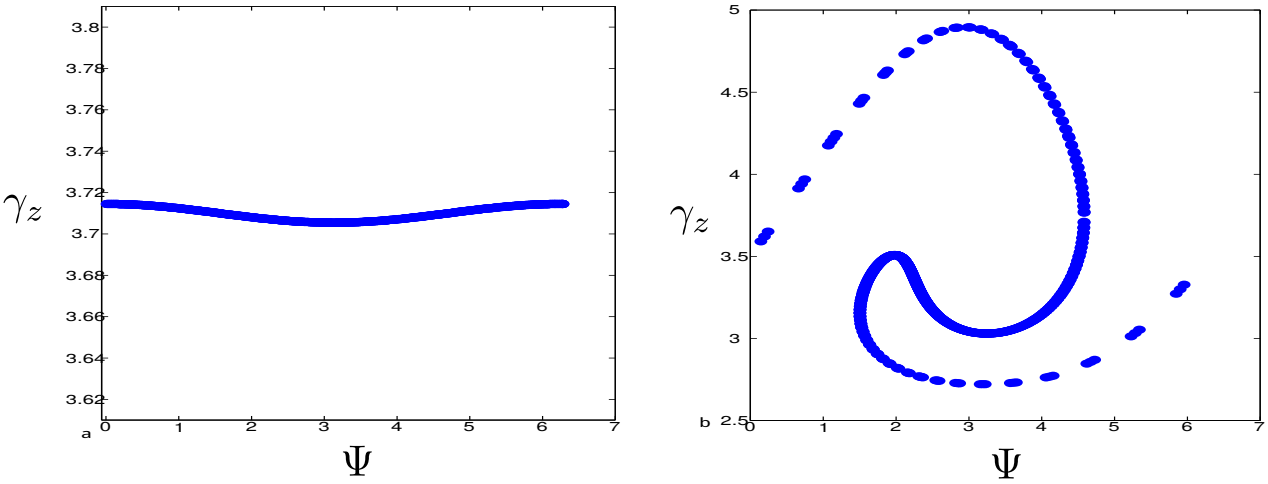

Figure 2.8: a. Phase space plot for the electron beam at the onset of linear amplification using selected samples of electron coordinates from the simulated electron bunch. b. Phase space plot for the same bunch at the onset of nonlinearity. Simulated with the same parameters as in Fig. 2.5

The electrons, evenly distributed along the ψ axis at the onset of amplification, become concentrated in small regions separated by intervals of no electron, i.e., forming small "bunches" in the phase space, at the onset of nonlinearity. The electron bunches tend to concentrate near the centre of the ψ axis, where $\psi = \pi$, and become more sparsely distributed

at both ends of the axis, where $\sin(\psi) = 0$, meanwhile, the electron distribution along the γ axis shows similar features, symmetrically forming bunches on both sides of the line $\gamma = 3.3$, the average value of γ of the electrons at saturation.

We check the simulation result with the energy conservation relation (2.81), which gives the error of energy conservation to below $\epsilon \approx 0.4\%$. Simulations using different energy spreads σ_γ and betatron amplitude spread σ_{r_β} are also carried out, showing different degrees of reduction to the saturation power. The cut-off energy spread for the amplification is at $\sigma_\gamma = 28\%$, about ρ, in rough agreement with the theory.

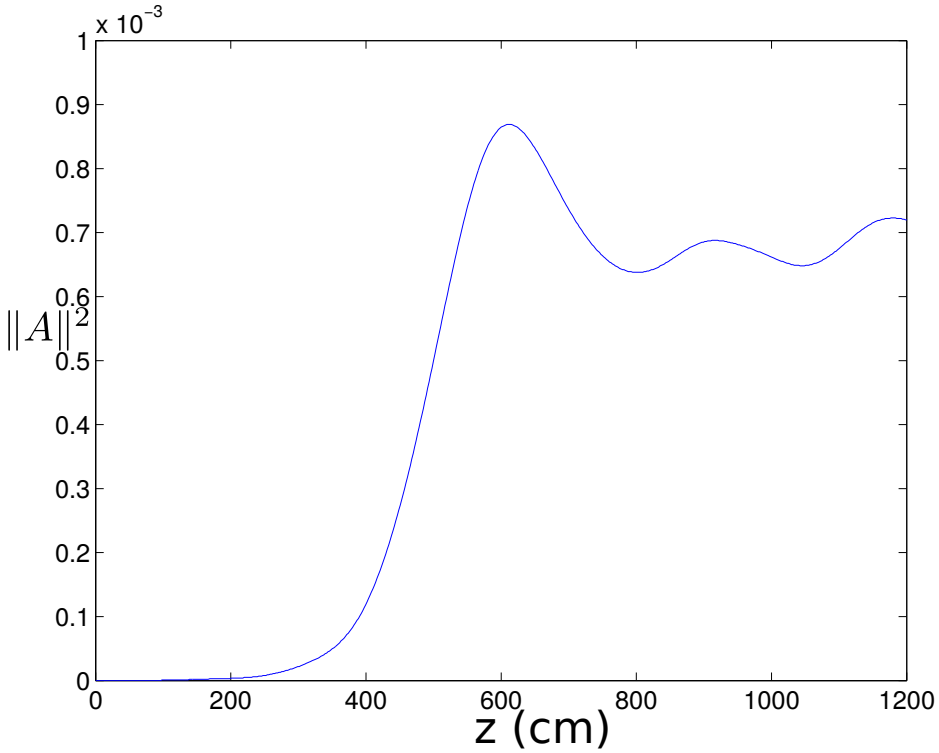

Figure 2.9: The radiation power plot for σ_γ=0.14 simulated with the parameters in Table 2.1

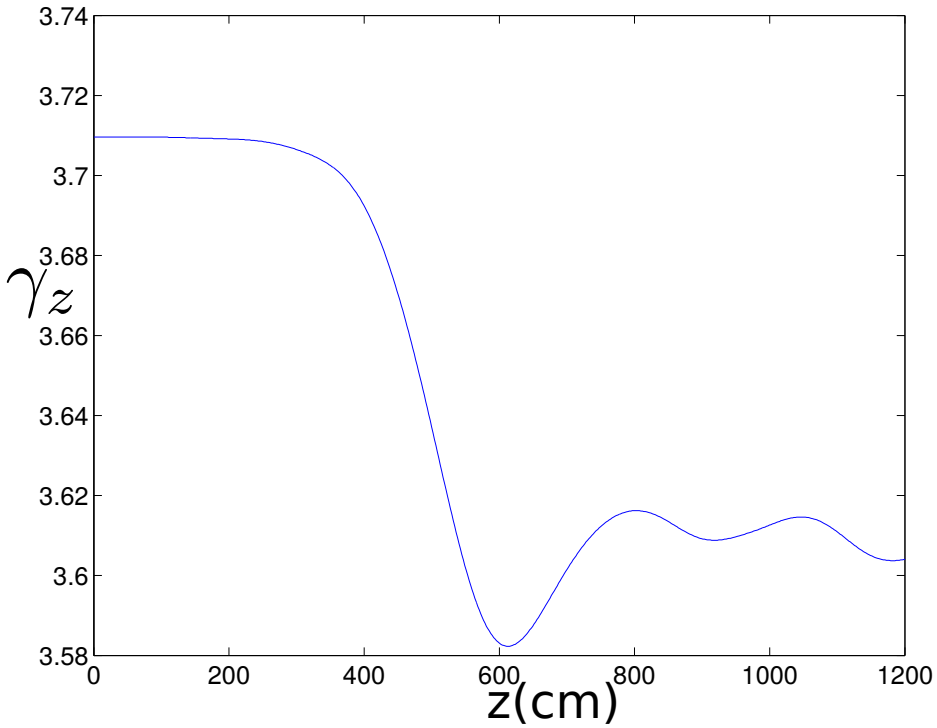

Figure 2.10: The beam energy evolution plot for σ_γ=0.14 simulated with the parameters in Table 2.1

2.4.6 Sub-millimetre Example

In this section, we present a simulation for sub-millimetre radiation wavelength using the parameters in the following Table:

Table 2.2: **Sub-millimetre Parameters**

$\lambda(\mu\text{m})$	484
$E(\text{MeV})$	4
$I(\text{kA})$	4
$n_p(\text{cm}^{-3})$	7×10^{12}
$\lambda_\beta(\text{cm})$	4.84
$r_b(\text{cm})$	6×10^{-2}

The overlap integral can be estimated to be 0.018 using Equation (2.166) with $V = 0.8$,which leads to a ρ parameter of 0.108 (FEL equivalent ρ of 0.027). The total beam power is about 16 GW, which could thus generate a radiation power of $2.7\% \times 16$ GW $= 425$ MW, the gain length is thus 8.16 cm, for an input power P_0 of 2 kW, the saturation length should be $L_g \ln(9P_{sat}/P_0) = 1.18$ m, while the simulation gives a saturation length of 1.29 m, confirming the theoretical prediction.

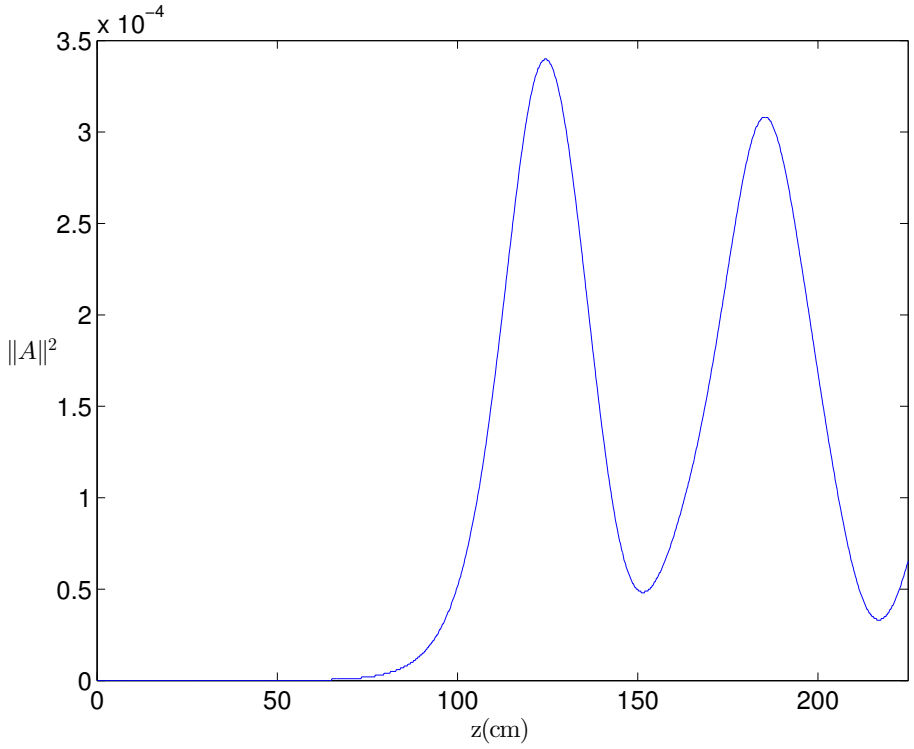

Figure 2.11: Plot of simulation result for the evolution of radiation power, obtained by numerically solving (2.41)-(2.43) with parameters set forth in the Table 2.2

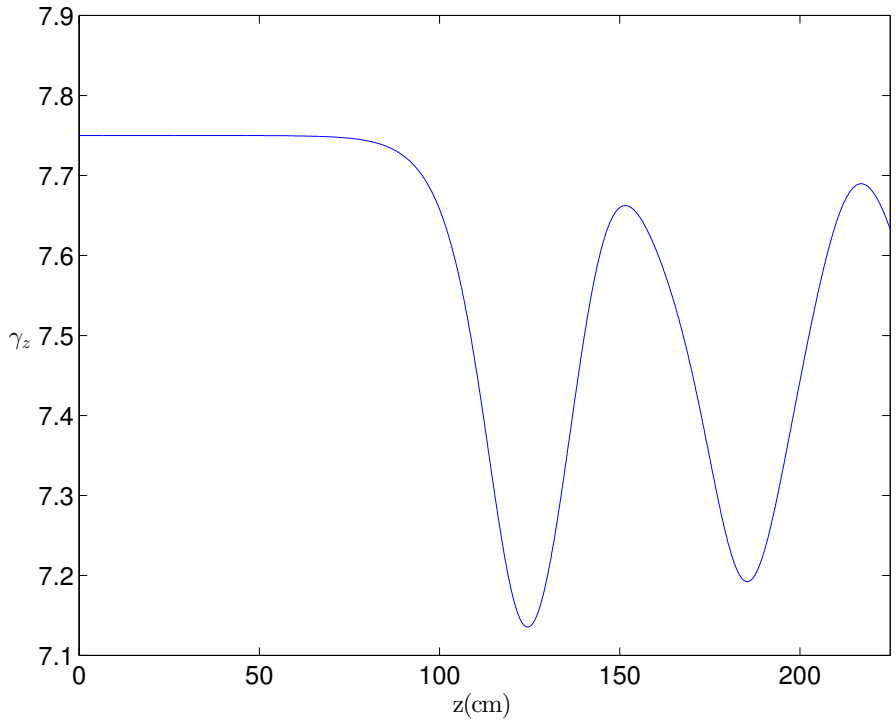

Figure 2.12: Plot of simulation result for the evolution of electron beam energy in units of mc^2, obtained by numerically solving (2.41)-(2.43) with parameters set forth in the Table 2.2

2.4.7 Infra-red Regime

In this section, we consider one example in the infrared regime, the amplification of 10 μm radiation, with the typical wavelength of a CO_2 laser, and a great number of industrial applications.

We simulate for the following parameters:

Table 2.3: **Infrared Parameters**

$\lambda(\mu\text{m})$	10
$E(\text{MeV})$	10
$I(\text{kA})$	4
$n_p(\text{cm}^{-3})$	1×10^{15}
$\lambda_\beta(\text{cm})$	0.7
$r_b(\text{cm})$	3×10^{-3}

The overlap integral is estimated to be 0.007 for $V = 0.62$ using Equation (2.166), which gives a ρ parameter of 0.0385. The total beam power is about 38 GW, which could can generate a radiation power of 350 MW. The gain length is 3.34 cm for an input power P_0 of 140 kW, the saturation length should be $L_g \ln(9P_{sat}/P_0) = 33.47$ cm, while the simulation gives a saturation length of about 29.4 cm, roughly confirming the prediction of the theory.

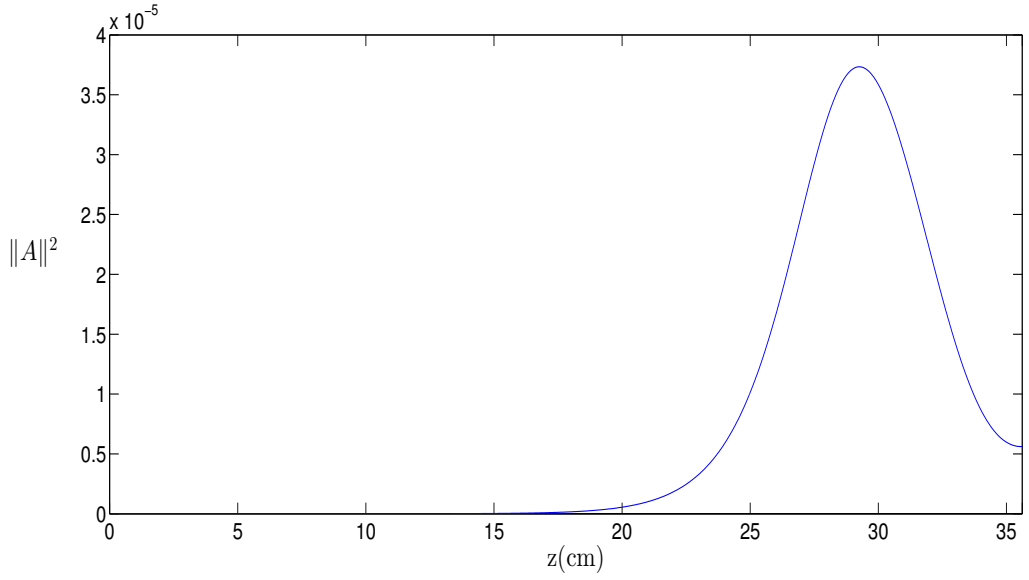

Figure 2.13: Plot of simulation result for the evolution of radiation power, using Eqs. (2.41)-(2.43) and parameters set forth in the Table 2.3

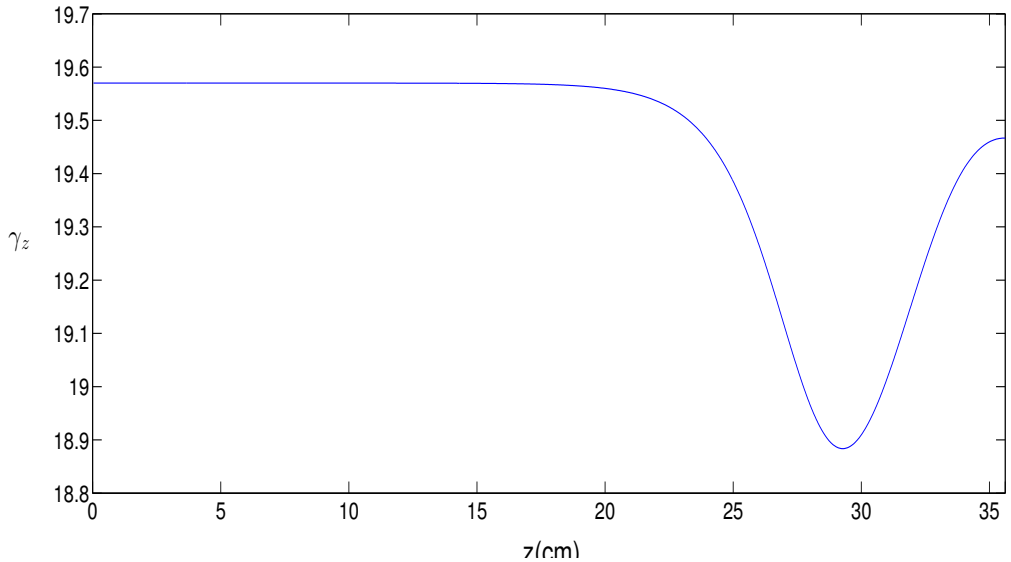

Figure 2.14: Plot of simulation result for the evolution of electron beam energy in units of mc^2, using Eqs. (2.41)-(2.43) and parameters set forth in the Table 2.3

2.4.8 X-Ray Regime

Due to the difficulty of producing a small-betatron amplitude electron beam, the careful adjustment of beam and channel parameters is essential to the production of coherent X-ray radiation using an ion channel, since the resonance condition must be satisfied within the experimental limitations. The following figure shows for a fixed combination of γ and r_β that, as the plasma wavelength increases, the radiation wavelength decreases at a rapid rate until it reaches about 5 nm, where the steep curve flattens out. The wavelength should thus ideally be chosen within the region of the greatest curvature, to minimize the output wavelength and the plasma wavelength (which determines the gain length L_g along with ρ) together, so that X-ray radiation can be sufficiently amplified within an ion channel of experimentally realistic length.

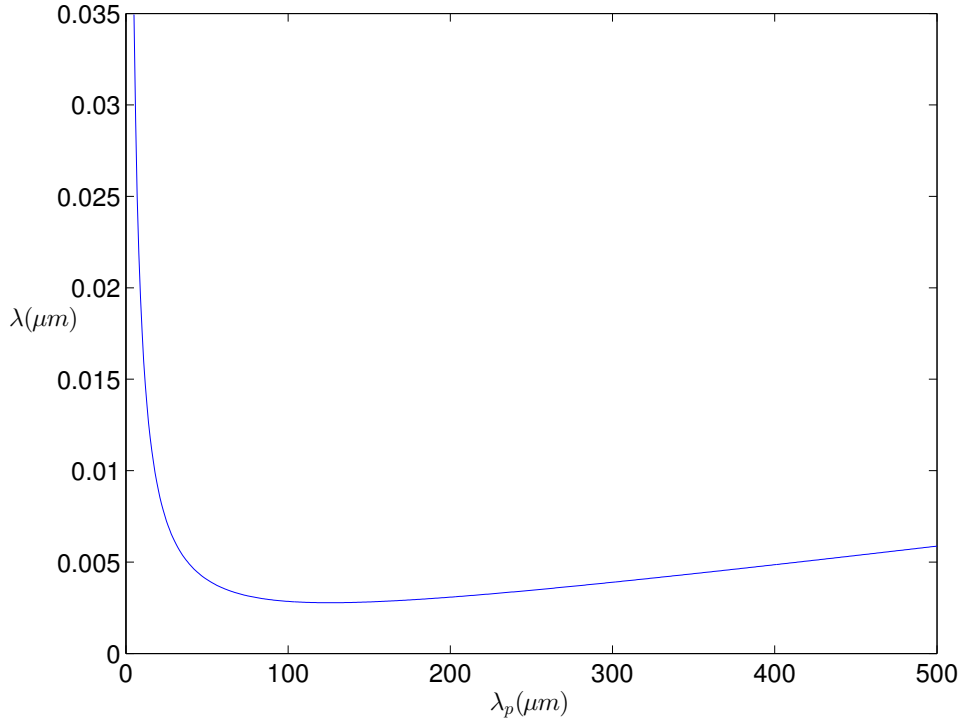

Figure 2.15: Resonant wavelength λ as a function of channel plasma wavelength λ_p for $\gamma = 1600$, $r_b = 1\mu m$

Table 2.4: **Soft X-ray Simulation Parameters**

λ(nm)	6
E(MeV)	800
I(kA)	4
$n_p(\text{cm}^{-3})$	1×10^{18}
λ_β(cm)	0.181
$r_b(\mu\text{m})$	1
$R_\beta(\mu\text{m})$	2

In the X-ray regime with the parameters above, we can calculate an overlap factor of 0.0553 for a channel radius of about 45 μm. This leads to a ρ parameter of 0.026 (FEL equivalent ρ of 0.0065), the total electron beam power is about 3.2 TW, which can generate a radiation power of 0.0065×3.2 TW $= 20.8$ GW. The gain length is 12.79 mm. For an experimentally achievable input power P_0 of 10 W, the saturation length is $L_g \ln(9P_{sat}/P_0)$ = 27.3 cm. While a channel of such a length may be difficult to maintain experimentally, 10-15 cm of amplification medium can produce a significant amount of coherent X-ray radiation. However, creating a channel with a radius at least an order of magnitude larger than the betatron amplitude could prove to be a significant engineering challenge. Radiation of Ångström wavelength could potentially be produced if electrons with an energy of 2.5 GeV or more are used, and the 1μm betatron amplitude is maintained; the ρ value in this case is in the range of 0.01-0.015, indicating that an amplifier efficiency of an order of magnitude larger than can be achieved by state-of-the-art XFEL such as the LCLS [17].

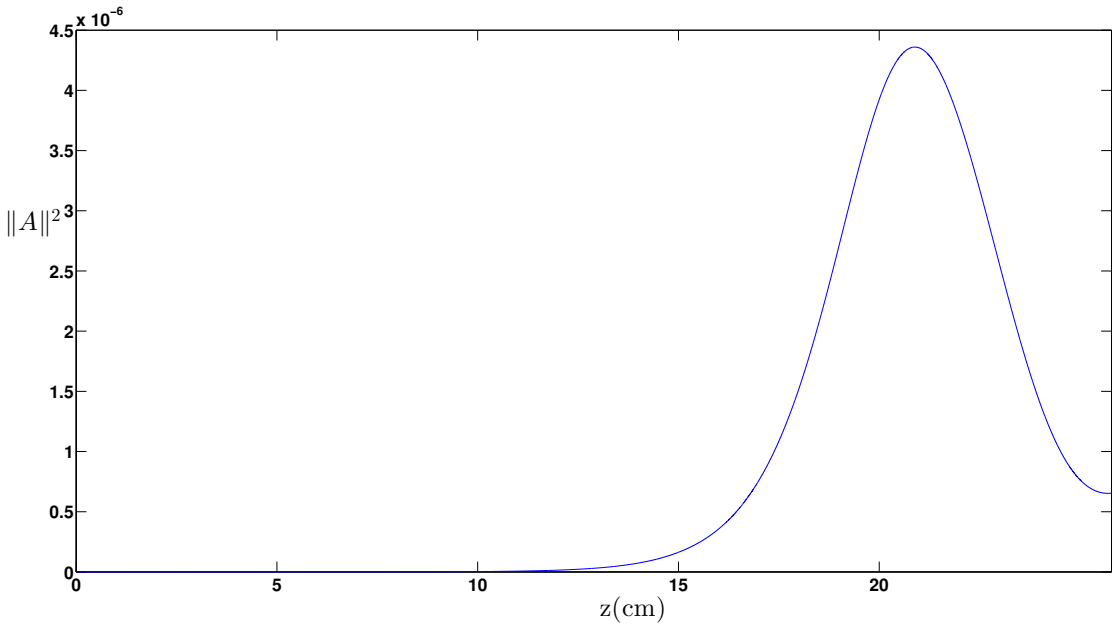

Figure 2.16: The field intensity evolution generated by solving Eqs. (2.41)-(2.43) using the X-ray parameters given in the Table.2.4.

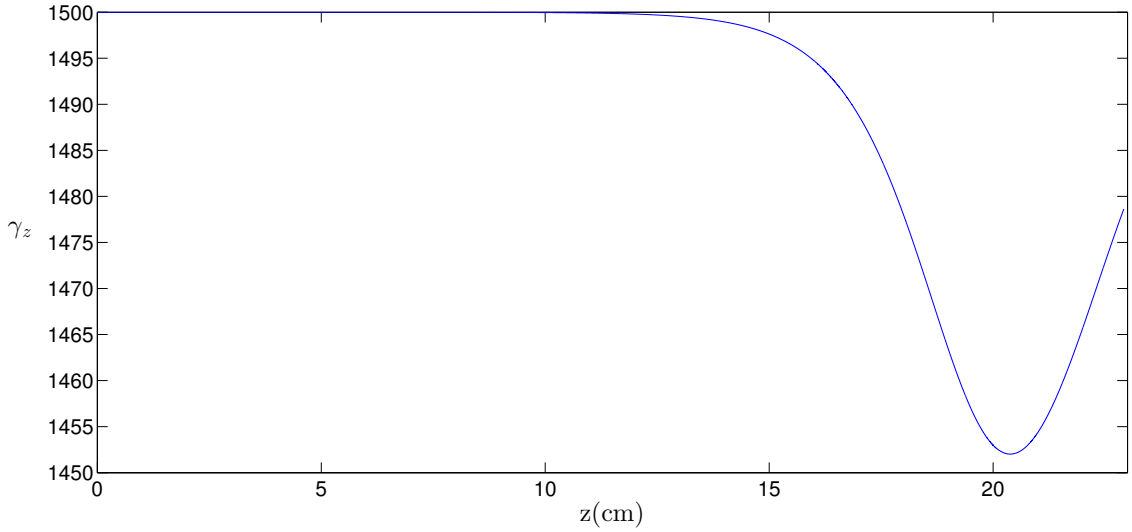

Figure 2.17: The electron beam energy evolution generated by solving Eqs. (2.41)-(2.43) using the X-ray parameters given in the Table 2.4.

We can see that the simulation indicates an efficiency of about 3%, which is in good agreement with the analytical prediction; the saturation took place after about 20 cm.

2.4.9 Large Betatron Amplitude Beam Simulation in the UV Regime

As can be calculated using Eq.(2.157), when $R_c \approx R_\beta \propto \lambda_p$, the overlap factor will be close to 1 thanks to the weak guiding effect, which makes ICL very useful for generating high-power UV radiation. Consider $R_\beta = 2$ μm, $r_b = 0.12$ μm. The condition $r_b \ll R_\beta$ requires the electron beam to have an intrinsic betatron amplitude spread; for a uniform distribution, we have $r_b = \sigma(r_b) \approx 0.12$ μm where $\sigma(f) = (\langle f^2 \rangle - \langle f \rangle^2)^{1/2}$. The simulation parameters can be derived from these conditions to be:

Table 2.5: **Ultraviolet Parameters with Large Betatron Amplitude**

λ(nm)	73
E(MeV)	400
I(kA)	0.07
n_p(cm^{-3})	3.2×10^{18}
λ_β(cm)	0.054
$r_b(\mu$m)	0.12
$R_\beta(\mu$m)	2

This give a ρ value of 0.07 (FEL equivalent ρ of 0.0175), the efficiency is thus 1.75% for a beam without detuning.

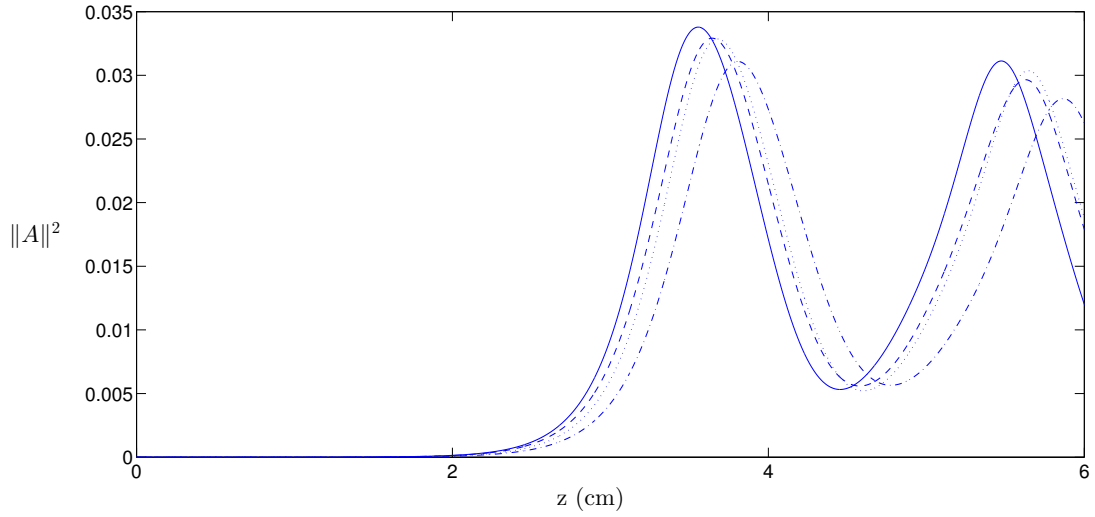

Figure 2.18: Evolution of field intensity under small spread conditions obtained via solving Eqs. (2.41)-(2.43) with parameters in Table 2.5 and a variety of initial spread conditions: The solid line corresponds to the on-resonance result ($\mu_{\bar{q}} = \mu_{\bar{s}} = 0$), while the data obtained with only energy/ betatron amplitude spread are shown with the dashed ($\mu_{\bar{q}} = 0.5$, $\mu_{\bar{s}} = 0$) and dotted ($\mu_{\bar{s}} = 0.5$, $\mu_{\bar{q}} = 0$) lines, respectively. The dash-dotted line indicates the data obtained using the condition $\mu_{\bar{q}} = \mu_{\bar{s}} = 0.5$.

The simulation result is in good agreement with the Compton regime analysis for the small-spread condition: the values of the peak intensity and gain factor obtained using only energy and betatron amplitude spread conditions are nearly equal, but smaller than that in the resonant case, while the peak intensity and gain obtained using both spread conditions is even smaller. In the large spread scenario, however, the theory in Sec.2.2.8 has predicted larger ρ, and correspondingly shorter gain length for electrons with both energy and betatron amplitude spreads, which we will try to determine in the following large spread simulation.

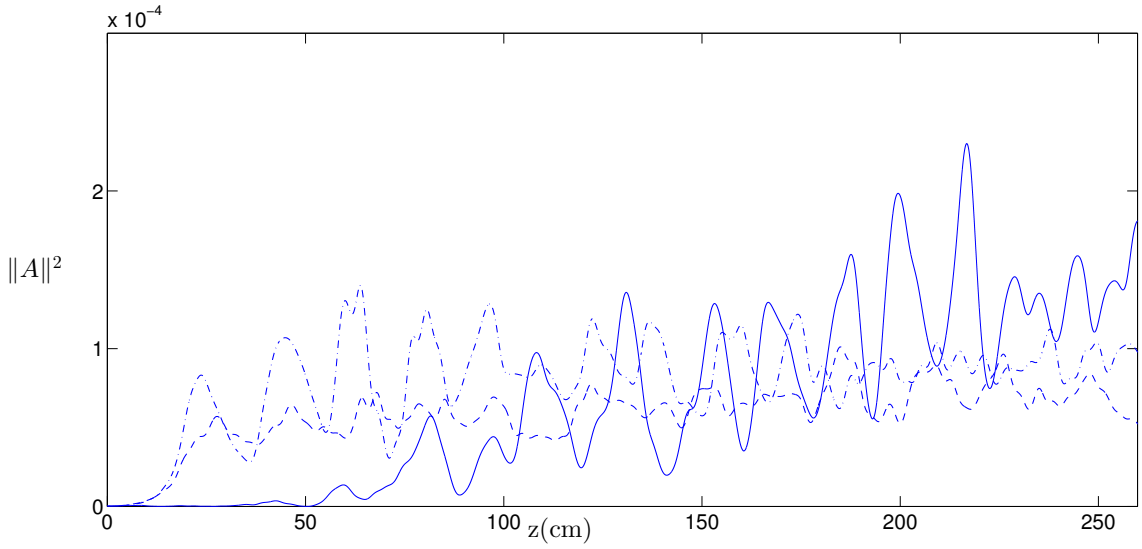

Figure 2.19: Evolution of field intensity under large spread conditions from solving Eqs. (2.41)-(2.43) with $\sigma(r_\beta) = 2.5\%$ and beam radius $r_b = 0.36\mu m$: the solid line corresponds to the betatron amplitude spread only case, while the dotted and dashed lines show the data obtained with additional energy spread condition ($\sigma(\gamma)$=10% for the dashed line and $\sigma(\gamma)$=7.5% for the dash-dotted line respectively.)

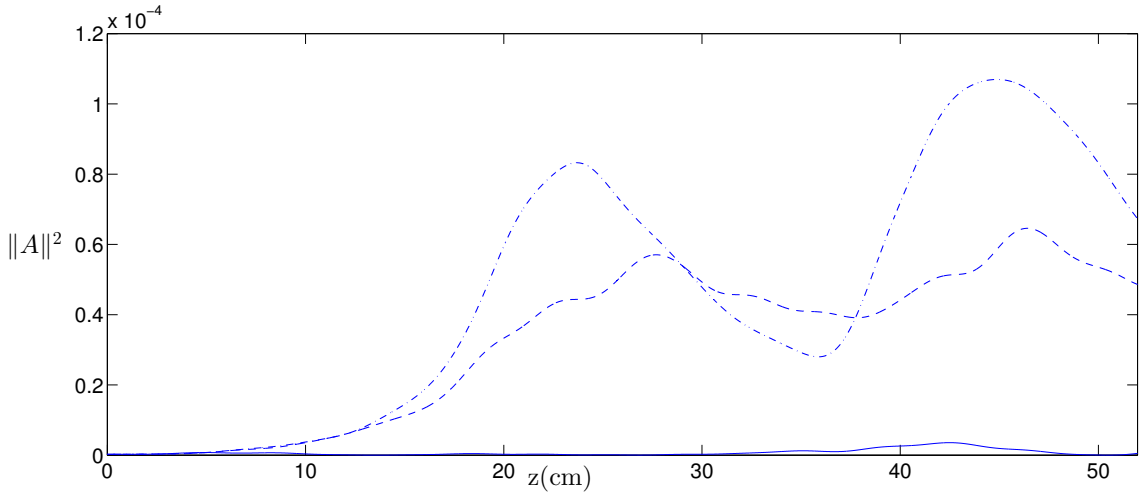

Figure 2.20: The blow-up of the Figure 1.20 for the first 50 centimeters of propagation.

The simulation result qualitatively confirms the prediction of the analysis in Sec. 1.2.8: for $\sigma(r_\beta)$ values larger than $\rho/4$, the linear regime gain is significantly larger when a γ spread is also present. Within the nonlinear regime, the peak intensity of the curve without energy spread is still the largest, which is not considered in the model described in Sec. 1.2.8. Such effects however, will not take place fully until after the laser field is propagated through a meters-long, experimentally unsustainable plasma wiggler. Therefore, it would be potentially beneficial to the amplification of the laser power to introduce an additional energy spread to the electron beam, if beams with large intrinsic betatron amplitude spread have to be used, albeit the need for unrealistically sharp edges in the electron distribution likely limits its practical benefits.

2.4.10 Raman Regime Simulation

With large curreents the ρ value could get close to 0.1 even in the UV regime, which makes the space charge and betatron variation effect non-negligible, as being shown in Sec. 1.2.7. The influence of the space charge and betatron variation effects on the value of Im(λ) is expressed through the coefficient in the first-order term of the dispersion relation, like the energy/ betatron amplitude spread. In the following plot the field intensity evolution curves simulated with such effects included are plotted side-by-side with a curve simulated under the Compton regime conditions.

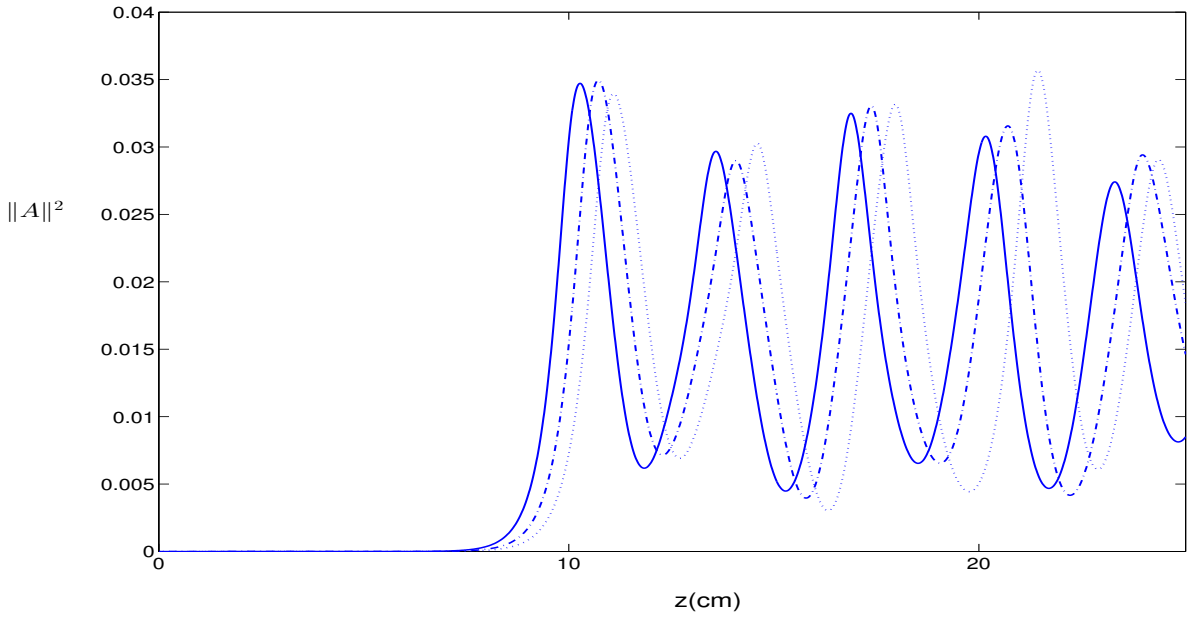

Figure 2.21: Field intensity $\|A\|^2$ versus z using the parameters in 2.5 under different theoretical assumptions, obtianed by solving Eqs. (2.41)-(2.43) and (2.48): the solid line is the Compton regime result, while the dotted line takes into account the space charge effect, and the dashed line takes into account both the space charge and the betatron variation effects.

The simulation clearly shows the reduction in the gain due to the space charge effect, as both the dashed and dotted lines display a longer saturation length compared to the solid line, the dashed line, however, exhibits a slightly shorter saturation length due to the betatron amplitude variation effect.

Chapter 3

Steady-State Theory for High-Harmonics ICL Radiation

3.1 Concept

It has been pointed out in the previous chapter that coherent radiation at wavelengths shorter than XUV would be very difficult to achieve, utilizing only the resonance between the betatron phase and the radiation phase, since a high frequency up-conversion factor can hardly be achieved for large R_β. Nevertheless, it is well understood [53] that a highly relativistic electron oscillating transversely will have a longitudinal velocity oscillating about its average, which could be integrated to give an oscillating contribution to the longitudinal (z) coordinate. When observed in the co-moving average rest frame, said electron will perform a so-called "figure-of-eight" motion. The corresponding rapid acceleration and deceleration will produce a rich spectrum of frequency components, including many harmonics, which is especially the case for large R_β oscillations performed by ICL electrons. Previous works have shown that by adjusting the γ value of the electrons, optimum gain can be achieved for a desired wavelength, with the biggest part of the total energy emitted by the electrons being released into the desired frequency component. In this section, the amplification of higher harmonics will be analyzed in a similar way, with the relation between the gain factors of the harmonics and the electron dynamic variables being derived, and the possibility of a realistic high-harmonics ICL being discussed.

3.2 Field Equation

As pointed out in the introduction, longitudinal velocity oscillations will lead to radiation emission at higher frequencies. The steady state self-consistent equations thus have to be rewritten accordingly to take into account the resonant energy exchange at higher frequencies. It is convenient to transform the wave equation to the frequency domain, using the Fourier transform relation:

$$A_y(z,t) = \frac{-i}{2}\left[\int_{-\infty}^{\infty} d\nu\, A_\nu(t) e^{i\nu k_0(z-ct)}\right] + c.c.. \tag{3.1}$$

Inserting this expression into the paraxial wave equation Eq. (2.31), we obtain:

$$\left(\frac{\partial^2}{\partial z^2} - \frac{\partial^2}{c^2\partial t^2}\right)\int_{-\infty}^{\infty} d\nu\, A_\nu(t) e^{i\nu k_0(z-ct)} = -\mu_0 J_y, \tag{3.2}$$

$$2\nu k_0 \frac{\partial A_\nu(t)}{\partial t} + \frac{\partial^2 A_\nu(t)}{\partial t^2} = -\mu_0 \int_{-\infty}^{\infty} dz\, e^{-i\nu k_0(z-ct)} J_y, \tag{3.3}$$

which after applying the SVEA approximation gives:

$$\begin{aligned}\frac{\partial A_\nu(t)}{\partial t} &= -\frac{\mu_0}{2\nu k_0}\int_{-\infty}^{\infty} dz\, e^{-i\nu k_0(z-ct)} J_y \\ &= \frac{\mu_0 e n_x}{\nu k_0 N_e}\sum_j \int\int_{-\infty}^{\infty} dz dy\, e^{-i\nu k_0(z-ct)}\omega_{\beta,j} r_{\beta,j}\sqrt{1-y^2/r_\beta^2}\,\delta(y-y_j)\,\delta(z-z_j),\end{aligned} \tag{3.4}$$

where the index j refers to a single electron, with betatron phase $\theta_j(t)$ and longitudinal position $z_j(t)$.

3.3 Particle Trajectories

To evaluate the integral on the RHS of the equation (3.4), the ponderomotive phase under the integral sign must be expressed in a form that explicitly includes jittering effect. To do this the longitudinal velocity must be expressed using $\gamma^{-2} = 1 - \beta_z^2 - \beta_y^2$ and the expression of the transverse velocity in terms of a_β and θ, $\beta_y = (a_\beta/\gamma)\cos(\theta)$, which for $1 + a_\beta^2 \ll \gamma^2$ yields

$$\beta_z = 1 - \frac{1 + a_\beta^2\cos^2(\theta)}{2\gamma^2}. \tag{3.5}$$

For constant γ this can be integrated to give

$$z = z_0(t) + \xi \sin(2\theta), \tag{3.6}$$

with $z_0(t) = ct[1-(1+a_\beta^2/2)/(2\gamma^2)]$ and $\xi = a_\beta^2 c/(8\omega_\beta\gamma^2) = a_\beta r_\beta/(8\gamma)$. The ponderomotive phase is thus

$$\psi = \theta + kz_0(t) - \omega t + k\xi \sin(2\theta). \tag{3.7}$$

The $\sin(2\theta)$ term thus introduced into the exponent gives rise to high harmonic terms, following the expansion of the exponential function

$$e^{-ik\xi\sin(2\theta)} = \sum_{m=-\infty}^{\infty} \mathrm{J}_m(k\xi)e^{-i2m\theta}, \tag{3.8}$$

where $\mathrm{J}_m(k\xi)$ is the m-th order Bessel function, with n also corresponding to the harmonic order. When γ and r_β values satisfy the resonance condition $\omega_\beta - \omega(1+a_\beta^2/2\gamma^2) = 0$, the argument of the Bessel function can be further simplified to $k\xi = a_\beta^2/[2(1+a_\beta^2)]$. These values are therefore limited to the interval between 0 (when $a_\beta = 0$) and 0.5 (when a_β approaches ∞). The field amplitude in frequency domain is then given by substituting Eq. (3.8) into the steady state wave equation in the frequency domain Eq. (3.4)

$$\begin{aligned}
&\frac{\partial A_\nu(t)}{\partial t} \\
&= \frac{\mu_0 e n_x}{\nu k_0 N_e} \sum_j \int dy \int_{-\infty}^{\infty} dz_0 e^{-i\nu k_0(z_0-ct)} \sum_{m=-\infty}^{\infty} \mathrm{J}_m(k\xi)e^{-2im\theta}\omega_{\beta,j}r_{\beta,j}\sqrt{1-y^2/r_\beta^2}\,\delta(y-y_j)\delta(z_0-z_{0,j}) \\
&= \frac{\mu_0 e n_x}{2\nu k_0 N_e} \sum_j \sum_{m=-\infty}^{\infty} \int d\eta \mathrm{J}_m(k\xi)e^{-i2m\theta}\omega_{\beta,j}r_{\beta,j}(\eta^{2m+1}+\eta^{2m-1})\delta(\eta-\eta_j)e^{-i\nu k_0(z_{0,j}-ct)} \\
&= \frac{\mu_0 e n_x}{2\nu k_0 N_e} \sum_{m=-\infty}^{\infty} \langle J_m e^{i\delta\nu_m\theta_j}(e^{-i(\nu k_0(z_{0,j}-ct)-(2m+1)\theta_j)} + e^{-i(\nu k_0(z_{0,j}-ct)-(2m-1)\theta_j)})\rangle,
\end{aligned} \tag{3.9}$$

where $\eta = e^{i\theta}$. If the resonance condition is chosen such that $\langle\psi'_{0,j}\rangle = 0$, with $\psi_{0,j} = n\theta_j + \nu k_0(z_{0,j} - ct)$, to generate amplification at the fundamental wavelength, the above equation can be averaged over the betatron period λ_β, whereupon the RHS of the equation

vanishes unless $\nu = n$ (as long as there is no detuning $\overline{\delta}_t$). Eq. (3.9) can thus be further simplified to an ODE(ordinary differential equation)

$$\frac{dA_n}{dt} \propto -\langle F_n(k_0\xi)\exp(-in\psi_0)\rangle, \tag{3.10}$$

with $F_n(\zeta) = \mathrm{J}_{(n-1)/2}(n\zeta) - \mathrm{J}_{(n+1)/2}(n\zeta)$.

3.4 Energy and Phase Equations

We can now derive the averaged equations for the electron energy and phase in the presence of the vector potential of the harmonic wave given above, inserting the expressions of β_y and (3.10) into equation (2.42) we have

$$\frac{d\gamma_j}{dt} = -\sum_{n\ \mathrm{odd}} \frac{\omega\omega_\beta r_{\beta j} a_n}{2c} F_n(k\xi_j)\cos(n[kz-\omega t]+\phi)\cos(\theta_j). \tag{3.11}$$

The harmonic wave number n satisfies a more general resonance condition $n\lambda_n = \lambda = \lambda_\beta(1+a_\beta^2)/2\gamma_r^2$, the ponderomotive phase variation equation should then be modified accordingly to reflect this change in harmonic wave number

$$\frac{d\psi_j}{dt} = \omega_\beta - \frac{\omega_n}{n}\left(\frac{1}{2\gamma_j^2} + \frac{\omega_p^2 R_\beta^2}{8\gamma_j c^2}\right). \tag{3.12}$$

3.5 Compton Regime, Universal Scaling and Linear Analysis

Defining $\overline{\delta}_t$ as the total detuning in the previous chapter, in the limit $\overline{\delta}_t \ll 1$, Eqs.(3.10), (3.11), (3.12) reduces to the following system

$$\begin{cases} \dfrac{d\psi_j}{dt} &= \omega_\beta \dfrac{\gamma-\gamma_r}{2\gamma_r}, \\ \dfrac{d\gamma_j}{dt} &= -k\dfrac{a_{\beta_r}}{\gamma_r} a_n F_n(k\xi_j)\exp(in\psi_{0,j}) + c.c., \\ \dfrac{dA_n}{dt} &= \dfrac{-\omega_b^2}{2\omega c}\langle F_n(k\xi) v_\beta \exp(-in\psi_{0,j})\rangle, \end{cases} \tag{3.13}$$

which after applying the universal scaling introduced in Chapter. 2

$$p_j = \frac{\gamma_j}{\gamma_{0,j}} - 1, \tag{3.14}$$

$$\overline{a}_n = 4c^3 \rho A_n e^{i\phi} / \omega_b^2 \omega_\beta R_\beta^3, \tag{3.15}$$

$$\bar{t} = \rho \omega_\beta t / 2, \tag{3.16}$$

$$a_\beta = \frac{\omega_p R_\beta \sqrt{\gamma_r}}{2c}, \tag{3.17}$$

can be transformed into

$$\begin{cases} \dfrac{d\psi_j}{d\tau} & = p_j, \\ \dfrac{dp_j}{d\tau} & = -\displaystyle\sum_{n \text{ odd}} F_n(k\xi_j)(\overline{a}_n \exp(in\psi_j) + c.c.), \\ \dfrac{d\overline{a}_n}{d\tau} & = \langle F_n(k\xi) \exp(-in\psi) \rangle. \end{cases} \tag{3.18}$$

The two generalized constants of motion can thus be written in a way similar to those in Chap. 2, namely

$$\langle p \rangle + \sum_n \|\overline{a}_n\|^2 = const; \qquad \frac{\langle p^2 \rangle}{2} - i \sum_n \frac{F_n}{n} (\overline{a}_n b^* - \overline{a}_n^* b) = const. \tag{3.19}$$

The gain coefficients for different harmonics can then be obtained by performing the same linear analysis as in Chap. 2, looking for solutions of the form $e^{i\lambda \bar{t}}$. Using the cubic dispersion relation $\lambda^3 = \langle F_n(k\xi)^2 n \rangle$, we can find the growth factor λ_n of the n-th harmonic

$$\lambda_n = (n \langle F_n^2(k\xi) \rangle)^{(1/3)} \left(-\frac{1}{2} + \frac{\sqrt{3}i}{2} \right), \tag{3.20}$$

and the gain parameter:

$$g_n = n^{1/3} \langle F_n^2(k\xi) \rangle^{1/3} g, \tag{3.21}$$

where $g = 4\sqrt{3}\rho/\lambda_\beta$ is the gain parameter of the fundamental wavelength, and the relation between the gain at higher-order and fundamental wavelength is shown in Fig. 3.1: The above graph demonstrates that compared with a fixed gain parameter in the fundamental wavelength, under conditions of fixed γ_r and r_{β_r}, gain parameters at higher harmonics will

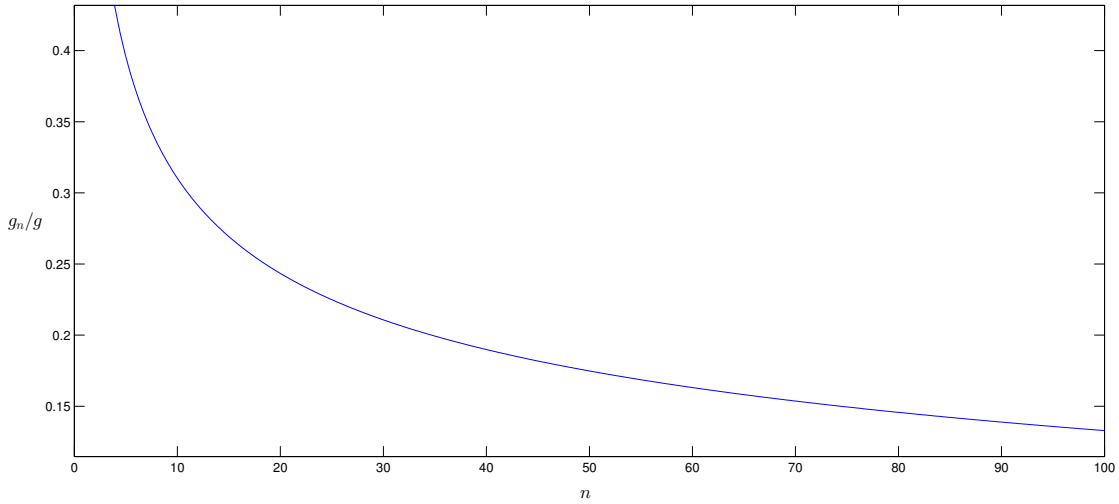

Figure 3.1: Plot of the ratio of gain coefficient at higher harmonics to fundamental gain g_n/g versus harmonic order n for the first 100 harmonics, with $a_\beta^2 = 49$

always be smaller, and become relatively negligible at high orders, making high-harmonics production difficult. This could be partly remedied by adjusting the value of γ_r and r_{β_r}, so that a desired radiation wavelength λ_n is forced to be produced at higher orders of harmonics of the fundamental resonant frequency. The lowest frequency component in the seeding field would satisfy the following generalized resonance condition, under the condition of fixed R_β:

$$\begin{aligned} \gamma_r &= \lambda_p^2(1+a_\beta^2)^2/(8n^2\lambda^2) \\ &= \lambda_p^2(1+\gamma_r k_p^2 R_\beta^2/2)^2/(8n^2\lambda^2). \end{aligned} \tag{3.22}$$

A cubic dependence of γ on n can be obtained from the above relation, with $\gamma_r \propto n^{-2}$, and $\gamma_r \propto n^2$ for $a_\beta \ll 1$ and $a_\beta \gg 1$, respectively. Instead of the resonance relation $\omega_\beta = kv_z - \omega$, γ will instead satisfy the relation $kv_z - \omega = n\omega_\beta$. Due to the dependence of γ on n, the gain coefficient with tunable γ_r is proportional to a higher power of n, through the relation $g \propto n^{1/3}\rho \propto n^{1/3}\gamma^{-1/3} \propto n^{-1/3}$ for $a_\beta^2 \gg 1$. However, because ξ also depends on γ_r through a_β, it also has to be redefined to reflect the tunability of γ_r. The relation of the gain coefficient $g_n(\gamma)$ to n becomes:

$$g_n^\gamma \propto n^{-1/3}\langle F_n(k\xi^\gamma)\rangle^{2/3}. \tag{3.23}$$

For $a_\beta^2 \ll 1$, the relation between γ_r and n is $\gamma_r \propto n^{-2}$, therefore we have:

$$g_n^\gamma \propto nF_n(k\xi^\gamma)^{2/3}. \tag{3.24}$$

It can be seen that tuning γ_r to produce higher frequency radiation becomes more productive when $a_\beta \gg 1$. At the same time R_β^2 also has a n dependence, which translates into a $g \propto n^{1/3}\rho \propto n^{1/3}R_\beta^{2/3} \propto n^{2/3}$ relation. Such tuning, as suggested in [46], can theoretically achieve for any seeding radiation wavelength a more favourable scaling of power gain, even if the values of γ and R_β do not satisfy the fundamental resonance condition of the seeding wavelength. Experimentally, γ_r does not usually have as large a tunable range as R_β, and therefore it is more desirable to tune R_β towards large values to achieve harmonic amplification.

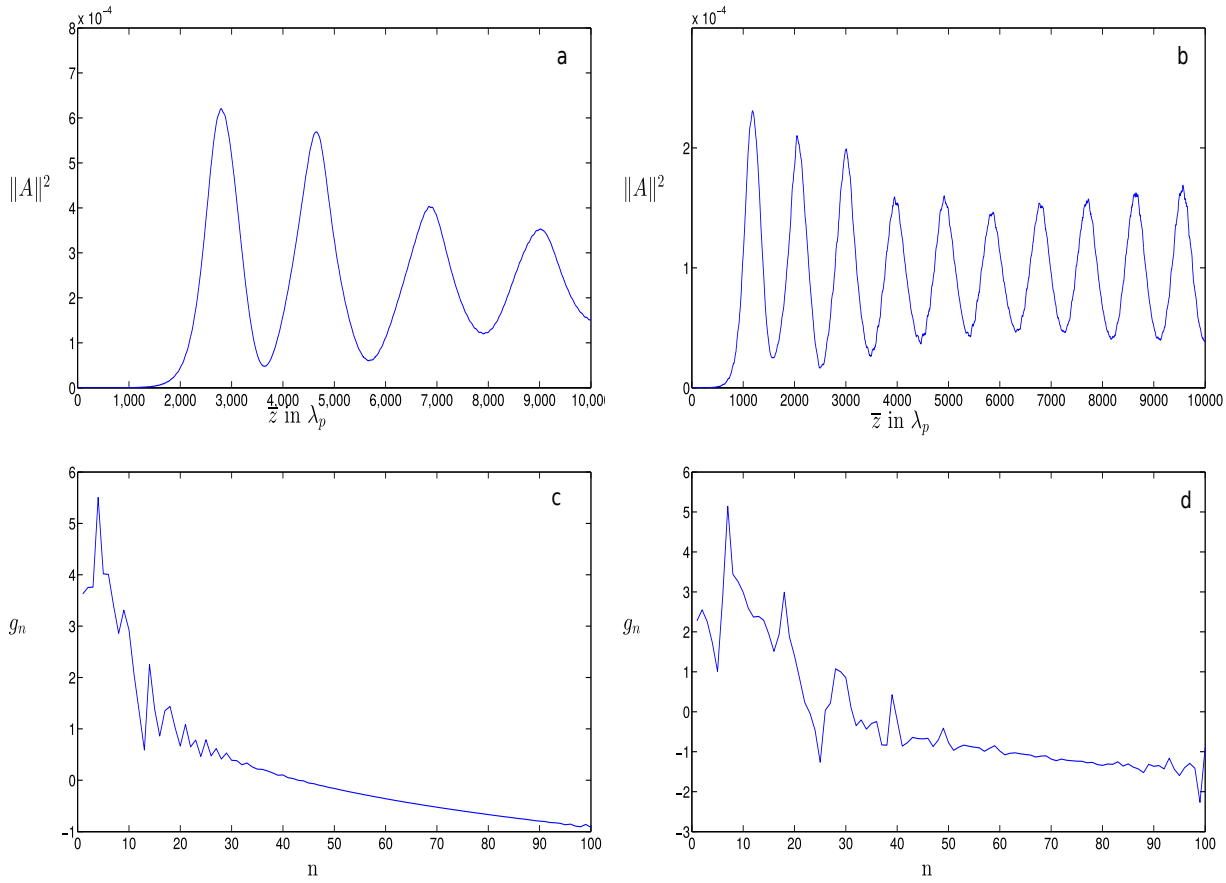

Figure 3.2: From top to bottom, the figure panels (a) and (c) show the evolution of radiation amplitude in $\overline{z}$ obtained by solving (3.13) and the harmonic frequency distribution of this radiation field for an initial seeding field with a wavelength of 3916 ω_p and $R_\beta = 0.022\lambda_p$ on fundamental resonance, while the figure panels (b) and (d) show the same simulation carried out with $R_\beta = 0.08\lambda_p$ which satisfies a 9-th order harmonic resonance relation with the same wavelength. The radiation power is normalized and the length unit is normalized with λ_p; $\gamma_r = 400$. The amplitude of the field in harmonic resonance oscillates at about 1.7 times the frequency of that in fundamental resonance, and the maximum gain points (the 4th point in the first plot and the 7th in the second) in the two frequency plots can be seen to satisfy the same ratio. Thus we know that the dominant frequency of the two simulation results are equal, and the second simulation saturates quicker than the first one, albeit with only 40% of the output power.

3.6 High Harmonics with Detuning

To further verify that amplification occurs through harmonic resonance, a series of simulations using the same γ_r and radiation wavelength as in Fig. 3.2, but with different R_β

detuning has been carried out. The results show that the saturated radiation field intensity is significantly larger when R_β satisfies a harmonic resonance condition than when it does not, confirming our theoretical analysis.

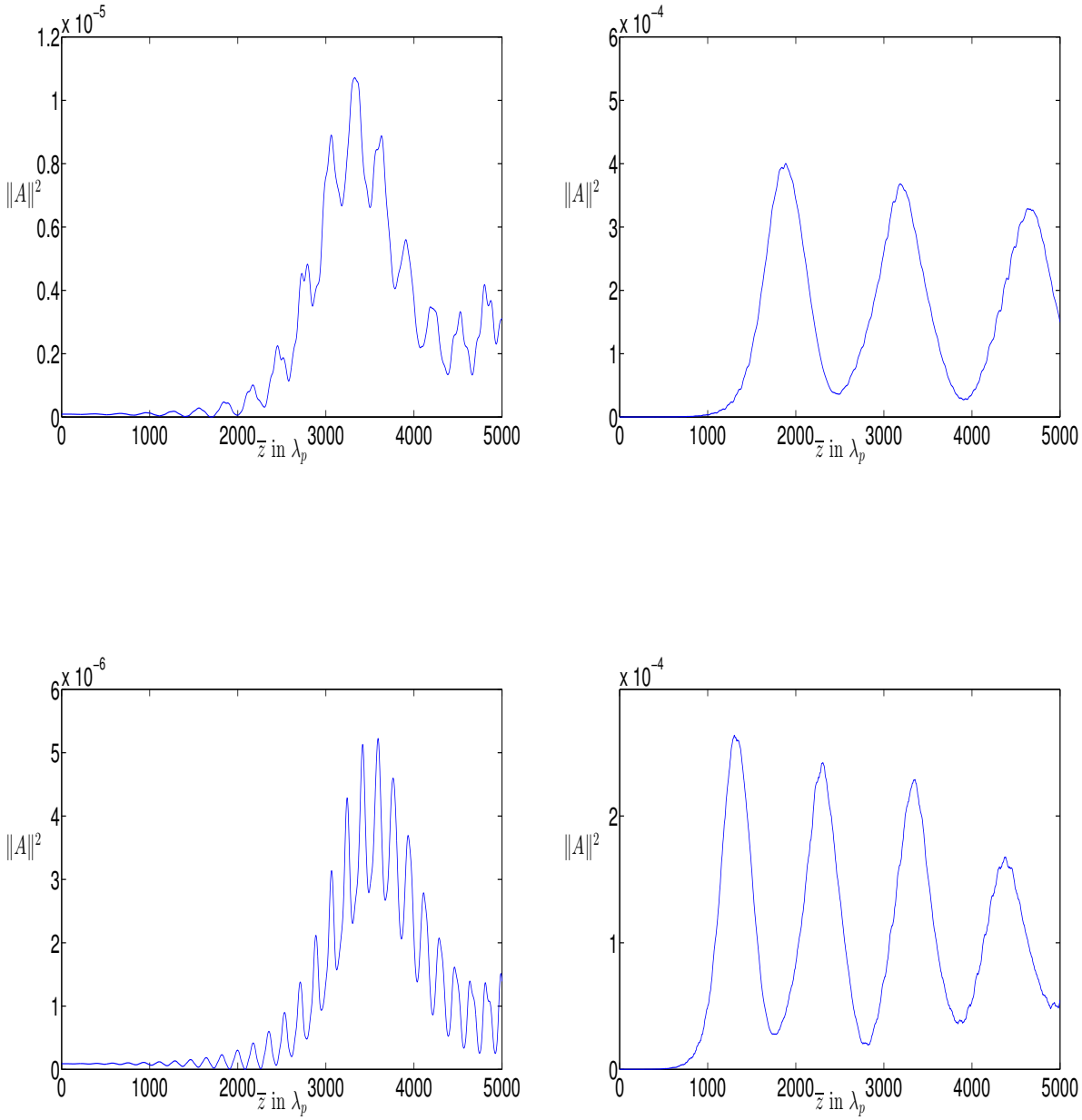

Figure 3.4: From top to bottom: the graphs on the left show dimensionless field intensities evolving with only fundamental frequency resonance, while the graphs on the right show the combined field intensities with resonances at harmonics included.

3.7 Enhanced Coherent Radiation at the Fundamental Frequency

An interesting characteristic of the ICL is identified from the group of eqns. (3.10)-(3.12): The direct modulation of the betatron frequency by the Lorentz factor γ gives rise to an additional slowly varying-component in the expression of the ponderomotive phase in Eq. (3.7) when $a_\beta \gg 1$. The "jittering" motion therefore not only produces radiation at high harmonics, but also enhances radiation at the fundamental resonant frequency. This can be seen by assuming $k_0 z_0 - \omega t = -\theta$ and $\psi_j = k z_{0j} - \omega t + \theta_j$, while keeping the product of all four lowest order terms in the expansion of (3.9), rather than just the two resonant ones, which can be summed to give

$$\frac{dA_1}{d\tau} = \langle e^{-i(kz-\omega t)}\{(e^{-i\theta} + e^{i\theta})[\mathrm{J}_0(k_0\xi) - \mathrm{J}_1(k_0\xi)(e^{-i2\theta} - e^{i2\theta})]\}\rangle. \tag{3.25}$$

(Calculations for higher order, less significant terms which contribute to the gain at the fundamental frequency can be carried out, these transform the ICL dispersion relation into a fourth-order algebraic equation, but are beyond the scope of this thesis.)
By calculating the third-order derivative of A_1, we obtain:

$$A_1''' = 2i\langle \mathrm{J}_0(k_0\xi) F_1^2(k_0\xi)\rangle^{1/3} A_1. \tag{3.26}$$

Therefore in this case, the growth factor and gain parameter should be redefined as:

$$\lambda_1 = \langle 2\mathrm{J}_0(k_0\xi) F_1^2(k_0\xi)\rangle^{1/3} \left(-\frac{1}{2} + \frac{\sqrt{3}i}{2}\right), \tag{3.27}$$

$$g_1 = \langle 2\mathrm{J}_0(k_0\xi) F_1^2(k_0\xi)\rangle^{1/3} g, \tag{3.28}$$

for the fundamental resonant frequency. For $0 < k_0\xi < 0.5$, the value of $(2\mathrm{J}_0(k_0\xi))^{1/3}$ will remain above the unity, therefore the gain at the fundamental frequency is enhanced via the direct modulation of the betatron frequency.

Chapter 4

Superradiance and SASE in the ICL

4.1 SASE in the ICL

The relativistic Doppler effect makes the FEL/ICL a suitable candidate for high-frequency coherent radiation generation. In the X-ray regime, however, the capability of an FEL/ICL amplifier to radiate coherently is adversely affected by the scarcity of high reflective mirrors in this frequency range. An alternative amplification scheme to a resonant cavity, must be sought for the amplification of X-ray radiation. By adjusting ρ and the energy of the electron beam, a FEL wiggler can produce coherent radiation beam in a single pass, in the so-called single pass high gain process of FEL, thereby avoiding the need of mirrors. When the electron bunch's shot noise is used to seed the single pass high gain amplification, the FEL is consider to work in the Self-Amplified Spontaneous Emission(SASE) [3, 19, 21] regime. An ICL works in the SASE regime could potentially further reduce the size of an X-ray FEL, where undulators are usually tens and even hundreds of metres long, to a size that could fit in a University laboratory and considerably reduce the cost as well. As in the FEL, however, SASE amplification in the ICL is an inherently noisy process, because it relies on amplification of synchrotron radiation of an electron bunch at startup, which has a bandwidth covering the whole spectrum. This section is devoted to the statistical and frequency analysis of the SASE process, the SASE phenomenon with the slippage effect will be discussed in the next section.

4.1.1 Characteristics of the Startup

Of great interest and importance to the FEL and ICL theory is the shot noise inherent in any realistic electron bunch, which originates from the discrete nature of the free electrons. The positions of the electrons are not correlated with energy but rather random, whose phases can sum to a non-zero bunching factor which serves as the initial signals that set off the amplification. Unlike FEL electron bunches, where the randomness comes from the random arrival times of electrons at the wiggler entrance, the initial ponderomotive phases of electrons in an ICL wiggler can be split into two terms: a longitudinal term produced by the different arrival times of electrons at wiggler entrance as in a FEL wiggler, and an independent random transverse phase θ_0 related to the random initial transverse position $y_0 = r_\beta \cos(\theta_0)$. This initial random phase distribution. unlike the FEL initial transverse phase $k_w z_0$, is not determined by the initial electron pulse shape or their longitudinal positions in the wiggler.

Defining z_m as the random longitudinal position of an electron m relative to the wiggler entrance, and θ_m as the initial transverse betatron phase at time $t = 0$, these random positions yield a sum of random phases $\exp(i(\theta_m - kz_m))$ as the source term of the Maxwell's equation, with a non-zero average value. An ICL starting from a shot noise will have initial power $|b_0|^2 = 1/N$, which is uniformly distributed in all frequencies. If the bunch length is much longer than the radiation wavelength, the phases can be consider to be uniformly distributed over the interval $[0, 2\pi]$. Under this assumption we can conclude that the real and imaginary parts of $b_0(\omega)$ are distributed in accordance with a Gaussian law. $b_0(\omega) = \langle \exp(-i(\theta_m - kz_m)) \rangle$ is the mean value of the bunching factor at frequency $\omega = kc$, and the frequency domain expression of b_0. which satisfies a negative exponential probability distribution [54]

$$p(|b(\omega)|^2) = \frac{1}{\langle |b(\omega)|^2 \rangle} \exp\left(-\frac{|b(\omega)|^2}{\langle |b(\omega)|^2 \rangle} \right). \tag{4.1}$$

Next we will analyze the temporal and spectral characteristics of the startup bunch noise. Due to its random nature statistical approaches [51] must be applied. Typical statistical properties, including spectral and temporal correlation functions will be discussed in the following paragraphs.

Defining the expression of the beam current as

$$I(t) = (-e) \sum_{m=1}^{N} c\beta_{\|} \delta(z - z_m) = (-e) \sum_{m=1}^{N} \delta(t - t_m). \tag{4.2}$$

Because shot noise comes from the aperiodicity of the electron distribution in space, its frequency-domain expression should be obtained using a Fourier transform, rather than Fourier series, which assumes negligible initial noise for the betatron phase distribution. We can write down the Fourier transform of $I(t)$ as

$$I(\omega) = \frac{I(k)}{c} = \frac{1}{c}\int_{-\infty}^{\infty} e^{ikz} I(z) dz = (-ec)\sum_{m=1}^{N} e^{ikz_m}. \tag{4.3}$$

The spectral correlation function of $I(\omega)$ and $I(\omega')$ can then be expressed as

$$\langle I(\omega) I^*(\omega')\rangle = \left\langle e^2 c^2 \sum_{m=1}^{N}\sum_{n=1}^{N} \exp(ikz_m - ik' z_n) \right\rangle. \tag{4.4}$$

Here the angle brackets denoting the averaging over ensemble of bunches.

Assuming that the electron bunch profile can be described by a profile function $F(t) = \langle -I(t)\rangle/(eN)$, it is easy to obtain the relation

$$\langle \exp(ikz_m)\rangle = \int_{-\infty}^{\infty} F(z_m) e^{ikz_m} dz_m = \overline{F}(k). \tag{4.5}$$

Using the property of a stationary process, which assumes that the mean, variance and autocorrelation function of the probability distribution does not change over time, the correlation function can be further expressed and normalized as

$$\frac{\langle I(\omega) I^*(\omega')\rangle}{\sqrt{\langle I(\omega)\rangle\langle I^*(\omega')\rangle}} = F(\omega - \omega') + (N-1) F(\omega) F^*(\omega'). \tag{4.6}$$

The second term on the RHS of the above equation corresponds to coherent emission due to the bunch profile, which is usually negligible when the bunch length is much longer than the radiation wavelength, even for a high current beam, because the resonant frequency is large compared to the characteristic frequency of the bunch profile.

The spectral correlation function of the electric field can therefore be derived with the expression of the current correlation function

$$S_1(\omega, \omega', \bar{t}) = \exp\left(i\frac{\omega - \omega'}{2\omega_\beta \rho}\bar{t}\right) F(\omega - \omega'). \tag{4.7}$$

with $\bar{t}$ being the scaled time defined in Chapter 2. The second-order correlation function

$S_2(\omega, \omega', \bar{t})$ can be derived in an analogous way

$$S_2(\omega, \omega', \bar{t}) = \frac{\langle |I(\omega) I^*(\omega')|^2 \rangle}{\langle |I(\omega)|^2 \rangle \langle |I^*(\omega')|^2 \rangle}. \tag{4.8}$$

For a bunch of electrons with completely randomized positions, S_2 can be written in terms of S_1 as

$$S_2(\omega - \omega') = 1 + \|S_1(\omega - \omega', \bar{t})\|^2. \tag{4.9}$$

The two correlation functions are useful in deriving the fluctuation of the radiation pulse energy σ_W^2, using the formula in [51]

$$\sigma_W^2 = \frac{\langle (W - \langle W \rangle)^2 \rangle}{\langle W \rangle^2} = \frac{\int_0^\infty \int_0^\infty \langle |E(\omega, \bar{t})|^2 \rangle \langle |E^*(\omega', \bar{t})|^2 \rangle |S(\omega - \omega')|^2 d\omega d\omega'}{[\int_0^\infty \langle |E(\omega, \bar{t})|^2 \rangle]^2}, \tag{4.10}$$

where $\langle W \rangle$ is the expression of the radiation energy $|E(\omega, \bar{t})|^2 \propto |I(\omega)|^2$ measured by a detector averaged over many shots, which is derived using Parseval's theorem

$$\langle W \rangle = \frac{2\Sigma}{Z_0} \int_0^\infty |E(\omega, \bar{t})|^2 d\omega, \tag{4.11}$$

where Σ is the cross section of the radiation pulse and Z_0 the vacuum impedance. The expression of the radiation energy must be derived using a similar method used in Chapter 2.

4.1.2 Time-domain Characteristics of a SASE Radiation Field

If we use the same approximation as in Chapter 2, where the value of betatron amplitude for each electron is considered to be time-independent within a betatron period, then the solution of steady state amplification with no seeding field, but initial bunching factor b_0 can be directly used with little modification, namely

$$A(\bar{t}) = \frac{b_0}{3i} \exp\left(\frac{\sqrt{3}}{2} \Big(1 - \frac{1}{9}\overline{\delta}_t^2\Big) \bar{t} + i \Big(\frac{1}{2} - \frac{2}{3}\overline{\delta}_t + \frac{1}{18}\overline{\delta}_t^2 \Big) \right), \tag{4.12}$$

for the growing mode, the $\overline{\delta}_t$ within the exponential, which represents the total detuning $\overline{\delta}_t = \overline{\delta}_\gamma + \overline{\delta}_{r_\beta}$ is obtained from a Taylor expansion of the amplifying solution of the cubic

characteristic equation $\lambda^3 - \overline{\delta}_t\lambda^2 + 1 = 0$ for a detuned ICL, around the point $\overline{\delta}_t = 0$, where the growth rate reaches its maximum. This steady state solution implicitly depends on ω through the detuning $\overline{\delta}_t$, which is related to ω by the resonance condition:

$$\overline{\delta}_t = -\frac{\omega - \omega_0}{2\rho\omega_0}, \tag{4.13}$$

the k-dependent form of which is:

$$\overline{\delta}_t = -\frac{k - k_0}{2\rho k_0}. \tag{4.14}$$

It can be seen that the frequency-domain expression depends on the wavenumber k, thus the propagation is dispersive. In an ICL amplifier only a single frequency propagates through the electron beam, and is amplified only when the values of γ and r_β satisfy the resonance relation, in a SASE ICL, the radiation is seeded by broadband spontaneous emission, which ensures that the electorn beam is atuomatically in resonance at a certain frequency. A different set of values of γ and r_β only changes the frequency at which amplification achieves maximum growth, without changing the growth rate, therefore in the SASE regime $\overline{\delta}_t$ can be taken to represent the frequency rather than energy deviation.

Thus for a startup noise defined as in Subsection 4.1.1, the absolute square of the vector potential expression in the frequency domain is

$$\begin{aligned} \|A(\overline{\omega}, \overline{t})\|^2 &= \frac{\|b_0\|^2}{9} \exp\left(\sqrt{3}\Big[1 - \frac{1}{9}\overline{\delta}_t^2\Big]\overline{t}\right) \\ &= \frac{\|b_0\|^2}{9} \exp(\sqrt{3}\overline{t}) \exp\left(-\frac{\sqrt{3}(\omega - \omega_0)^2}{36\rho^2\omega_0^2}\overline{t}\right), \end{aligned} \tag{4.15}$$

which exhibits a Gaussian-shape amplification band around the resonant frequency ω_0, with the RMS bandwidth σ_A determined by ρ and ω_0. Eq.(4.15) shows that the radiation amplitude should fluctuate in the same manner as the Fourier component of the shotnoise. The Fourier amplitude of the electric field, using the SVEA approximation, can be expressed as

$$E(\overline{\omega}, \overline{t}) = \frac{E_0}{3i} \exp\left(\Big[\frac{\sqrt{3}}{2}\Big(1 - \frac{1}{9}\overline{\delta}_t^2\Big) + i\Big(\frac{-\omega}{2\omega_\beta\rho} + \frac{1}{2} - \frac{2\overline{\delta}_t}{3} + \frac{\overline{\delta}_t^2}{18}\Big)\Big]\overline{t}\right) \frac{I(\omega)}{I_0}. \tag{4.16}$$

The power spectrum density then follows the same negative exponential probability distribution, which becomes a gamma distribution [51] if the integration is carried out over part

of the frequency spectrum.

We define the effective angular frequency as

$$\omega_k = \frac{-ck}{2\omega_\beta \rho} + \frac{1}{2} - \frac{2\bar{\delta}_t}{3} + \frac{\bar{\delta}_t^2}{18}. \tag{4.17}$$

The group velocity of the field can be readily obtained from $E(\bar{\omega}, \bar{t})$

$$v_g = \left.\frac{d\omega_k}{dk}\right|_{k=k_0} = c\left(1 - \frac{1+a_\beta^2}{3\gamma_0^2}\right). \tag{4.18}$$

The time domain expression of the field can then be obtained through a Fourier transform

$$E(\bar{z}, \bar{t}) = \sqrt{\frac{8\pi}{\sqrt{3}\bar{t}}}\frac{ec\omega_0}{I_0}\rho \exp\left(\frac{i+\sqrt{3}}{2}\bar{t}\right)\sum_m \exp\left(-\sigma_A^2[z - z_t - z_m]^2 + ik_0 z_m\right), \tag{4.19}$$

which can be related, in the limit of a long electron bunch $\Delta\omega_C \ll \sigma_A$, to the spectral power.

The statistical analysis demonstrates two important properties of the noise spectrum: (1) The startup is noisy with multiple spikes; (2) The spectrum should narrow as $1/\sqrt{\bar{t}}$ when the radiation beam propagates in the wiggler. This understanding of the noise properties will form the starting point of numerical investigation of the SASE ICL.

4.2 The Superradiant Theory of ICL

In Chapter 2, the electrodynamics of the ICL is studied with the assumption that the electron and radiation beam propagate at nearly the same velocity, which is equivalent to the case that the radiation beam interacts with a infinitely long electron beam, with electrons in every section of the beam radiating equally and simultaneously. When the energy deviation of the electrons from resonance becomes larger than the limit of linear analysis permits, and nonlinear effects come into play, the amplification of the radiation beam amplitude saturates and the amplitude starts to oscillate. In reality however, electrons always propagate at a slower speed than the radiation in the vacuum. The radiation beam then slowly overtakes the electrons from which it gains its energy, at the same time continuing to extract energy from the succeeding sections of the electron beam, until it reaches the end of the bunch. A radiation pulse amplified in such a way does not enter into the saturation regime, rather, its power continues growing until it completely slips out of the electron bunch. Therefore,

the radiation pulse will experience a variation in the electron density as it propagates, which makes it necessary to take into account propagation effects on the length scale of the electron bunch, rather than the wiggler-wavelength scale. The amplified radiation power will be proportional to the square of the electron current. If electrons enter the amplifier in a unprepared state randomly distributed, and only evolve to emit radiation with an intensity proportional to n_e^2 under the influence of spontaneous radiation from the bunch itself, such a self-organizing phenomenon, called "superradiance" in the FEL literature to reflect the defining features of the radiation process.

It is thus immediately clear, that the radiation pulse will evolve in distinct ways at different positions relative to the bunch. Defining the scaled propagation distance difference $\overline{z}_1$ as

$$\overline{z}_1 = \frac{4\pi\rho}{\lambda}(z - \overline{v}t), \tag{4.20}$$

and adopting slightly different definitions for scaled z and t from Chap. 2,

$$\overline{z} = \frac{4\pi\rho z}{\lambda}, \tag{4.21}$$

$$\bar{t} = \frac{4\pi\rho t}{\lambda}, \tag{4.22}$$

the propagation volume can be divided into three regions, depending on the value of $\overline{z}_1$, the first region is the leading edge of the light pulse, which has escaped the electron bunch and is no longer amplified. This area is characterized by

$$\frac{4\pi\rho\, l_b}{\lambda} < \overline{z}_1 \leq \frac{4\pi\rho\, l_b}{\lambda} + c\bar{t}, \tag{4.23}$$

followed by the region occupied by the electron bunch, where the radiation undergoes steady-state amplification, which is defined by

$$c\bar{t} \leq \overline{z}_1 \leq \frac{4\pi\rho\, l_b}{\lambda}. \tag{4.24}$$

The last region is the trailing edge at the end of the light pulse with

$$\overline{z}_1 < c\bar{t}, \tag{4.25}$$

where radiation evolves non-uniformly since electrons occupying this region have already

been pre-bunched by the light pulse slipping over them. Sect. 4.3 will be dedicated to the study of radiation dynamics in these three different regions.

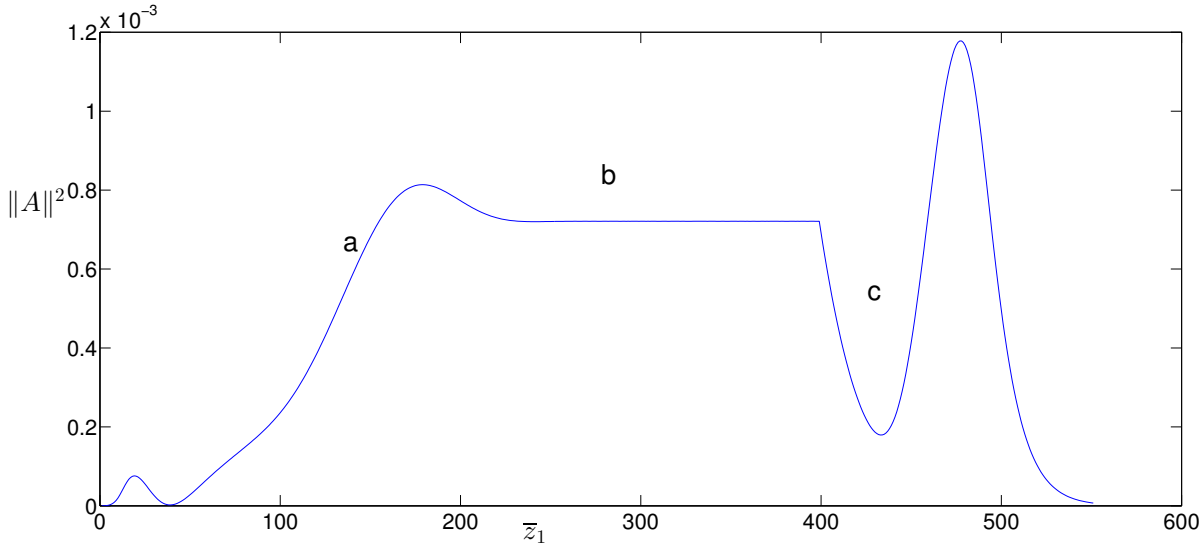

Figure 4.1: Schematic plot of the three regions in strong superradiance. (a) Slippage region, (b) steady-state region, (c) radiation escaping from the electron bunch.

The study of superradiance is also vital to the study of the SASE regime of the ICL. Since a SASE ICL starts from noisy spontaneous emission of the electron bunch, it is mostly used for radiation at frequencies above the ultraviolet regime, and as a single-pass amplifier, where a short electron bunch and a comparatively long undulator are utilized, and propagation effects cannot be neglected. Such propagation effects are called "weak superradiance", as will be discussed in Subsect. 4.4.2. Moreover, even in the long bunch case it's still possible to generate superradiant radiation with an electron beam prebunched by modulating its energy with a seeding laser field. There is always a region at the trailing edge of the electron bunch that evolves as a short pulse, and emits radiation superradiantly. This region occurs because no radiation enters from behind and all radiation propagates in the forward direction. The radiation intensity emitted in such a way is much greater than the steady-state saturation value, such a phenomenon is called "strong superradiance", due to its high power output, as will be discussed in Subsect. 4.5.3.

4.3 Dynamics and Parameters of ICL Pulse Propagation in the Superradiant Regime

4.3.1 Scaled Spatio-Temporal ICL Equations

We start by writing down the self-consistent equations describing the evolution of the electron variables and the complex field of the radiation in the one dimensional case

$$\left(\frac{\partial}{\partial\overline{z}}+\frac{\partial}{c\partial\overline{t}}\right)\overline{a}_r=\chi(\overline{z}-\overline{v}_\parallel\overline{t})(1+\delta)\langle(1+s)\exp(-i\psi)/(1+q)^{1/2}\rangle, \tag{4.26}$$

$$\frac{d\psi_j}{d\overline{t}}=(2/\rho)(1+q_j)^{-1/2}-(1+a_\beta^2)^{-1}(1+q)^{-2}-(1+s_j)^2/[(1+\delta)(1+1/a_\beta^2)(1+q_j)], \tag{4.27}$$

$$\frac{dq_j}{d\overline{t}}=-\rho\overline{a}_r(1+s_j)\exp(i\psi_j)/[(1+\delta)(1+q_j)^{1/2}]-i\rho^2\frac{(1+a_\beta^2)^2}{(3+a_\beta^2)a_\beta^2}\langle\exp(-i\psi)\rangle\exp(i\psi_j)+c.c., \tag{4.28}$$

$$\frac{ds_j}{d\overline{t}}=-i(\rho^2/8)\langle\exp(-i\psi)\rangle\exp(i\psi_j)/(1+q_j)^{1/2}+c.c.. \tag{4.29}$$

The macroscopic electron density fluctuation function $\chi(\overline{z}-\overline{v}_\parallel\overline{t})$ is introduced into the source term to reflect the influence of the propagation effect on the source term. The ρ parameter also needs to be slightly modified to reflect this change

$$\rho=\left(\frac{R_\beta^2\widetilde{\omega}_b^2}{2\gamma c^2}\right)^{1/3}, \tag{4.30}$$

by changing the plasma frequency into $\widetilde{\omega}_b=\sqrt{\widetilde{n}_e e^2/(m_e\epsilon_0)}$, where $\widetilde{n}_e$ is the peak electron density such that $\widetilde{n}(\overline{z},\overline{t})=\chi(\overline{z}-\overline{v}_\parallel\overline{t})\widetilde{n}_e$. The definition of the averaging $\langle...\rangle$ is also modified correspondingly; it is now carried out over $N(\overline{z},\overline{t})$ electrons around position $\overline{z}$ at a fixed time $\overline{t}$, instead of over all electrons in the beam.

The spatio-temporal ICL equations formally resemble the time-dependent FEL equations, and therefore we can apply the same standard transformation of coordinates

$$\overline{z}'=\overline{z}, \tag{4.31}$$

$$\overline{t}'=\overline{t}-\overline{z}/\overline{v}_\parallel, \tag{4.32}$$

as defined in Chap. 2, to Eqs. (4.26) to (4.29). The transformed equations are

$$\frac{d\psi_j}{d\overline{t}'} = q_j - \rho s_j + \delta, \tag{4.33}$$

$$\frac{dq_j}{d\overline{t}'} = -[\overline{a}_r + i\rho\langle\exp(-i\psi)\rangle\exp(i\psi_j)] + c.c., \tag{4.34}$$

$$\frac{\partial\overline{a}_r}{\partial\overline{z}'} - \frac{(1-\beta_\parallel)}{c\beta_\parallel}\frac{\partial\overline{a}_r}{\partial\overline{t}'} = -i\langle\delta\psi\exp(-i\psi_0)\rangle - \frac{\rho}{2}\langle q\exp(-i\psi_0)\rangle, \tag{4.35}$$

$$\frac{d\overline{s}_j}{d\overline{t}'} = -\frac{i}{2}\Big(\frac{\partial\overline{a}_r}{\partial\overline{z}'} - \frac{(1-\beta_\parallel)}{c\beta_\parallel}\frac{\partial\overline{a}_r}{\partial\overline{t}'}\Big)e^{i\psi_j} + c.c.. \tag{4.36}$$

The influence of slippage on the interaction can now clearly be seen: when the velocity difference between the radiation and electron beam is not appreciable during the interaction in the wiggler, i.e., the so-called "short wiggler" limit, in which the slippage length, defined as the number of wiggler periods times the radiation wavelength $N_\beta\lambda_r$ is much smaller than the electron pulse length l_b. This limit can be easily understood by normalizing $\overline{z}$ to L_β, and $\overline{t}$ to l_b/c. In this case the ratio between the time and space derivative becomes

$$\frac{L_\beta(1-\beta_\parallel)}{\beta_\parallel l_b} = \frac{N_\beta\lambda_r}{\beta_\parallel l_b}, \tag{4.37}$$

using the resonance condition $\lambda_r = \lambda_\beta(1-\beta_\parallel)$. Hence if the value of $N_\beta\lambda_r/l_b$, defined to be the slippage parameter U, is much smaller than one, the time variation can be neglected within the electron pulse length l_b, except for a small region in the trailing edge. Under this condition, radiation evolution in most parts of the electron beam will be governed by the steady state ICL equations (4.26)-(4.29). When the slippage parameter is much larger than one,however, the non-uniformity of the electron distribution will affect the amplification, the following subsections are dedicated to the discussion of the difference between these two different kinds of superradiance.

4.3.2 Scaled co-moving coordinates

To understand the phenomenon of the cooperative radiation effect, the scale in which it takes place must be understood first. In the discussion of the steady-state SASE effect, we have found the parameter characterizing the RMS bandwidth of the SASE spectrum to be $\sigma_A = (k-k_s)/(2\rho k_s)$, the FWHM(Full width at half maximum) bandwidth of the spectrum is thus $\Delta k = 4\pi\rho/\lambda_s$. recalling that the coherence time of a radiation field is inversely

proportional to its bandwidth, we define a unit of length characterizing the scale in which the electrons interact cooperatively via the radiation field

$$l_c = \frac{\lambda}{4\pi\rho}, \tag{4.38}$$

i.e., the "cooperation length" as defined in [55]. It can immediately be seen that this length scale of cooperative radiation is the length scale of the slippage effect, which depends on the difference between the velocities of the radiation propagation and bunch propagation. Although both beams propagate at a speed close to the light in the vacuum, the relative velocity between the two is quite small, and the dynamics of the interaction can thus be better analysed on two different length scales: One length scale is, certainly, the wiggler (betatron) wavelength, the other is the length of the bunch. We transform to the following coordinates

$$\begin{cases} \overline{z}_1 &= \dfrac{z - \overline{v}_\parallel t}{l_c}, \\ \overline{z}_2 &= \dfrac{ct - z}{l_c}, \end{cases} \tag{4.39}$$

which satisfy the condition $\overline{z}_1+\overline{z}_2 = (4\pi\rho(c-\overline{v}_\parallel)/\lambda)t = c(4\pi\rho/\lambda_\beta)t = c\bar{t}$, under the resonance relation $\omega_\beta = \omega - k\overline{v}_\parallel$. The coordinate transformation used here is different from that adopted by Bonifacio et al in [56]. Due to the difference in the resonance relation in ICL compared with the FEL, the phase of electron synchrotron motion within an ion channel is a function of $\bar{t}$ and unlike the FEL, does not depend on the longitudinal position of the electron. Thus the electron-frame moves at a speed of $\overline{\beta_\parallel} = 1 - \omega_\beta/\omega$, rather than $1/(1 + \omega_\beta/\omega)$, as in FEL theory. In fact, if the FEL co-moving frame is used, the scaled ponderomotive phase transforms in terms of the FEL co-moving coordinates to :

$$\psi_j = \frac{\overline{z}_1}{\rho} - \Big(\frac{1}{\beta} - 1\Big)\frac{\overline{z}_2}{\rho}, \tag{4.40}$$

which is not constant when the resonance condition is satisfied.

4.3.3 ICL Equations in Transformed Coordinates

Applying the coordinate transformations (4.39) to the ICL equations (4.26)-(4.29), under the Compton regime condition $\rho \ll 1$yields

$$\frac{\partial \psi_j(\overline{z}_1, \overline{z}_2)}{\partial \overline{z}_2} = p_j(\overline{z}_1, \overline{z}_2), \tag{4.41}$$

$$\frac{\partial q_j(\overline{z}_1, \overline{z}_2)}{\partial \overline{z}_2} = -(a(\overline{z}_1, \overline{z}_2) \exp\big(i\psi_j(\overline{z}_1, \overline{z}_2)\big) + c.c., \tag{4.42}$$

$$\frac{\partial \overline{a}_r(\overline{z}_1, \overline{z}_2)}{\partial \overline{z}_1} = \chi(\overline{z}_1)\langle \exp\big(-i\psi_j(\overline{z}_1, \overline{z}_2)\big)\rangle, \tag{4.43}$$

where the variation in s_j is neglected, and ψ_j, p_j and A are scaled using the same universal scaling as used in the previous chapter.

To facilitate our discussion regarding the radiation evolution in different regions, we introduce the superradiant parameter K as in [56]:

$$K = \frac{l_c}{l_b}, \tag{4.44}$$

that is, the ratio between the cooperation and the bunch length. A slippage parameter U can also be defined using K and gain parameter G as $U = KG$, where $G = 4\pi\rho N_\beta$

If we assume a uniform electron density distribution over the whole bunch length, the region occupied by the electron bunch is thus $0 < z - \overline{v}_\parallel t < l_b$, which can be rewritten using the scaled coordinate as $0 < \overline{z}_1 < 1/K$. Similarly, the limits of the three regions defined in (4.2) can also be expressed using the transformed coordinates and the K parameter, with the "steady-state" region defined as $c\bar{t} < \overline{z}_1 < 1/K$, where slippage has no effect on the growth of the field amplitude, the trailing edge region $0 < \overline{z}_1 < \overline{z}$, where the radiation pulse is affected by propagation effect and is non-uniform, and the leading edge $1/K < \overline{z}_1 < c\bar{t} + 1/K$, where the radiation is no longer amplified.

The parameters K and U are also important for the radiation pulse evolution in the trailing edge, which further determines the radiation power and other characteristics of the pulse. Therefore, radiation amplification with different K and U are discussed separately in the next section.

4.4 Superradiant Regime

4.4.1 Linear Analysis

In this section, we proceed to discuss the linear regime of the (4.41)-(4.43), following the approach described in [57]. (4.26)-(4.29) can be generalised using a set of dimensionless variables that are slightly different from (4.39)

$$\begin{cases} \overline{z}_1 = & \dfrac{4\pi\rho}{\lambda}(z - \overline{v}_{\parallel}t) = \dfrac{z - c\overline{\beta}_{\parallel}t}{l_c}, \\ \overline{t} = \bar{t}, \end{cases} \tag{4.45}$$

and the collective variables

$$B = \langle \delta\psi \exp(-i\psi_0) \rangle, \tag{4.46}$$

$$P = \langle \overline{q} \exp(-i\psi_0) \rangle, \tag{4.47}$$

$$A = \overline{a}_r. \tag{4.48}$$

The self-consistent linearized ICL equations can be transformed to

$$\frac{1}{c}\frac{\partial \mathcal{B}}{\partial \bar{t}} = \mathcal{P} - \rho\mathcal{S} + \overline{\delta}, \tag{4.49}$$

$$\frac{1}{c}\frac{\partial \mathcal{P}}{\partial \bar{t}} = -\mathcal{A} - \rho\mathcal{B} + c.c., \tag{4.50}$$

$$\Big(\frac{1}{c}\frac{\partial}{\partial \bar{t}} + \frac{\partial}{\partial \overline{z}_1}\Big)\mathcal{A} = -i\mathcal{B} - \frac{\rho}{2}\mathcal{P} + i\overline{\delta}\mathcal{A}, \tag{4.51}$$

following the method devised in [58] by applying the coordinate transformation from $(\overline{z}, c\bar{t})$ to $(c\bar{t}, \overline{z}_1)$, thus eliminating the partial dependences of the particle evolution equations on $c\bar{t}$, and making the equations directly solvable using the Laplace transform method. If we set the following initial condition at the wiggler entrance

$$\begin{aligned} A(\overline{z}_1, \bar{t} = 0) &= A_0, \\ B(\overline{z}_1, \bar{t} = 0) &= 0, \\ P(\overline{z}_1, \bar{t} = 0) &= 0, \end{aligned} \tag{4.52}$$

the Laplace-transformed fields using the given conditions are

$$\begin{cases} \mathcal{A}(w) & = A_S(w) + A_{SR}(w), \\ A_S(w) & = -A_0 \dfrac{-iw^2}{\Delta w}, \\ A_{SR}(w, \overline{z}_1) & = A_0 \dfrac{iw^2}{\Delta w} \exp\Big(- i \dfrac{\Delta w}{w^2} \overline{z}_1 \Big), \end{cases} \tag{4.53}$$

where Δw is the polynomial on the left hand side of the steady-state dispersion relation $w^3 - \delta w^2 + 1 = 0$. It is easy to see that A_S is just the frequency domain expression for the steady-state solutions, with three singularities, each corresponding to the respective growth rates of the three steady-state modes. The term A_{SR}, which also depends on $\overline{z}_1$, has one additional essential singularity $\omega = 0$, which appears in the exponential factor. We invert the Laplace transform to evaluate the singularities of A_{SR}, and obtain:

$$A_{SR}(\bar{t},\overline{z}_1) = \exp(i[\delta_\gamma + \delta_{r_\beta}]\overline{z}_1) \frac{A_0}{2\pi} \int_{\mathrm{B}} \frac{-iw^2}{\Delta w} \exp\Big(i\omega c\bar{t} - i \frac{w^3+1}{w^2} \overline{z}_1 \Big] d\omega,$$

which can be simplified to give

$$A_{SR} = \exp(i[\delta_\gamma + \delta_{r_\beta}]\overline{z}_1) \frac{A_0}{2\pi} \int_{\mathrm{B}} \frac{-iw^2}{\Delta w} \exp\Big(iw(c\bar{t} - \overline{z}_1) - i \frac{1}{w^2} \overline{z}_1 \Big) d\omega, \tag{4.54}$$

where the contour B is parallel to the real axis and lies below all the singularities of A_{SR}, δ_γ and δ_{r_β} are the detunings in the kinetic energy and betatron amplitude, respectively. In the regime where $\overline{z}_1 \geq c\bar{t}$, the integral contour B can be closed in the lower-half complex plane, since all of the singularities are out of the region enclosed by the contour and the integral vanishes. Hence for $c\bar{t} \leq \overline{z}_1$, we have $A = A_s(\bar{t})$.

When $\overline{z}_1 \leq c\bar{t}$, the contour can be closed in the upper half plane and the integral value is given by $2\pi i$ times the sum of residues at the singularities of the function A_{SR}. Evaluating all the simple poles of the above contour integration will exactly cancel that of $A_S(\omega)$, leaving only the contribution of the essential singularity $\omega = 0$. Therefore, for $\overline{z}_1 \leq c\bar{t}$ we have $A = A_{SR}$, where

$$A_{SR} = \exp(i[\delta_\gamma + \delta_{r_\beta}]\overline{z}_1) \frac{A_0}{2\pi} \int_{\mathrm{B}} \frac{-iw^2}{\Delta w} \exp\Big(iw\overline{z}_2 - i \frac{1}{w^2} \overline{z}_1 \Big) d\omega, \tag{4.55}$$

where $\overline{z}_2 = c\bar{t} - \overline{z}_1$ and B is a contour enclosing the essential singularity $\omega = 0$.

When $1/K \leq \overline{z}_1 \leq c\bar{t} + 1/K$, we have radiation escaping from the leading edge of the

electron pulse, no longer interacting with the electrons, while keeping track of the steady-state exponential growth. A noticeable difference from FEL pulse propagation can be seen here: In the FEL, the radiation pulse extends out of the electron beam head and thu always maintains a region where the pulse is no longer amplified, with minimum length $K_1\lambda/\lambda_w$, while in the case of ICL the length of the region starts at 0. This difference arises from the fact that in the ICL theory the $t = 0$ point is defined as the starting point of the bunch-field interaction and when the bunch head enters the wiggler, while in FEL theory, it is the $z = 0$ point, with the $t = 0$ point being implicitly defined as when the entire electron bunch is injected into the wiggler, and the radiation field generated by the preceding parts of the bunch has already propagated outside of the bunch.

We can rewrite the integral (4.55) using the following variables, which are particularly suitable for the discussion,

$$\kappa = \Big(\frac{\overline{z}_2}{\overline{z}_1}\Big)^{1/3}\omega,$$
$$y = \sqrt{\overline{z}_1}\overline{z}_2,$$

into

$$A_{SR} = \exp(i[\delta_\gamma + \delta_{r_\beta}]\overline{z}_1)\frac{A_0\overline{z}_1^{\frac{3}{2}}}{2\pi y}\int_{\mathrm{B}}\frac{-i\kappa^2}{\Delta\kappa}\exp\big(iy^{2/3}\phi(\kappa)\big)d\kappa. \tag{4.56}$$

The integral of $A_{SR}(\overline{z}, \overline{z}_1)$ can then be evaluated asymptotically using the stationary phase method. The principal contribution to the integral is due to the regions lying close to the value $k = k_s$, which satisify the condition $\phi'(\kappa_s) = 0$. There are three points of stationary phase, which correspond to a growing, an oscillatory, and a decaying exponential respectively. By only keeping the growing exponential $\kappa_s = 2^{1/3}(1 - \sqrt{3}i)/2$, we obtain

$$A_{SR} = \frac{\exp(i\overline{\delta}_t\overline{z}_1)}{\sqrt{3\pi}y^{4/3}}\frac{A_0\overline{z}_1}{Q(\overline{z}_1, \overline{z}_2)}\exp\Big(\frac{3}{2}(\sqrt{3}+i)(y/2)^{2/3} - \frac{i\pi}{4}\Big), \tag{4.57}$$

where

$$Q(\overline{z}_1, \overline{z}_2) = 1 + \overline{\delta}_t\exp\Big(i\frac{\pi}{3}\Big)\Big(\frac{2\overline{z}_1}{\overline{z}_2}\Big)^{2/3} - \frac{2\overline{z}_1}{\overline{z}_2}. \tag{4.58}$$

The signal A_{SR} exhibits an exponential growth that depends asymptotically on $y^{2/3}$ (for $y > 1$) in the exponential factor, and does not depend on δ_γ and δ_{r_β}, unlike the steady state

signal A_S.

If the initial field is $A_0 = 0$, while the initial bunching factor $b = b_0 \neq 0$, as required for SASE to take place, the expression for the signal A_{SR} can be obtained as:

$$A_{SR} = \frac{\exp(i\bar{\delta}_t \bar{z}_1)}{\sqrt{3\pi}y} \frac{b_0 \bar{z}_1}{Q(\bar{z}_1, \bar{z}_2)} \exp\Big(\frac{3}{2}(\sqrt{3}+i)(y/2)^{2/3} - \frac{i\pi}{4}\Big). \tag{4.59}$$

4.4.2 Weak Superradiance

Electron bunches with pulse lengths as short as a few radiation wavelengths can now be measured in plasma accelerators [59] [60], which translates to a K value close to unity. The utilization of such electron beams as coherent radiation sources will give rise to U values ranging from 1-5 to sometimes 50-100. In fact, if the high gain condition $G > 1$ is valid, U is always greater than 1 when $K > 1$, thus a short wiggler length and a short electron pulse length combination cannot produce high gain amplification and will not be discussed.

For $y \gg 1$ the relationship between $\bar{z}_1/\bar{z}_2$ and U is

$$0 < \frac{\bar{z}_1}{\bar{z}_2} < \frac{1}{U-1}. \tag{4.60}$$

Under such a condition, $c\bar{t} - \bar{z}_1$ will always be larger than 0 within the electron beam, except for a very short distance at the entrance of the interaction region. The term A_S in the expression (4.53) can thus be neglected, and $Q(\bar{z}_1, \bar{z}_2)$ can be replaced with 1. We can then simplify (4.59) to

$$A_{SR} = \frac{\exp(i\delta \bar{z}_1)}{\sqrt{3\pi}y^{4/3}} A_0 \bar{z}_1 \exp\Big(\frac{3}{2}(\sqrt{3}+i)(y/2)^{2/3} - \frac{i\pi}{4}\Big). \tag{4.61}$$

Expressions of A_{SR} and b_{SR} with no initial radiation field but an initial noise-induced bunching factor can also be easily obtained as:

$$A_{SR} = \frac{b_0 \bar{z}_1}{\sqrt{3\pi}y} \exp\Big(\frac{3}{2}(\sqrt{3}+i)(y/2)^{2/3} - \frac{i\pi}{4}\Big), \tag{4.62}$$

$$b_{SR} = \frac{b_0 \bar{z}_1}{\sqrt{3\pi}(4y)^{1/3}} \exp\Big(\frac{3}{2}(\sqrt{3}+i)(y/2)^{2/3} - \frac{i\pi}{4}\Big). \tag{4.63}$$

If we consider the entire slippage region for a point with fixed $\bar{z}_1$, expression (4.61) can

be written as:

$$A_{SR} = \frac{\exp(i\delta\overline{z}_1)}{\sqrt{3\pi}(c\bar{t} - \overline{z}_1)^{4/3}} A_0 \overline{z}_1^{2/3} \exp\Big(\frac{3}{2}(\sqrt{3}+i)[\overline{z}_1^{1/2}(c\bar{t} - \overline{z}_1)/2]^{2/3} - \frac{i\pi}{4}\Big), \tag{4.64}$$

using the variables $\bar{t}$ and $\overline{z}_1$. At the pulse leading edge, we have $\overline{z}_1 = 1/K$. If we observe the field in this point of the electron pulse, given that it is the point where radiation leaves the pulse, the asymptotic formula (4.64) will turn into:

$$A_{SR} = \frac{A_0}{\sqrt{3\pi}(c\bar{t} - 1/K)^{4/3} K^{1/3}} \exp\Big(\frac{3}{2}(\sqrt{3}+i)(c\bar{t}/2\sqrt{K})^{2/3} - \frac{i\pi}{4}\Big), \tag{4.65}$$

with $y \sim c\bar{t}/\sqrt{K}$, the intensity grows exponentially if $(c\bar{t}/\sqrt{K})^{2/3} > 1$. Superradiant gain can thus be defined in a form similar to the steady-state gain

$$G_{SR} \sim \Big(\frac{c\bar{t}}{\sqrt{K}}\Big) = \frac{G}{U^{1/3}}. \tag{4.66}$$

For a short bunch, U is always larger than 1, and as a result the peak power of the weak superradiant regime is always smaller than the steady-state regime; due to the short bunch length the radiation generated at the tail of the bunch propagates out of the bunch before it is sufficiently amplified. For $K \ll 1$, the averaged energy extraction in dimensionless units in the linear regime can be defined by integrating $\|A_{SR}\|^2$ in the expression Eq. (4.64) over $\overline{z}_1$ on the entire bunch length

$$E_L = \frac{1}{l_b} \int_0^{\bar{l}_b + c\bar{t}} d\overline{z}_1 \langle |A_{SR}| \rangle^2. \tag{4.67}$$

Due to the strong slippage, the radiation inside the bunch can be neglected. The above integration can then be carried out solely in the region $\overline{l_b} < \overline{z}_1 < \overline{l_b} + c\bar{t}$. An asymptotic evaluation of E_L, using the stationary phase method similar to [58] leads to the following expression

$$E_L = \frac{1}{3\sqrt{4\pi\sqrt{3c\bar{t}}N_{l_c}}} e^{\sqrt{3}c\bar{t}}. \tag{4.68}$$

It is easy to see that $E_L = P_{\text{ave}}/(\rho P_w)$, where P_{ave} is the unscaled average emitted power, and P_w is the total electron beam power.

Simulation Results

Simulations of pulse propagation in the weak superradiance regime are conducted, by solving the equations (2.40)-(2.42) numerically, and plot the normalised field intensity $\|A\|^2$ against $\overline{z}_1 = z - \overline{v}_\| t/\lambda$, to demonstrate the charateristics of the weak superradiance radiation pulse, with the numerical methods used for the simulation be detailed in section 4.5.

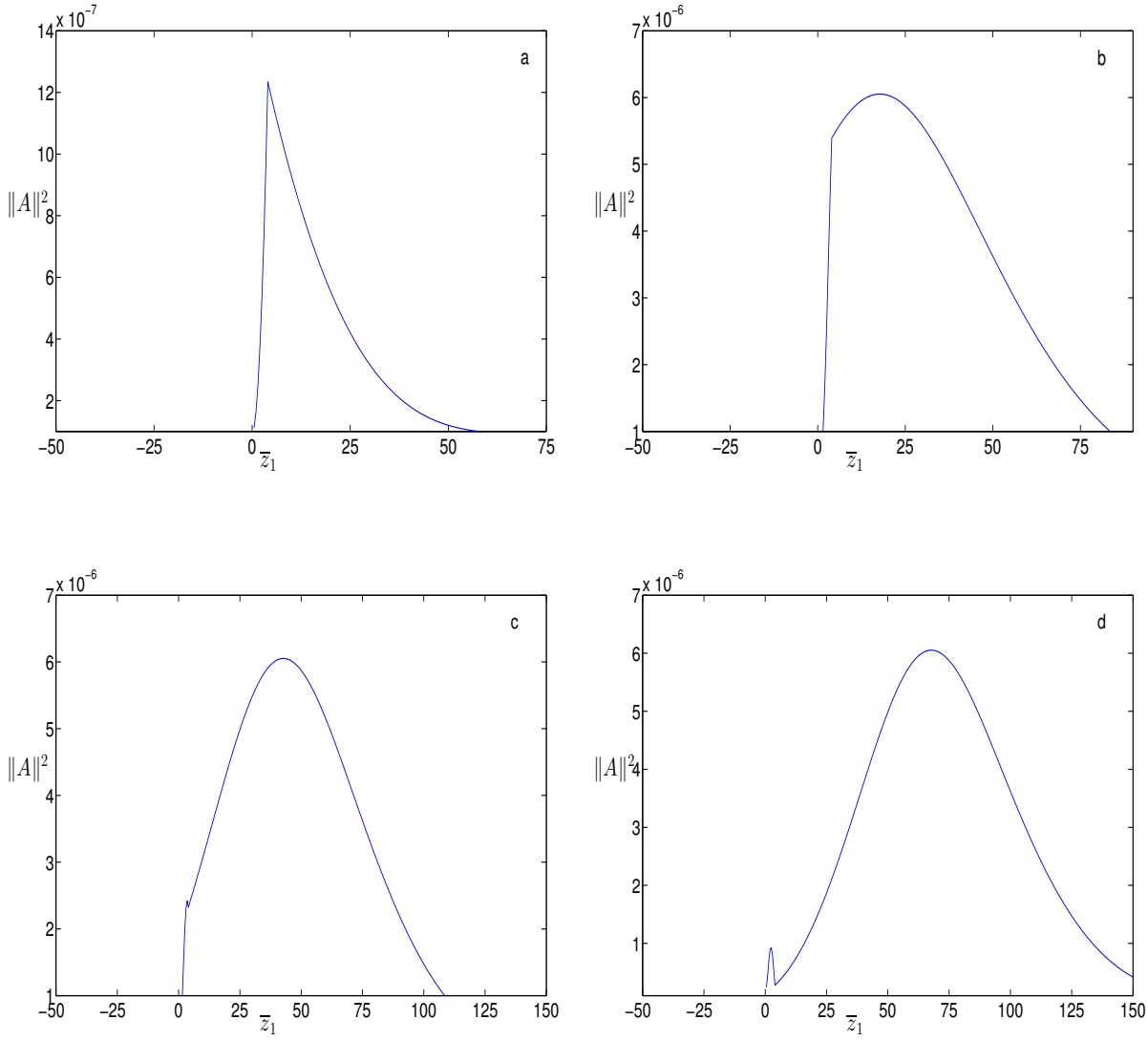

Figure 4.3: From (a) to (d), the four graphs show the gradual formation of a single radiation pulse envelope at positions $\overline{z}$=250, 300, 350, 400, by solving the equations for the weak superradiance parameters $\|\overline{A_0}\|^2 = 1.6 \times 10^{-9}$, $G = 15$, $K = 2$, $U = 30$.

We also plot the spectrum of a radiation pulse seeded with a plane wave. After in-

teracting with a sub-cooperation length electron pulse, the pulse will retain its spectral monochromaticity, all frequency components other than the resonant one have negligible power.

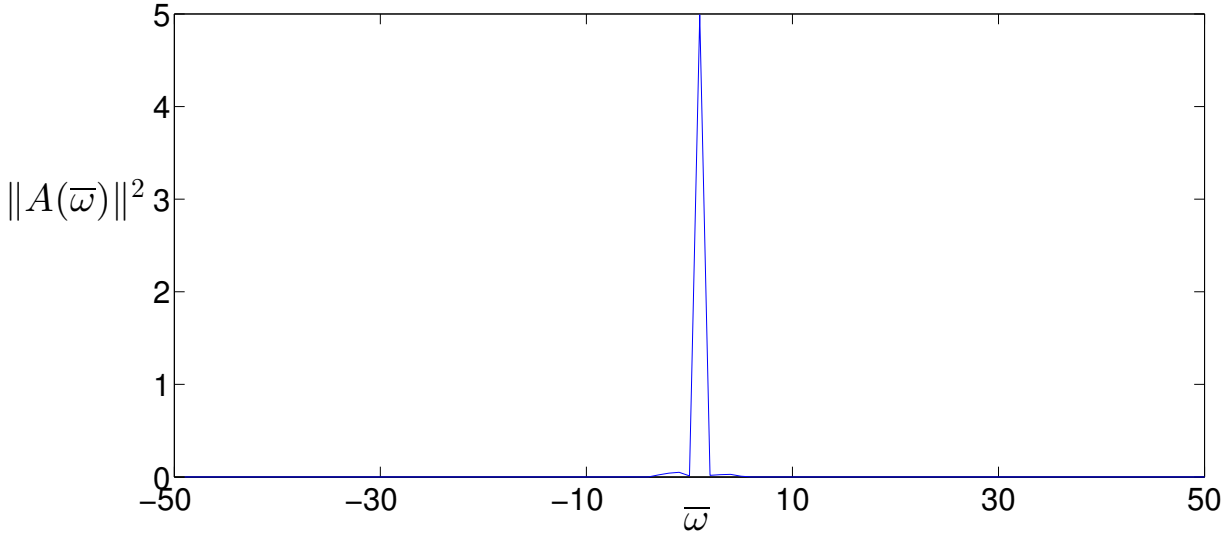

Figure 4.4: Spectrum of the radiated pulses for short electron pulse with $K = 1$, $\overline{z} = 400$, and $\overline{\omega} = (\omega - \omega_0)/\omega_0$, other parameters are $G = 10$, $\gamma = 400$.

4.4.3 Nonlinear Regime

Superradiant results from the linear analysis can be extended to the nonlinear regime in the short-pulse limit, by applying the ansatz used in [58] on the field and electron variables in Eq.(4.34)-Eq.(4.36)

$$\overline{a}_r = \overline{z}_1 \exp(i\overline{\delta}_t \overline{z}_1) A_1(y), \tag{4.69}$$

$$\psi_j = \psi_{1j}(y) - \delta \overline{z}_1, \tag{4.70}$$

$$q_j = \sqrt{\overline{z}_1} p_{1j}(y), \tag{4.71}$$

$$s_j = \sqrt{\overline{z}_1} s_{1j}(y). \tag{4.72}$$

Eqs (4.34)-(4.36) are reduced to a system of ordinary differential equations

$$\begin{cases} \dfrac{d\psi_{1j}}{dy} & = p_{1j}, \\ \dfrac{dp_{1j}}{dy} & = -A_1 \exp(i\psi_{1j}) + c.c., \\ \dfrac{y}{2}\dfrac{dA_1}{dy} + A_1 & = \langle \exp(-i\psi_{1j}) \rangle. \end{cases} \tag{4.73}$$

With all effects of order ρ neglected, it can be observed that the solution of Eqs. (4.73) does not depend on $\overline{z}_1$ and δ, but only on the initial condition b_0. Such independence implies that $\overline{a}_r$ only depends on ρ through $\overline{z}_1$, thus we have $|\overline{a}_r|^2 \propto \overline{z}_1^2 |A_1|^2 \propto \rho^2 |A_1|^2$. It is already known that $|\overline{a}_r|^2 \propto \rho n_e$, thus the radiation intensity is propotional to $\rho^2 \times \rho n_e \propto n_e^2$, If we define N_e as the number of electrons in the bunch with n_e being used for the peak number density in the spatio-temporal formulation, then the scaling of $|\overline{a}_r|^2 \propto N_e^2$ can be obtained as well, compared with $N_e^{4/3}$ in the steady state regime.

Another observation is that the electrons will be forced to radiate at their spontaneous frequency by the phase factor $\exp(i\overline{\delta}_t \overline{z}_1)$, regardless of the value of $\overline{\delta}_t$ or any predetermined radiation frequency. This can be easily seen from the following relation

$$A \exp(i[kz - \omega t]) \propto A_1 \exp(i\overline{\delta}_t \overline{z}_1), \tag{4.74}$$

where the relation $\overline{z}_1 + \overline{z}_2 = c\overline{t}$ has been used, which can turn the radiation phase into $k_s(z - ct)$, hence the detuning factor $\exp(i\overline{\delta}\overline{z}_1)$ shifts the carrier frequency from ck to ck_s. The solution (4.64) describes a superradiant process, with intensity scaling as n_e^2 and frequency of ck_s, formally identical to what is described in [58].

Setting $x \equiv y^2$, the wave equation of $A_1(y)$ can be written as

$$(d/dx)(xA_1) = \langle \exp(-i\theta_1) \rangle \equiv b_1. \tag{4.75}$$

Integrating both sides of (4.75), we have

$$A_1 = \frac{1}{x} \int_0^x dx' b_1(x') \equiv \overline{b}_1, \tag{4.76}$$

where $\overline{b}_1$ is defined as the average of b_1 with respect to x. This result gives rise to an interesting and useful interpretation of the superradiant process: in the electron rest frame, an electron with betatron amplitude r_β in the laboratory frame will "see" the electrostatic wig-

gler field as a counter-propagating pseudo-radiation field with amplitude R_β and wavelength λ_β, and transfers the pump energy into the radiation by scattering the pseudo-radiation field, a process dubbed as coherent relativistic Thomson scattering. If we take the square modulus of both sides of the above equation, the power radiated out of the electron bunch in the superradiant regime can be expressed using the original dimensionless quantities defined in Chapter 2: $A = 2A_y/(\rho^2 a_\beta)$, the relations $P = cn_e\epsilon_0\|E\|^2\pi r_b^2/2$ and $E \approx -i\omega a_r$

$$P_c = (R_\beta^2/S_b)\omega^2 r_e^2 C N_e^2 \|\bar{b}_1\|^2 \propto \|\bar{b}_1\|^2 N_e^2, \tag{4.77}$$

with $S_b = \pi r_b^2$ and $r_e = e^2/(4\pi\epsilon_0 m_e c^2)$ being the classical electron radius, and $C = 16\pi^2\epsilon_0 m_e^2 c^3/e^2$. Equation (4.77) is the power radiated by the electrons in a coherent Thomson backscattering of the pseudo-radiation field. We notice that the power expression depends on $N_e^2\|\bar{b}_1\|^2$, which becomes N_e^2 when $\|\bar{b}_1\|$ approaches 1, indicating a cooperative process. In the limit $\bar{b}_1 \propto 1/N_e^{-1/2}$ it becomes N_e and the power expression becomes

$$P_{inc} = N_e(R_\beta^2/r_b^2)\omega^2 r_e^2 C. \tag{4.78}$$

Compare expression (4.78) with the spontaneous betatron radiation power expression for a highly relativistic electron bunch in an ion channel wiggler oscillating with phase θ, defined in [37]

$$P_{sp} = \frac{2}{3} N_e c e^2 \gamma_r^4 r_b^2 k_\beta^4 \cos^2(\theta), \tag{4.79}$$

which after averaging is

$$\overline{P}_{sp} = \frac{1}{3} N_e c e^2 \gamma_r^4 r_b^2 k_\beta^4. \tag{4.80}$$

For $a_\beta \gg 1$, the expression can instead be simplified to

$$\overline{P}_{sp} = \frac{1}{3} c e^2 N_e \gamma_r^4 R_\beta^2 k_\beta^4. \tag{4.81}$$

The coherent radiation power is proportional to the square of the beam electron density, and linearly proportional to the plasma density, while the spontaneous betatron radiation power is proportional to the square of the plasma density, but linearly proportional to the beam density.

4.4.4 Strong Superradiance

In the last section, we describe the slippage effect for an electron bunch length of several radiation wavelengths, for which the influence of slippage on the field evolution is best observed, the requirement of an extremely short bunch for weak superradiance, however, is too much of a limitation for real-world radiation amplification, and the sub-saturation power output is also less than ideal. In addition, the usually large ρ value of ICL amplifier usually makes the conditions for weak superradiance hard to satisfy. Therefore it is necessary to investigate superradiance effect with a comparatively long bunch, with $K \ll 1$. Although the electron beam used is sufficiently long that the slipping radiation does not propagate out of the beam, at the trailing edge of the beam, where $\overline{z}_1 \ll c\bar{t}$ a short pulse forms as a result of the superradiant effect, and slips through the electron beam. This pulse, propagating at a group velocity of $v_g = 1 - (1 + a_\beta^2)/3\gamma_0^2$, obtained using the same dispersion relation as (4.17)

$$\omega(k) = c\Big[k + \Big(\frac{1}{2} - \frac{2}{3}\overline{\delta}_t + \frac{1}{18}\overline{\delta}_t^2\Big)2\rho k_\beta\Big], \tag{4.82}$$

is then continuously amplified by absorbing the spontaneous radiation emitted from the electrons entering the slippage region, with its width inversely proportional to the square root of its height.

The intensity of such a radiation field can be described by a transformed version of the expression of A_{SR},. When $\overline{z}_1 \gg 1$, the exponential factor in the expression (4.64) becomes dominant, with $y = \sqrt{\overline{z}_1}\overline{z}_2$ as a function of $\overline{z}_1$ for a fixed $\bar{t}$ and, reaching a maximum value at $\overline{z}_1 = c\bar{t}/3$, at which point, for nonzero $\overline{\delta_t}$(when $\overline{\delta}_t$=0 the stationary phase approximation used to obtain the time-domain expression (4.57) for A_{SR} is no longer valid), the expression of the intensity can be written as

$$\|A_{SR}\|^2 = \frac{\|b_0\|^2}{4\pi c\bar{t}\overline{\delta}_t}\exp(\sqrt{3}c\bar{t}). \tag{4.83}$$

This expression grows exponentially with $\bar{t}$ as the steady state intensity expression, with the difference being the $\bar{t}$ and the detuning factor in the denominator. In addition to the superradiant pulse propagation, from the discussion in section 4.2 we know that the long pulse also produces a steady-state-like radiation field in the region where $\overline{z}_1 > c\bar{t}$. Such a mixture of different kinds of pulses is evident in the following simulation results:

Simulation Results

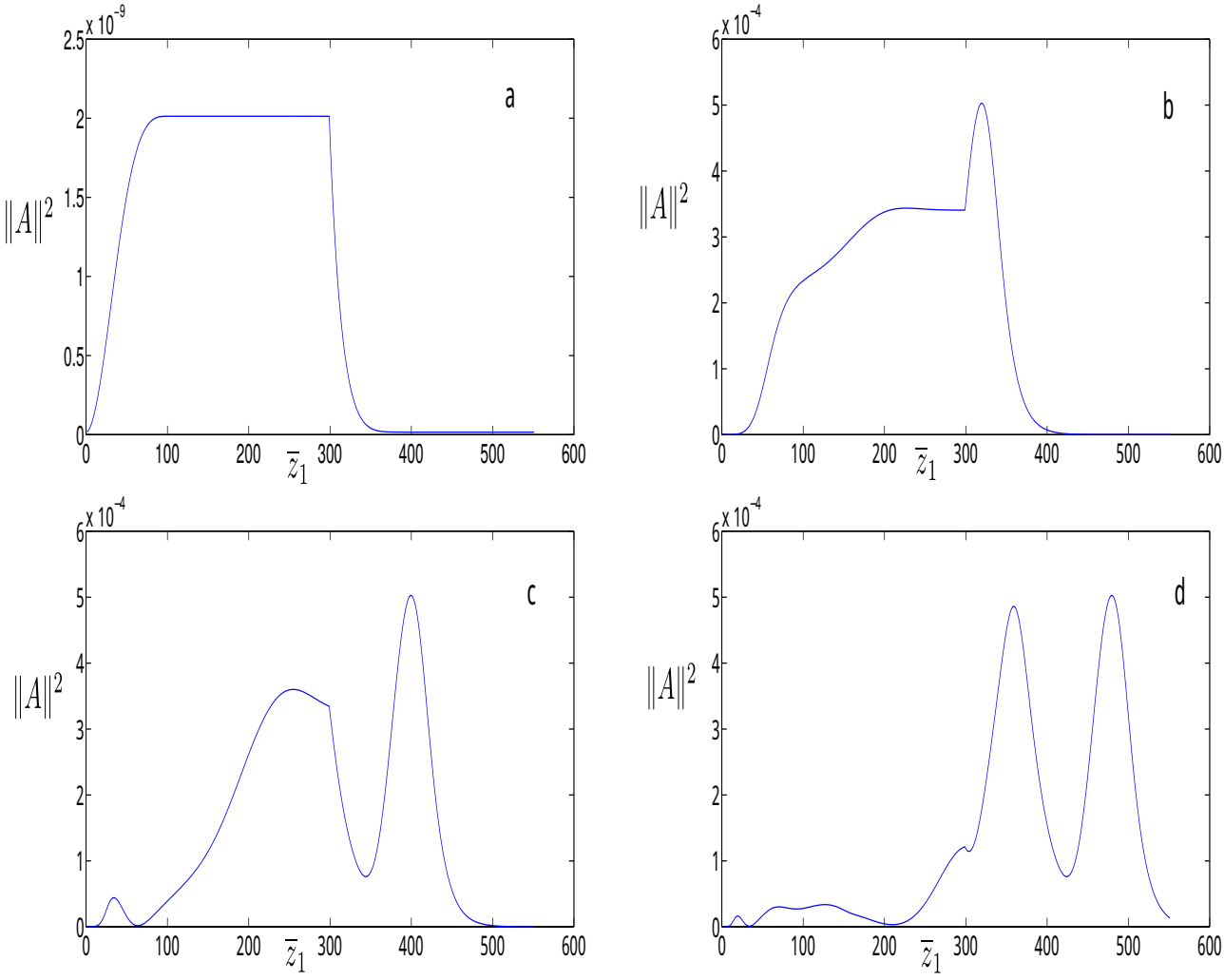

Figure 4.5: From (a) to (d), the four graphs show radiation and electron pulses at positions $\bar{z}(\bar{z} = z/\lambda_w)$=120, 360, 480, 600,respectively, produced by numerically solving $\|A\|^2$ from Eqs. (2.40), (2.41), and (2.42) with strong superradiance parameters $\|\overline{A_0}\|^2 = 1.6 \times 10^{-9}$, $G = 15$, $K = 0.042$, $U = 0.63$, $\gamma = 400$.

At the beginning of the undulator, the flat-top and low power of the radiation pulse are clearly indicative of a steady-state amplification process. As the pulse continues to develop, the spike produced by the trailing edge of the electron beam slips through the steady-state pulse and becomes clearly visible, with its power dominating that of the steady-state pulse. Meanwhile, the trailing edge continues to generate radiation, which in turn gets amplified superradiantly, at the end of the undulator, two spikes taking up most of the radiation power

are clearly visible.

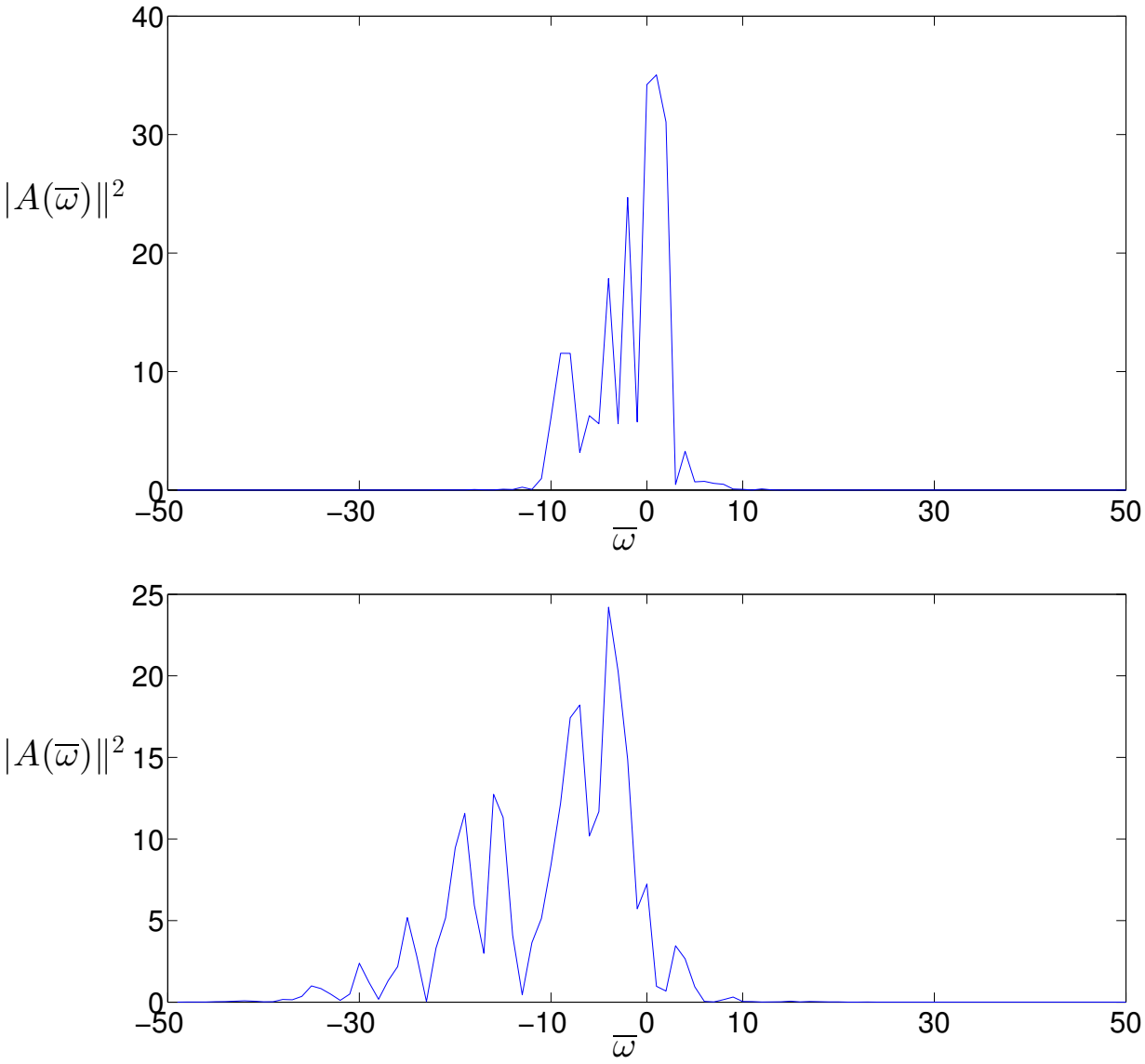

Figure 4.6: The frequency spectra of the strong superradiance at the middle (above, with $\overline{z}$=150) and the end of the interaction region (below, with $\overline{z}$ = 600) plotted against $\overline{\omega} = (\omega - \omega_0)/\omega_p$ (where ω_0 is the central frequency) using parameters same as the time-domain plots, showing the multiple frequency spikes.

Unlike the short-bunch weak superradiance simulation, in the long-bunch case the frequency spectrum extends beyond the central frequency value. This can be attributed to

the change in the distribution of the electron γ factors, which experiences a collective drop from the absorption of the laser pulse. As unamplified laser radiation continues to propagate through these electrons with reduced γ values, it will stimulate the electrons to emit radiation at, according to Eq. (4.74), their spontaneous frequencies rather than the frequency of the unamplified radiation field. In the following graph we plot the energy extraction efficiency E_L averaged over the whole bunch as defined in (4.67) as a function of $\bar{t} = ct/\lambda_w$, to examine the energy extraction efficiency of such long pulse scenario:

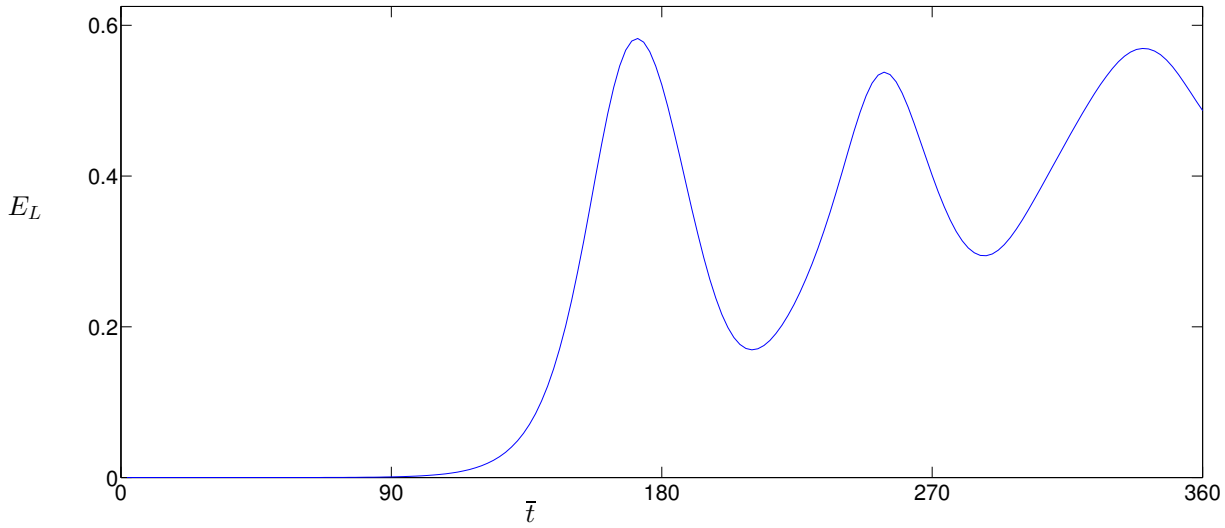

Figure 4.7: Long-pulse case: average energy extraction E_L vs $\bar{t} = ct/\lambda_w$ obtained using (4.68); the parameters are the same as in Fig. 4.5

Simulation Results

In Fig. 4.5, two different kinds of radiation evolution is clearly visible. In the leading edge, the steady-state amplification is dominant and $\|A\|^2$ is uniform while at the trailing edge we can clearly see a spike forming. The amplification of the spike is a purely superradiant effect, the pulse attains its power through continuous amplification of the spontaneous radiation pulse emitted by the trailing edge of the electron pulse, and therefore takes place no matter how large the detuning is. To verify this, we need to simulate a beam sufficiently detuned to prevent any steady-state amplification from taking place and compare this with the simulation of a on-resonant beam, with all other parameters set to be identical. The expression (4.83) shows that the signal will grow exponentially, as the steady state signal,

so the growth factor should be large enough to allow over-saturation level amplification of the superradiant signal to take place.

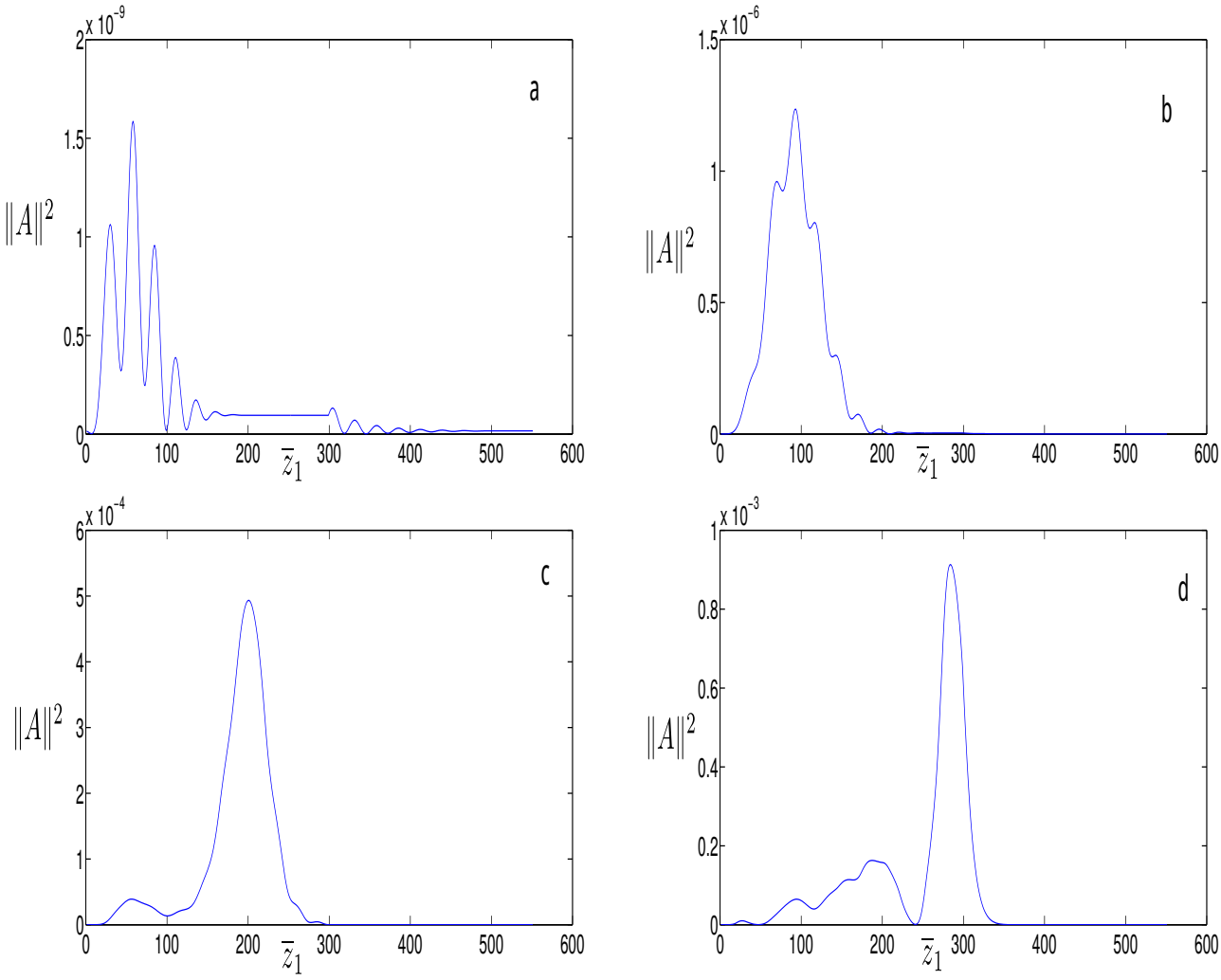

Figure 4.8: From a to d, the four graphs show radiation and electron pulses at positions $\overline{z}(\overline{z} = z/\lambda_w)$=160, 240, 320, 480 (the end of the interaction region), by solving Eqs. (2.40), (2.41), and (2.42) for the parameters $\|\overline{A_0}\|^2 = 1.6 \times 10^{-11}$, $G = 25$, $K = 0.042$, $U = 1.05$, γ=400.

As we have anticipated, the spike grows to a larger amplitude than the resonant case, while the steady-state amplification, albeit does not disappear completely, becomes much less pronounced. The energy extraction efficiency E_L along the undulator is also plotted:

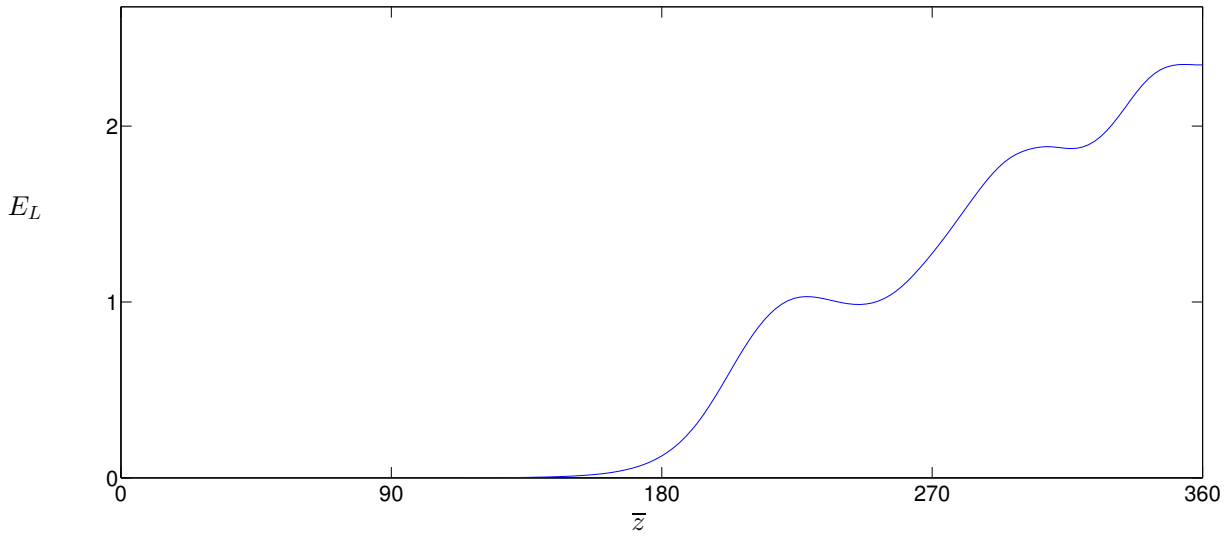

Figure 4.9: Energy extraction efficiency over the whole electron bunch plotted as a function of $\bar{t} = ct/\lambda_w$ showing the superradiant growth of radiation power, under the off-resonance condition, with $\overline{\delta} = 5$

4.5 Full SASE Numerical Simulation

4.5.1 Introduction

In this section, we describe the full simulation of a spatio-temporal SASE process in an ion channel wiggler. In the first subsection we describe the noise algorithm used to generate the phase drift in the initial phases of simulated particles, followed by the two subsections describing the discretization of the wave-equation in spatio-temporal coordinates, and the algorithm used to advance the partial equation solver, along with the conditions need to be satisfied to carry out the simulation.

4.5.2 The Noise Algorithm

The initial shot noise algorithm must satisfy three criteria: (1) In the absence of shot noise, the initial bunching at all harmonics of the fundamental frequency must be zero; (2) the initial mean value of bunching factor $|b|^2$ should be $1/N_e$, where N_e is the number of electrons in the bunch; (3) the initial macroparticles should be distinguishable not only in their longitudinal coordinates, but also in their transverse coordinates, to account for the transverse bunching effect. To achieve all three goals, we follow the approach described in [61] with minimal change. The electron bunch is first divided into a number of macroparticles, with each macroparticle, indexed by p only distinguishable from others by its longitudinal coordinate, the collection of macroparticles are subdivided into a number of "beamlets", each of which, indexed by q has its own, statistically independent longitudinal microbunching distribution spread among two or more macroparticles. Each of the macroparticles corresponding to a given beamlet is initialized with the same set of coordinates (y,p_y,p_z) but the different individual beamlets carry with them unique and physically distinguishable coordinates.

A small amount of phase drift $\delta\theta_{p,q}$ is then added to the phase of each macroparticle within a beamlet to simulate the effect of shot noise. From one beamlet to the next, there is no correlation in the amount of phase difference added, otherwise there would be anomalous temporal variation in $d\theta/dt$ from beamlet to beamlet; the random number used to generate $\delta\theta_{j,k}$ should also be completely independent among beamlets. Therefore the phase drift can be expressed as in [61]

$$\delta\theta_{p,q} = \sum_{m=1}^{m=M} (a_{m,q} \cos m\theta_{p,q} + b_{m,q} \sin m\theta_{p,q}) \tag{4.84}$$

This equation forms the basis of the algorithm for generating shot-noise in the simulation of this section.

4.5.3 Simulation of Propagation Effect

Discretization of the Wave Equation

Compared with the steady-state formulation, in the spatio-temporal simulation the slippage effect is non-negligible, the radiation beam will slowly overtake the electron bunch, and at the same time continue to absorb energy from less bunched electrons. The electron bunch length will thus have to be accounted for in the simulation. Consider an ion channel with a length of L_u, plasma wavelength λ_p, an electron bunch with a bunch length of L_b is injected into the channel, copropagating with a plane wave $A_r = A_0 e^{i(kz-\omega t)}$ initially. The wave equation of the radiation can be discretised using a Crank-Nicholson scheme, however, using such a scheme would require all phase-space coordinates of the macroparticles in all beam slices discretized in z to be stored in a tridiagonal matrix in the memory, which is quite demanding on the machine hardware. Instead, we choose to use a explicit differencing scheme, following the assumption made in Reiche's GENESIS [52] thesis, namely the interaction time between the electron bunch and a single slice of radiation beam is too short to change the collective instability significantly before the radiation field is advanced further. Such a scheme is much less demanding:

$$\left(\frac{\partial}{\partial z} + \frac{\partial}{c\partial t}\right) A_r = s(z,t) \rightarrow \frac{u_{n+1}^m - u_n^m}{\Delta z} + \frac{u_{n+1}^{m+1} - u_{n+1}^m}{c\Delta t} = s_n^m, \tag{4.85}$$

where n and m are the indices of the discretization in t and z in a Cartesian mesh, respectively: $t_n = n\Delta t$, $z^m = m\Delta z$, and u_n^m and s_n^m are the values of A_r and the source term at point(m,n), respectively. Using $c = 1$ and $\Delta z = c\Delta t$ we obtain

$$u_{n+1}^{m+1} - u_n^m = s_n^m \Delta z. \tag{4.86}$$

Simulation Methods

With the discretization used in the previous subsection, the time-dependent simulation code can be written without much modification to the steady state simulation code. At the end of every step integration in every run of steady state simulation the value of the radiation field, u_n^{m+1} is saved into a temporary array, which will be reused at the point r_{n+1}^{m+1}. However

to produce a physically meaningful simulation result, caution must be taken in terms of selection of simulation parameters.
Firstly, the stability of the differencing scheme (4.85) must be ensured through proper selection of the stepsizes in z and t coordinates. Rewriting Eq.(4.85) in the form

$$u_{n+1}^m - u_n^m = -\frac{c\Delta t}{\Delta z}(u_{n+1}^{m+1} - u_{n+1}^m) + s_n^m. \tag{4.87}$$

Performing a Von Neumann stability analysis [62], the amplification factor is

$$\|\xi\|^2 = 1 - 2\|\frac{c\Delta t}{\Delta z}\|\Big(1 - \|\frac{c\Delta t}{\Delta z}\|\Big)(1 - \cos k\Delta z). \tag{4.88}$$

The stability condition $\|\xi\|^2 \leq 1$ is the Courant-Friedrichs-Lewy condition $c\Delta t \leq \Delta z$. Therefore if the z coordinate is to be discretized in units of λ_β, the discretization unit of the t coordinate must be no more than λ_β/c to avoid numerical instability. This discretization, however, is not very useful, since there is no information on the different scales of the propagation to be obtained from such discretization, which would make, e.g., the representation of bunch length very difficult. To address this problem we transform the wave equation to the form established in (4.35)

$$\frac{\partial \overline{a}_r}{\partial \overline{z'}} - \frac{(1-\beta_\parallel)}{c\beta_\parallel}\frac{\partial \overline{a}_r}{\partial \overline{t'}} = s(\overline{z'}, \overline{t'}). \tag{4.89}$$

The natural step sizes for this discretization are λ_β for the $\overline{z'}$ coordinate and λ/c for the $\overline{t'}$ coordinate, respectively. The chosen stepsize in $\overline{z'}$ is smaller than λ_β, so as to make sure the fluctuation within one wavelength does not become the source of an undesired instability and at the same time improves accuracy. Also, to avoid instability in the Runge-Kutta solver, the integration step Δz should normally be relatively small compared to the gain length. Caution should also be taken with the value of M, the number of beam slices to be used in the simulation: Since each beam slice must be able to accommodate one radiation slice, the value of M should not be larger than L_u/λ. At the same time, to guarantee that at least one radiation slice remains in the simulated electron bunch, M should also fulfill the condition $M > \frac{L_u}{\Delta z}$. In addition, the interaction region length and the bunch length must be adjusted accordingly depending on the kind of superradiance expected to be observed.

Simulation of noise startup

To clearly observe the evolution of the noise spectrum within the bunch, we start with a simulation using a low gain parameter and short bunch length, so that the phase space coordinates (γ and r_β) of the bunch electrons do not change significantly due to the resonant absorption of energy by the laser pulse,

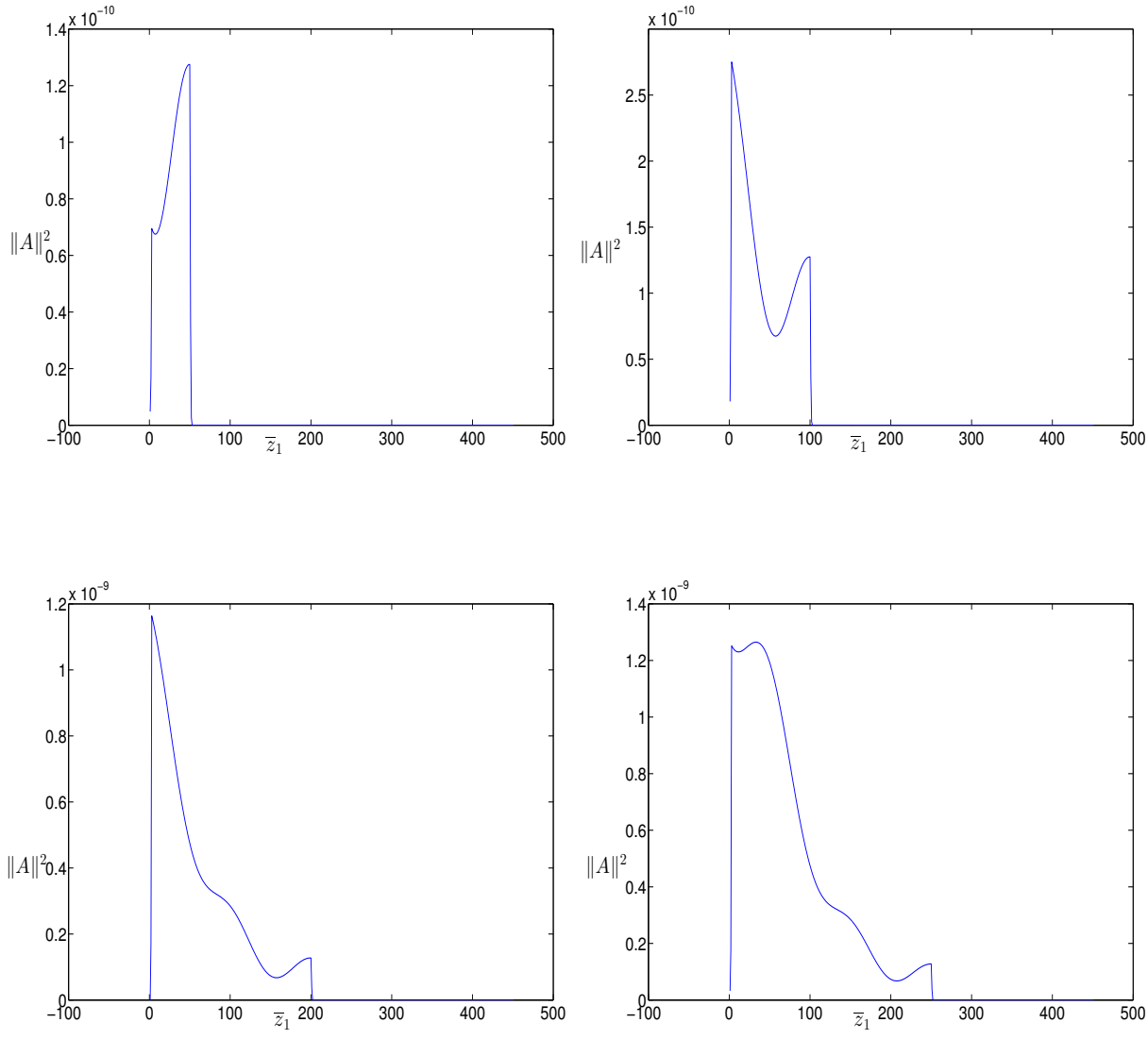

Figure 4.11: From top to bottom, left to right, shot-noise initiated radiation pulse as a function of $\overline{z}_1$ at $\overline{z} = 32, 64, 128, 160$; obtained by solving Eqs. (2.40), (2.41), and (2.42) for initial parameters $\langle|b_0|^2\rangle = 10^{-10}$, $G = 19$, $K = 2$, γ=400, $\overline{\delta}$=0

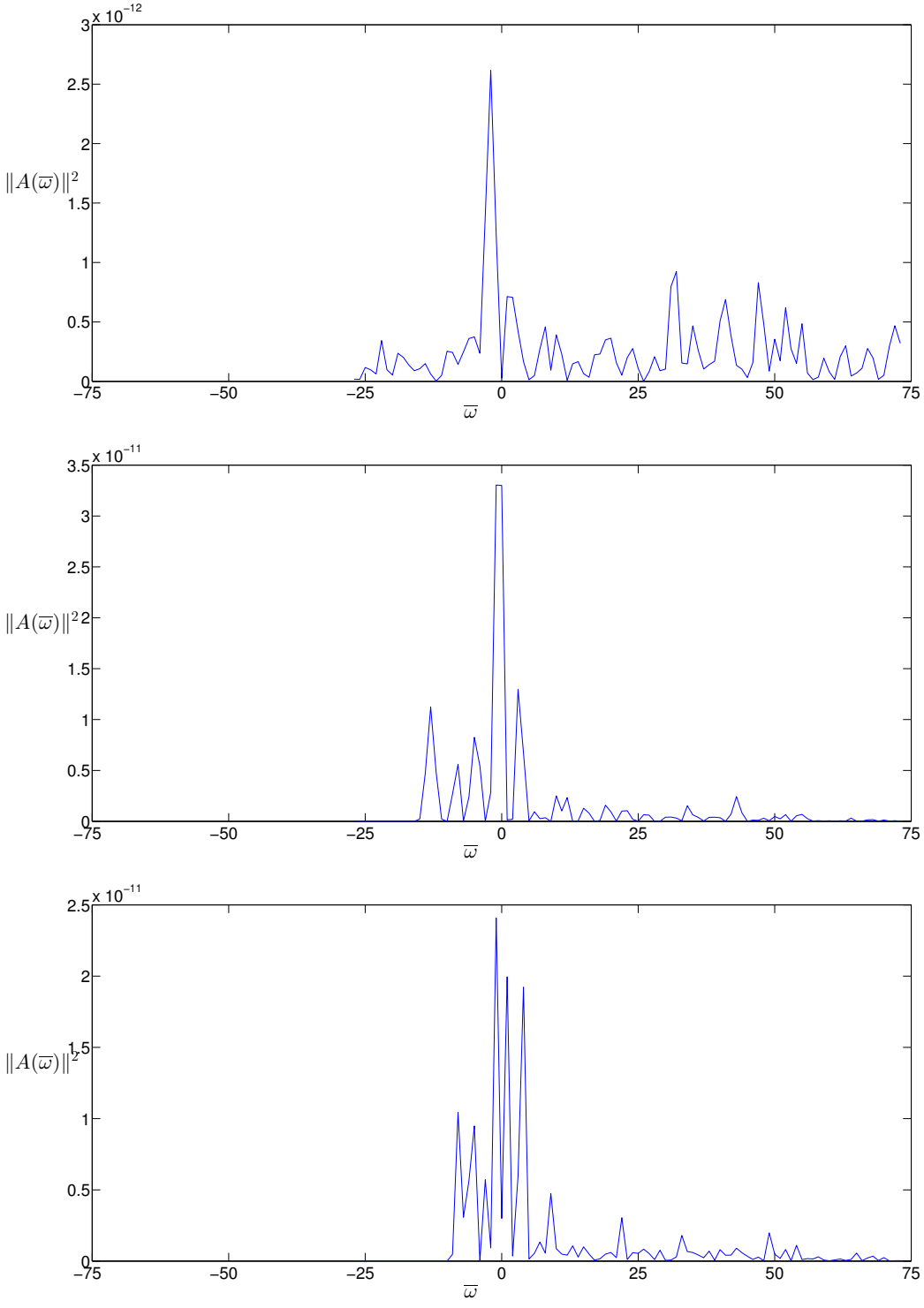

Figure 4.12: From top to bottom, the spectrum of a radiation pulse started up with shot-noise as a function of $\overline{\omega} = (\omega - \omega_0)/\omega_p$ (where ω_0 is the central frequency of the spectrum) at $\overline{z} = 0, 4, 9$ with $N_w = 70$, after filtering the frequency components generated by the rectangular profile of the current. Other parameters are $\langle |b_0|^2 \rangle = 10^{-10}$, $G = 66$, $K = 0.026$, γ=400, $\overline{\delta}$=0.

It is apparent from the spectral plots that the initial shot noise power spectrum is rather spiky, and the electron bunch with the narrow phase-space distribution serves as a monochromator which narrows the bandwidth, thus the sharper power spectra near the end of the interaction region.

The role of the bunch length in the formation of the temporal/spectral structure of a noise-initiated pulse is also investigated, in the short bunch case a single smooth uniform pulse shape is generated, while in the long bunch case, multiple spikes evenly spaced can be observed in the time-domain plot.

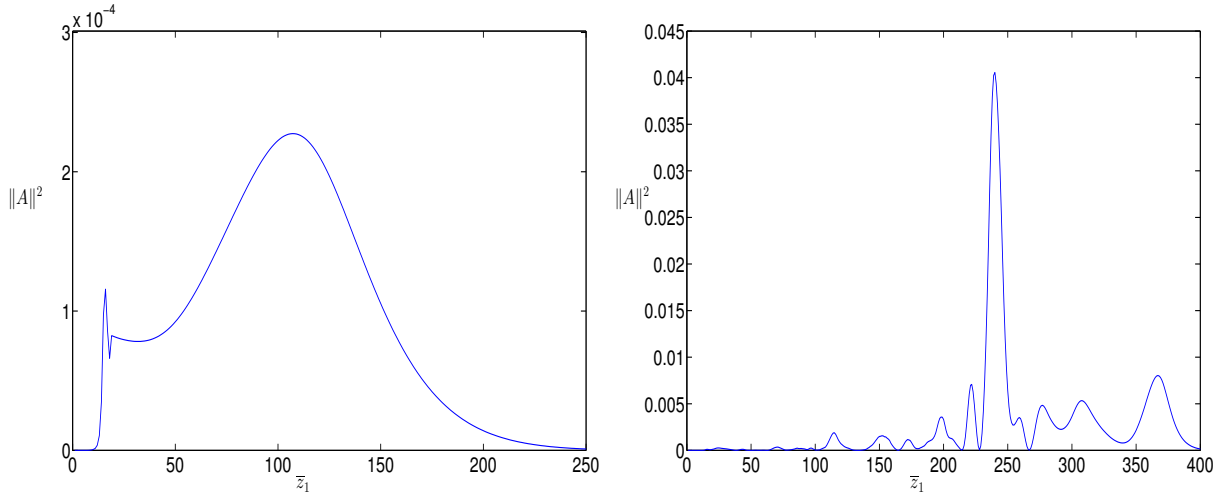

Figure 4.13: Temporal structure of the noise-initiated radiated pulse in the short bunch ($l_b = 3l_c$), weak superradiance case, and the long bunch ($l_b = 30l_c$), strong superradiance case, respectively, at the position of $\overline{z} = 20$, with $\langle |b_0|^2 \rangle = 1.6 \times 10^{-8}$. The temporal scale is in units of $\overline{z}_1 = (z - \overline{v}_\parallel t)/\lambda$.

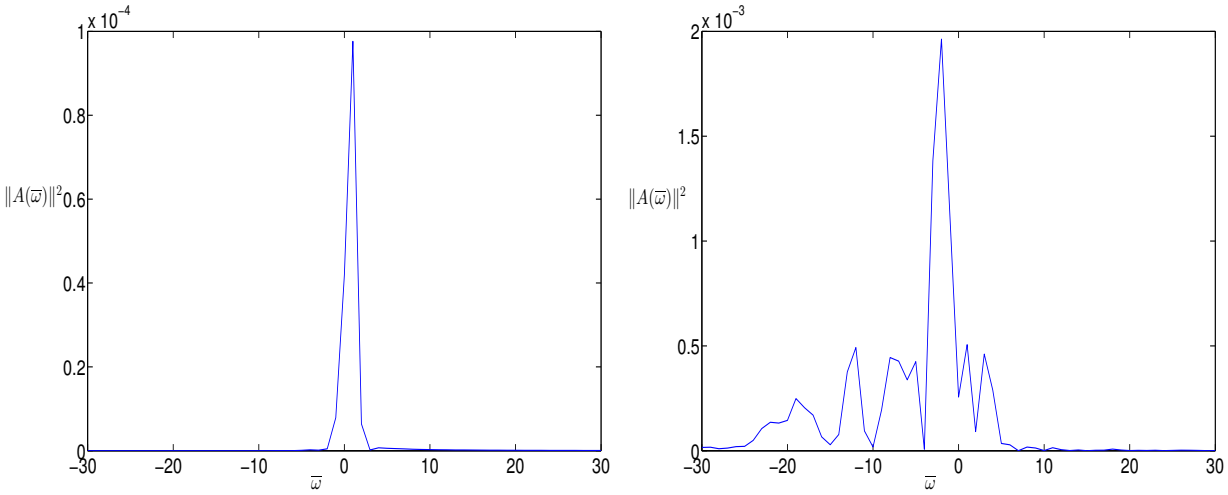

Figure 4.14: Spectrum of the radiated pulses, for the same cases of Fig. 4.13, $\overline{\omega} = (\omega - \omega_0)/\omega_p$, where ω_0 is the central frequency of the spectrum: the resonant frequency determined by the beam bunch parameters.

Chapter 5

Conclusion

This thesis has provided a theoretical investigation of the Ion Channel Laser (ICL) with large amplitude betatron oscillations using steady-state and spatio-temporal models, which have been compared with earlier works, in particular by Whittum [1]. To begin with, the collective motion of highly relativistic electrons in the electrostatic field of an ion channel has been studied in Chapter 2, using slab geometry and applying the universally scaled linear theory of the Free-Electron Laser (FEL) by Bonifacio *et al.* [3]. This model extends Whittum's ICL theory to the large-betatron amplitude case. The electron motion is entirely described by a set of ponderomotive coordinates obtained by separating the Hamiltonian into two parts, which correspond to the longitudinal and transverse electron motion, respectively. The energy exchange of a single electron with the radiation field is described by a first order equation giving the time derivative of the Lorentz factor γ in dependence of the ponderomotive phase, which is the difference between the electron betatron phase and the radiation phase; its time derivative, in turn, depends on both γ and the betatron amplitude r_β to first-order. This is in contrast to Whittum's ICL theory, where only the γ dependence is considered.

Next, the multi-particle equations and the steady-state field equation of the ICL have been formulated with collective variables defined in analogy to Ref. [3]. Scaling of the variables and linearization makes the form of the solution to the differential equation independent of the experimental parameters; the efficiency of the amplifier is determined by only two parameters, the "gain parameter" ρ and the betatron wavelength λ_β. The solution of the characteristic equation of ICL, which determines its complex growth rate, has been obtained, not only for the Compton regime where ρ is small, but for the Raman regime where the ρ value is large not just as a result of high beam electron density, but also because of

the high betatron amplitude and also for electron bunches with spreads in the kinetic energy and betatron amplitude as well.

The theory has then been directly compared with Whittum's theory to understand the differences resulting from the different approaches. Apart from the different expressions for ρ under the two approaches, we identify a caveat in Whittum's derivation of equations of motion, which introduces a redundant ponderomotive phase-dependent term into the phase evolution equation. In addition, we show that the assumption of small betatron amplitude in Whittum's model is practically unworkable after accounting for the space charge effect in the scaled model.

I have also analysed the effect of dielectric guiding on the amplification and shown that, given properly selected beam/channel parameters for large betatron amplitude, its impact on the gain of the ICL can be limited.

After having established the analytical model, the investigation proceeded with numerical simulations, which demonstrate the amplification of radiation with wavelengths ranging from microwaves to X-rays in an ion channel, under a variety of conditions, including different energy and amplitude spreads.

In Chapter 3, I discussed electron dynamics in the ICL that leads to the generation and amplification of high-order harmonics, which enables it to produce radiation at much higher frequencies than the fundamental resonance relation permits.

In Chapter 4, I presented the statistical properties of the electron bunch as a SASE radiation source. I have shown that radiation in the ICL can start from shot-noise and that the stochastic properties are preserved after amplification.

I have gone on to discuss the propagation model of the ion channel laser, which takes into account the slippage effect; an approximate solution to the 1D wave equation under the SVEA approximation has been obtained using the stationary approximation method, which in the time domain can be shown to depend on the length of the electron bunch relative to the total interaction length. The evolution of the radiation pulse can be characterized by two types of superradiant evolution: weak and strong superradiance respectively. The former applies to the short bunch – long wiggler scenario, which produces widening pulses in the time domain, with below-saturation radiation power, and the latter to the long bunch – long wiggler scenario, which generates multiple spikes with above-saturation radiation power, after evolving from a flat-top steady-state pulse, even at significant detuning.

The numerical simulations in chapter 3 not only demonstrate superradiant amplification, but also amplification of shot noise of the electron bunch. This confirms that the theoretical

method for analyzing the time-dependent FEL can be applied to the spatio-temporal analysis of the ICL.

On the basis of the analytical model and numerical simulations, we conclude that, unlike proposed in Whittum's thesis, an ICL generating high-frequency radiation is within the realm of experimental possibility for large betatron amplitudes, with gain parameter exceeding that of a traditional FEL by an order of magnitude.

Bibliography

[1] D. H. Whittum, A. M. Sessler, and J. M. Dawson, Phys. Rev. Lett. **64**, 2511 (1990).

[2] D. H. Whittum, Theory of the Ion-Channel Laser, Ph.D. Thesis, (Lawrence Berkeley Lab., CA (USA), 1990).

[3] R. Bonifacio, C. Pellegrini, and L. M. Narducci, Proc. of the 1984 AIP FEL Conference, **118**, 236 (1984).

[4] B. Ersfeld, R. Bonifacio, S. Chen, R. Islam, P. Smorenburg and D. Jaroszynski, New J. Phys. **16**, 093025 (2014).

[5] E. Esarey, B. A. Shadwick, P. Catravas, and W. P. Leemans, Phys. Rev. E. **65**, 056505 (2002).

[6] J. D. Jackson, Classical Electrodynamics (John Wiley & Sons, New York, 1998).

[7] C. Joshi, T. Katsouleas, J. Dawson, Y. Yan, and J. Slater, IEEE J. Quantum Electron. **23**, 1571 (1987).

[8] J. C. Clarke, The Science and Technology of Undulators and Wigglers (Oxford University Press, Oxford, 2004)

[9] L. R. Elias, W. M. Fairbank, J. M. J. Madey, H. A. Schwettman, and T. I. Smith, Phys. Rev. Lett. **36**, 717 (1976)

[10] D. A. G. Deacon, L. R. Elias, J. M.J. Madey, G. J. Ramian, H. A. Schwettman, and Ti I. Smith, Phys. Rev. Lett. **38**, 892 (1977).

[11] E. D. Courant, C. Pellegrini, and W. Zakowicz, Phys. Rev. A. **32**, 2813 (1985).

[12] J. Madey, J. Appl. Phys. **42**, 1906 (1971).

[13] R. Bonifacio and F. Casagrande, Nucl. Instr. & Meth. A. **239**, 36 (1985).

[14] R. Bonifacio, B. W. J. McNeil, and P. Pierini, Phys. Rev. A. **40**, 4467 (1989).

[15] D. A. Jaroszynski, R. J. Bakker, A. F. G. van der Meer, D. Oepts and P. W. van Amersfoort, Phys. Rev. Lett. **70**, 3412 (1993).

[16] R.Bonifacio, L. De Salvo, P. Pierini, N. Piovella and C. Pellegrini Phys. Rev. A, **73**, 70 (1994)

[17] P. Emma *et al.*, Nature. Photon. **4**, 641 (2010).

[18] T. Ishikawa, *et al.*, Nature. Photon. **6**, 540 (2012).

[19] A. Kondratenko and E. Saldin, Part. Accel. **10**, 207 (1980).

[20] R. Bonifacio, C. Pellegrini, and L. M. Narducci, AIP Conf. Proc. **118**, 236 (1984).

[21] K.J. Kim, Phys. Rev. Lett. **57**, 1871 (1986).

[22] R.Bonifacio, *et al.*, Phys. Rev. ST Accel. Beams **9**, 090701 (2006).

[23] R. H. Dicke, Phys. Rev. **93**, 99 (1954).

[24] W. Ackermann *et al.*, Nature. Photon. **1**, 336 (2007).

[25] C. Joshi, T. Katsouleas, J. Dawson, Y. Yan, and J. Slater, IEEE J. Quantum Electron. **23**, 1571 (1987).

[26] [1] I. Blumenfeld *et al.* Nature **445**, 741 (2007).

[27] M. V. Ammosov, N. B. Delone and V. P. Krainov, Sov. Phys. JETP Lett. **64**, 1191 (1986).

[28] H. A. Bethe and E. E. Salpeter, Quantum Mechanics of One- and Two Electron Atoms (Plenum, New York, 1977).

[29] T. Auguste *et al.*, J. Phys. B - At. Mol. Opt. Phys. **25**, 4181 (1992).

[30] D. Bauer, P. Mulser and W. Steeb, Phys. Rev. Lett. **75**, 4622 (1995).

[31] B. Quesnel and P. Mora, Phys. Rev. E. **58**, 3719 (1998).

[32] G.Z. Sun *et al.*, Phys. Fluids. **30**, 526 (1987).

[33] X. L. Chen and R. N. Sudan, Phys. Fluids. B. **5**, 1336 (1993).

[34] M.D.Felt *et al.*, Phys. Rev. E. **53**, 1068 (1996).

[35] G. P. Agrawal. Nonlinear Fiber Optics, Third Edition. (Acad- emic Press, San Diego, 2001).

[36] S. P. D. Mangles, *et al.*, Phys. Rev. Lett. **96**, 215001 (2006).

[37] Shuoqin Wang *et al.*, Phys. Rev. Lett. **88**, 135004 (2002).

[38] `http://qd.typepad.com/.shared/image.html?/photos/uncategorized/plasma_3.jpg`

[39] I. Kostyukov and A. Pukhov, Phys. Plasmas. **11**, 5256 (2004)

[40] S. Cipiccia *et al.*, Nature. Phys. **7**, 867 (2011).

[41] K. Nemeth, B. Shen, Y. Li, H. Shang, R. Crowell, K. C. Harkay, and J. R. Cary, Phys. Rev. Lett. **100**, 95002 (2008).

[42] S. Kneip *et al.*, Phys. Rev. Lett. **100**, 105006 (2008).

[43] F.T. Arecchi, R. Bonifacio, IEEE J. Quantum Electron. **QE1**, 169 (1965).

[44] R. A. Fonseca *et al.*, LNCS. **2331**, 342, (2002).

[45] R. Bonifacio, F. Casagrande and C. Pellegrini, Opt. Commun. **61**, 55 (1987).

[46] R. Bonifacio, F. Casagrande, G. Cerchioni, L. de Salvo Souza, P. Pierini, and N. Piovella, La Rivista Del Nuovo Cimento **13**, 1 (1990).

[47] R. Bonifacio, C. Maroli, and A. Dragan, Opt. Commun. **76**, 353 (1990).

[48] E. Esarey, B. A. Shadwick, P. Catravas, and W. P. Leemans, Phys. Rev. E. **65**, 056505 (2002).

[49] D. Marcuse, Theory of Dielectric Optical Waveguides, Second Edition, (Academic Press, 1991)

[50] E. Snitzer, JOSA, **51**, 491 (1961).

[51] E. L. Saldin, E. A. Schneidmiller, and M. V. Yurkov, Nucl. Instr & Meth. A. **407**, 291-295 (1998).

[52] S. Reiche, Numerical Studies for a Single Pass High Gain Free-Electron Laser, Ph.D. Thesis, (DESY, Germany, 2000)

[53] J. D. Jackson, Classical Electrodynamics (John Wiley & Sons, 1998).

[54] Joseph W. Goodman, New York, Wiley-Interscience, 1985, 567 P. 1, (1985).

[55] R. Bonifacio, F. Casagrande, Nucl. Instr & Meth. A. **239**, 36 (1985).

[56] R. Bonifacio, B. W. J. McNeil, and P. Pierini, Phys. Rev. A. **40**, 4467 (1989).

[57] R. Bonifacio, C. Maroli, and N. Piovella,Opt. Commun. **68**, 369 (1988).

[58] R. Bonifacio, L. Souza, P. Pierini, and N. Piovella, Nucl. Instr & Meth. A. **296**, 358 (1989).

[59] S.P.D Mangles, C.D.Murphy, Z.Najmudin *et al.*, Nature **431**, 535 (2004).

[60] M. R. Islam, E. Brunetti, R. P. Shanks *et al.*, New J. Phys. **17**, 93033 (2015).

[61] W. Fawley, Phys. Rev. ST Accel. Beams **5**, 070701 (2002).

[62] W.H. Press *et al.*, Numerical Recipes in Fortran 77, (Cambridge University Press, Cam- bridge, 1992)

[63] P. Mora and T. M. Antonsen, Phys. Plasmas. **4**, 217 (1997).

[64] L. V. Keldysh, Sov. Phys. JETP **20**, 1307 (1965).

[65] K Burnett, V. C. Reed and P.L. Knight, J. Phys. B - At. Mol. Opt. Phys. **26**, 561 (1993).

[66] Y. Gontier, M. Poirier and M. Trahin, J. Phys. B-At. Mol. Opt. **13**, 1381 (1980).

[67] B. W. Shore and P. L. Knight, J. Phys. B - At. Mol. Opt. **20**, 413 (1987).

[68] M. Ferray, A. L'Huillier, X. F. Li, L. A. Lompre, G. Mainfray and C. Manus, J. Phys. B - At. Mol. Opt. **21**, L31 (1988).

[69] Y. Gontier, M. Poirier and M. Trahin, J. Phys. B-At. Mol. Opt. **13**, 1381 (1980).

[70] A. L. Schawlow and C. H. Townes, Phys. Rev. **112**, 1940 (1958).

[71] A.Borisov, A.V.Borovskiy *et al.*,, Phys. Rev. A. **45**, 5830 (1992).

[72] A. M. Komashko *et al.*, JETP Lett. **62**, 860 (1995).

[73] Z.Sheng, K.Mima, J.Zhang and J.Meyer-ter-Vehn, Phys. Rev. E. **69**, 016407 (1996).

[74] R. W. Hellwarth, Advances in Quantum Electronics (Columbia University Press, New York, 1961).

[75] H. W. Mocker and R. J. Collins, App. Phys. Lett. **7**, 270 (1965).

[76] G. A. Mourou, T. Tajima and S. V. Bulanov, Rev. Mod. Phys. **78**, 309 (2006).

[77] F. Gires and G. Mayer, Compt. Rend. **258**, 2039 (1964).

[78] D. Strickland and G. Mourou, Opt. Commun. **56**, 219 (1985).

[79] Jaroszynski, D. A. *et al.*, Phil. Trans. R. Soc. A **364**, 689 (2006).

[80] Anna Enqvist, Geneartion of Ultrashort Laser Pulses Through Filamentation, Master thesis,(Lund University., Sweden, 2006).

[81] M. H. Key, M. D. Cable, T. E. Cowan *et al.*, Phys. Plasmas. **5**, 1966 (1998)

[82] K. B. Wharton, C. Brown, B. A. Hammel, S. Hatchett, M. H. Key *et al.*, Phys. Rev. Lett. **81**, 822 (1998).

[83] A. Pukhov and J. Meyer-ter-Vehn, Phys. Rev. Lett. **79**, 2686 (1997).

[84] A. Pukhov and J. Meyer-ter-Vehn, Phys. Rev. Lett. **76**, 3975 (1997).

[85] A. Pukhov and J. Meyer-ter-Vehn, Phys. Plasmas. **5**, 1880 (1998).

[86] G. I. Budker, Atomic Energy **1**, 673 (1956).

[87] I. Y. Kostyukov, G. Shvets, N. J. Fisch, and J. M. Rax, Phys. Plasmas. **9**, 636 (2002).

[88] F. S. Tsung, Ritesh Narang, W. B. Mori, C. Joshi, R. A. Fonseca, and L. O. Silva, Phys. Rev. Lett. **93**, 185002 (2004).

[89] Y. Glinec, J. Faure, A. Norlin, A. Pukhov, and V. Malka, Phys. Rev. Lett. **98**, 194801 (2007).

[90] K. R. Chen, T. C. Katsouleas, and J. M. Dawson, IEEE Trans. Plasma Sci. **18**, 837 (1990).

[91] I. Kostyukov, A. Pukhov, and S. Kiselev, Phys. Plasmas. **11**, 5256 (2004).

[92] P. Sprangle and A. T. Drobot, IEEE Trans. Microw. Theory Tech. **25**, 528 (1977).

[93] R. Bonifacio, F. Casagrande, L. De Salvo Souza, Opt. Commun. **58**, 259 (1986).

[94] C. S. Liu, V. K. Tripathi, and N. Kumar, Plasma Physics and Controlled Fusion **49**, 325 (2007).

[95] I. Kostyukov, S. Kiselev, and A. Pukhov, Phys. Plasmas. **10**, 4818 (2003).

[96] M. H. Key, M. D. Cable, T. E. Cowan *et al.*, Phys. Plasmas. **5**, 1966 (1998).

[97] K. B. Wharton, C. Brown, B. A. Hammel, S. Hatchett, M. H. Key *et al.*, Phys. Rev. Lett. **81**, 822 (1998).

[98] A. Pukhov and J. Meyer-ter-Vehn, Phys. Rev. Lett. **76**, 3975 (1997).

[99] A. Pukhov and J. Meyer-ter-Vehn, Phys. Plasmas. **5**, 1880 (1998).

[100] B.W.J. McNeil, N.R. Thompson, Nature. Photon. **4**, 814 (2010)

[101] P. Emma *et al.*, Phys. Rev. Lett. **92**, 074801 (2004)

[102] D.A. Jaroszynski *et al.*, Phys. Rev. Lett. **70**, 3412 (1993)

[103] S.M. Wiggins *et al.*, Plasma Physics and Controlled Fusion **52**, 124032 (2010)

[104] E. Brunetti *et al.*, Phys. Rev. Lett. **105**, 215007 (2010)

[105] N. Piovella *et al.*, Phys. Rev. E. **52**, 5470 (1995)

[106] D.A. Jaroszynski *et al.*, Phys. Rev. Lett. **78**, 1699 (1997)

[107] A.J.W. Reitsma and D.A. Jaroszynski, Phys. Plasmas. **14**, 053104 (2007)